

# **Compact Electromagnetic Flow Meters with Enhanced Sensitivity for Flow Measurement in Sodium Circuits**

by

**K.K.RAJAN**

**Enrollment No: ENGG02201104007**

**Indira Gandhi Centre for Atomic Research  
Kalpakkam**

**Thesis Submitted to Board of Studies in Engineering Sciences**

**for Total Fulfillment to the Requirements of**

**Doctor of Philosophy**

of

**Homi Bhabha National Institute, Mumbai**



**April, 2015**



## Homi Bhabha National Institute

### Recommendation of the Viva Voce Board

As members of the Viva Voce Board, we certify that we read the dissertation prepared by K.K.Rajan entitled "Compact Electromagnetic Flow Meters With Enhanced Sensitivity for Flow Measurement in Sodium Circuits " and recommend that it may be accepted as fulfilling the dissertation requirement for the degree of Doctor of Philosophy.

Chairperson	Dr.M. Sai Baba <i>m. saibaba</i>	Date: 24/4/15
Convener/Supervisor	Dr.T. Jayakumar <i>T. Jayakumar</i>	Date: 24/04/2015
Member-1	Prof. Udayakumar IISc, Bangalore <i>Udayakumar</i>	Date: 24/04/15
Member-2	Dr. B.P.C. Rao <i>B.P.C. Rao</i>	Date: 24/4/15
Member-3	Dr. K. Velusamy <i>K. Velusamy</i>	Date: 24/4/2015

Final approval and acceptance of this dissertation is contingent upon the candidate's submission of final copies of dissertation to HBNI.

I hereby certify that I have read this dissertation prepared under my direction and recommend that it may be accepted as fulfilling the dissertation requirement.

*T. Jayakumar*  
24/04/2015

(T. Jayakumar)

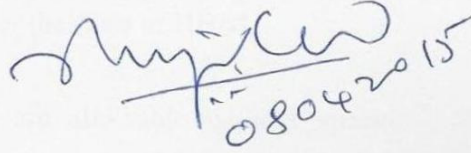
Convener/Supervisor

Place : Kalpakkam

Date : 24.04.2015

## CERTIFICATE

I hereby certify that I have read this dissertation prepared under my direction and recommend that it may be accepted as fulfilling the dissertation requirement.

A handwritten signature in blue ink, appearing to read 'T. Jayakumar', with the date '08.04.2015' written below it.

**(T. Jayakumar)**  
Convener/Supervisor

Place : Kalpakkam,

Date : 08.04.2015.

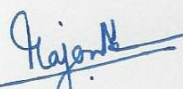
## STATEMENT BY AUTHOR

This dissertation has been submitted in partial fulfillment of requirements for an advanced degree at Homi Bhabha National Institute (HBNI) and is deposited in the library to be made available to borrowers under the rules of HBNI.

Brief quotations from this dissertation are allowable without special permission provided that accurate acknowledgement of source is made. Requests for permission for extended quotation from or reproduction of this manuscript in whole or in part may be granted by competent authority of HBNI when in his or her judgment the proposed use of materials in the interest of scholarship. In all other instances, permission must be obtained from the author.

Place: Kalpakkam

Date : 08.04.2015

  
(K.K. Rajan)

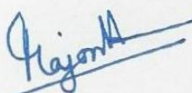
## DECLARATION

I declare that the thesis entitled "Compact Electromagnetic Flow Meters With Enhanced Sensitivity for Flow Measurement in Sodium Circuits " submitted to Homi Bhabha National Institute for the award of Doctor of Philosophy in Electrical Engineering is original research carried out by under the supervision of Dr. T. Jayakumar, Distinguished Scientist and Director, Metallurgy and Materials Group, Indira Gandhi Centre for Atomic Research, Kalpakkam.

The work reported in this thesis has not been used for award of any other degree or diploma.

Place: Kalpakkam,

Date : 08.04.2015

  
(K.K. Rajan)

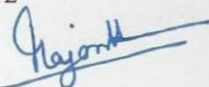
## List of Publications Arising from the Thesis

### Journal

- 1) **K. K. Rajan**, G. Vijayakumar and S. Sureshkumar; Indigenous Development of Sodium Flow meters for Prototype Fast Breeder Reactor; Journal of Instrument Society of India, ISSN 0970-9983, Vol.44, No.3, pp, 154-156, September, 2014.
- 2) Ranga Ramakrishna, P. Anup Kumar, M. Thirumalai, G. Vijayakumar, V.A. Sureshkumar, V. Prakash, C. Anand Babu and **K. K. Rajan**; In-situ calibration of permanent magnet flow meters in PFBR using noise analysis technique; Flow Measurement and Instrumentation, Vol. 34, pp, 76-82, December, 2013
- 3) **K. K. Rajan** and G. Vijayakumar; Stabilization of Magnet assemblies of Permanent Magnet Sodium Flow meters used in Fast Breeder Reactors, Nuclear Engineering and Design, 275(2014), pp, 368-374, May, 2014.
- 4) **K. K. Rajan**, Vijay Sharma, G. Vijaykumar and T. Jayakumar, Design and Development of 100 NB Pipe Size Samarium Cobalt based Permanent magnet Flow meter, Annals of Nuclear Energy, Volume 76, , pp 357-366, February, 2015
- 5) **K. K. Rajan**, Vijay Sharma, G. Vijaykumar and T. Jayakumar, Development of Side Wall type Permanent Magnet Flow meter for Sodium Flow Measurement in Large Pipes of SFRs, Flow Measurement and Instrumentation, communicated in June 2014, accepted for publication.
- 6) **K. K. Rajan**, T. Jayakumar, P K Aggarwal, V Vinod, Sodium flow measurement in large lines of Sodium cooled fast breeder reactors with bypass type flow meters, Annals of Nuclear Energy, communicated in February 2015, Under review.

### Seminars and Conferences

- 1) **K. K. Rajan**, G. Vijayakumar and Vijay Sharma; Design and Development of 100 NB Pipe Size Samarium Cobalt based PM Flow meter; NCESC-2013, Hindustan University, Chennai, 14-15, March, 2013
- 2) P.K. Aggarwal, I. Banerjee. G. Vijayakumar, G. Padmakumar and **K. K. Rajan**; Estimation of Bypass Flow Rate in PFBR Secondary Sodium Circuit by Numerical Analysis Thirty Ninth National Conference on Fluid Mechanics and Fluid Power, SVNIT, Surat, Gujarat, India, 13-15, December, 2012

  
(K K Rajan)

*Dedicated to my Parents,  
Wife and Daughter*

## ACKNOWLEDGEMENT

I am immensely grateful to my Research Guide Dr.T. Jayakumar, Distinguished Scientist and Director, Metallurgy and Materials Group, for his invaluable guidance in the right direction to complete this work.

I am thankful to Chairman of my Doctoral Committee Dr.M. Sai Baba and members of my Doctoral Committee Dr.B.P.C.Rao and Dr.K.Velusamy for their useful suggestions in my research work.

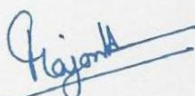
I owe my sincere thanks to Dr.P.R.Vasudeva Rao, Director, IGCAR for granting permission to do Ph.D and allowing me to use various facilities in IGCAR.

I am grateful to Dr. P Kalyanasundaram Former Director, FRTG for helping me to get permission and showing interest in my research work. I am thankful to Shri. R Prabhakar Former Director (Technical), BHAVINI for very useful discussions during the course of this research work.

I acknowledge the help rendered by my colleagues S/Shri G Vijayakumar, Vijay Sharma, Piyush Agarwal, S Suresh Kumar, V. A. Suresh Kumar, Ranga Ramakrishna, V Vinod and S Chandramouli in various studies carried out as part of this research work.

I am thankful to Shri R Ramalingam and Shri A. Kolanjiappan for the support they had rendered for preparing figures and graphs of this thesis.

I place on record my thanks to Smt. Shanthi Rajendran, Smt. Indra Ramdoss and Shri P. Varadan for providing typing, printing and binding support.

  
(K.K. Rajan)

## SYNOPSIS

Sodium cooled fast breeder reactors (SFRs) have primary, secondary and auxiliary circuits with liquid sodium as the coolant. Safe and economic operation of SFR systems depends on the successful monitoring of flow and other process parameters accurately in various circuits. The present research is directed towards development and characterization of high sensitive electromagnetic flow meters for sodium circuits of SFR.

Electromagnetic (EM) flow meters are used for sodium flow measurements in sodium cooled fast reactors. The pipe size in various circuits of a typical 500 MWe SFR ranges from 15 NB to 800 NB. An electromagnetic flow meter based on induced voltage basically consists of a pipe made of a non-magnetic material (SS) mounted in a transverse magnetic field between the two poles of a permanent magnet or electromagnet structure. If the field is produced by coil with DC power supply, it is known as saddle coil type EM flow meter. If the field is generated by a permanent magnet structure, it is known as permanent magnet flow meter (PMFM). Both these types work on the principle of DC generator and are based on the Faraday's law of electromagnetic induction. Electrical contacts (electrodes) positioned diametrically opposite to each other are welded to the outer surface of the pipe, with their central axis oriented normal to the direction of the lines of magnetic field and sodium flow. A small DC voltage is developed across the electrodes as conductive liquid metal (sodium) flows perpendicular magnetic field. The critical part of the PMFM is the magnet assembly.

The scheme for the measurement of sodium flow in pipelines using PMFM has been established and the flow meters have also been put to use for reactor applications. However, a few of the problems currently faced in pipeline flow meters are

- a) The ability of the Alnico-V magnet assembly to provide stable field is not known
- b) They are bulky and heavy for large size pipes
- c) Their sensitivity is relatively low for large size pipes
- d) Sodium calibration of PMFM is costly and time consuming
- e) Conventional PMFMs are not suitable for large pipes

Significant improvements are required in sodium flow measurement methods to achieve compactness, high sensitivity, better accuracy, stability and economy. These form the motivation for the present research and the following are the key areas where research work is focused:

- a) Studies on Alnico-V based pipe flow meters, factors affecting the sensitivity, establishing an effective calibration method and quantification of error and sensitivity
- b) Development of in-situ calibration techniques by cross correlation of noise signals from different pairs of electrodes of the same flow meter
- c) Investigation of loss of magnetism, stabilization of magnet assemblies of PMFM and stability studies at accelerated conditions
- d) Analysis, Design and development of Samarium Cobalt based PMFM with the objective of compactness and improved sensitivity
- e) Analysis and design of side wall type permanent magnet flow meter for sodium flow measurement in large pipes of SFRs.
- f) Modeling, design, optimization and validation of bypass flow meters to improve accuracy and resolution, specifically for the main secondary circuit flow measurement.

## **STUDIES ON ALNICO-V BASED PERMANENT MAGNET FLOW METERS**

As part of the research a permanent magnet flow meter with Alnico-V magnet assembly suitable for 100 NB pipe is designed and manufactured. Many novel features are incorporated in this flow meter. Among the various factors affecting sensitivity, air gap flux density surrounding electrode was found to be a critical parameter. Hence flux density has been measured at many points in the air gap of the magnet assembly where the sodium duct is positioned and average air gap flux density has been estimated. EMF, output from the flow meter is estimated based on established formula. Sodium calibration of flow meters has been carried out in a setup by absolute constant volume method. A procedure for error analysis has been established and from the errors associated with voltage volume and time measurements, the overall error in the flow meter sensitivity has been determined as  $\pm 1.2\%$ .

In-situ calibration of permanent magnet flow meters has been carried out by cross correlation of voltage fluctuations from two sets of electrode pairs in a PMFM. The transit time of fluctuation is found from the peak value of the cross correlation function. From the known spacing between the electrode pairs, flow rate is calculated. The accuracy of the flow rate estimated using cross-correlation technique was found to be within  $\pm 5.5\%$ .

## **STABILITY STUDIES ON ALNICO-V MAGNET ASSEMBLIES**

Alnico-V flow meters are the best choice of flow meters for pipe size below 100 NB. A magnet assembly is subjected to different types of losses in magnetic flux density during its service life. Magnet assemblies are electrically stabilized by a process known as AC knockdown and thermally stabilized by rapid heating and cooling cycles (RHC) and gradual heating and cooling cycles (GHC). The process of stabilization has been established based on literature survey and experimental studies.

The stability of magnet assembly with respect to time at around 100 °C is the main concern. To simulate the long term operation of permanent magnet at low temperature stability test of magnet at high temperatures below 550 °C were conducted for shorter duration. 5000 hours of accelerated endurance test has been conducted on the same assembly at four different temperatures of 380 °C, 480 °C and 530 °C after stabilizing the magnet assembly at temperatures around 50°C above the endurance test. The result shows minimum variation in flux density even in the accelerated test. To measure the recoverable losses in indigenous Alnico-V material, the magnet assembly stabilized at 580 °C and tested at different temperatures was used. Total reduction in magnetic flux density of the magnetic assembly, measured at air gap centre, when magnet temperature is varied from 30°C to 500 °C is found to be 12.8%. This corresponds to a (Tc) value of -0.0272%/°C which is comparable to the values reported in standards.

### **SAMARIUM COBALT BASED PERMANENT MAGNET FLOW METER**

For the operating conditions of SFR sodium circuits, magnet assemblies with Sm<sub>2</sub>Co<sub>17</sub> are found to be suitable and selected as the magnetic material for the compact design. A flow meter for 100 NB pipe with Sm-Co magnet assembly have been designed, analyzed, fabricated and tested in a sodium calibration setup. Multiphysics modelling of this PMFM has been carried out in FEM code COMSOL 3.5a. For modelling magnetostatics, incompressible Navier Stokes and DC conduction application modules of the software were used. The sensitivity of the Sm-Co PMFM at various process conditions has been estimated. Also sodium testing and calibration of the Sm-Co PMFM have been carried out. Calibration accuracy is estimated as 1.06%. Sm-Co flow meter sensitivity increased by 202% with a net weight reduction of 55% in comparison with Alnico-V PMFM.

Experimental and simulation results of the flow meter output voltage signal and the sensitivity have been compared. At a low flow rate of 14 m<sup>3</sup>/h, the variation between the experimental and the computational results is only 1.91%. This increases with increase in flow rate and reaches a maximum value of 7.38% at the maximum flow rate of 133 m<sup>3</sup>/h. This variation is justifiable. Long term

stability test,  $\text{Sm}_2\text{Co}_{17}$  magnet assemblies were carried out on two assemblies. There was no significant reduction in the flux density after the endurance test at operating temperature and higher temperature. The temperature coefficient of reversible losses is found to be  $0.0312\%/^\circ\text{C}$  for the range of temperatures from  $28^\circ\text{C}$  to  $100^\circ\text{C}$ , which is the expected range of temperatures of the magnet during its service and matches well with the value reported in Magnet materials producers association (MMPA) standard.

### **SIDE WALL TYPE PMFM FOR FLOW MEASUREMENT IN LARGE PIPES**

As part of the research work one side wall flow meter (SWFM), in which an Alnico-V permanent magnet block mounted on one side of a SS pipe of 100 NB size has been designed, fabricated, analyzed and tested. Two pairs of electrodes are provided at  $60^\circ$  and  $120^\circ$  angle. SWFM has been tested and calibrated in a calibration set up and the relationship between its voltage amplitude and sodium flow rate has been established. Calibration of the SWFM flow meter has been done at various process conditions. The calibration accuracy is  $\pm 1.4\%$ . Three dimensional Finite Element Method (FEM) modeling of SWFM has been carried out using COMSOL 3.5a software and the results of the modeling have been validated with experimental results. FEM model has been then used to analyze the effect of electrodes position and sodium flow rates on SWFM sensitivity.

From the calibration results, it is found that the electrode pair at  $120^\circ$  angle is more sensitive than the electrodes pair at  $60^\circ$  angle at low sodium flows, while the trend reverses at higher flows. The maximum value of the variation in sensitivity in the full flow range is around  $9\%$  for  $60^\circ$  angle electrodes pair and  $4\%$  for  $120^\circ$  angle electrodes pair.

### **BY PASS FLOW METERS FOR FLOW MEASUREMENT IN LARGE PIPES**

For sodium flow measurements in large main secondary pipelines of SFRs bypass type flow meters are used. The hydraulic characteristics of the

bypass flow meter system have been evaluated numerically and experimentally using water as simulant for a scaled-down model of the Proto type fast breeder reactor (PFBR) secondary bypass flow meter. The scaling down has been only done for the main line from 792.6 to 254.5 mm diameter, by keeping the bypass line geometry same. The same scale-down geometry has been modelled and analyzed with three dimensional 180° symmetric model using a computational fluid dynamics (CFD) code. The bypass flow covering the full range of main flow velocity has been evaluated by numerical calculations and experimentally validated. The results were in good agreement. Using the same numerical tool with suitable correction factor, flow ratio for full scale actual Proto Type Fast Breeder Reactor (PFBR) circuit has been computed. The overall accuracy achieved  $\pm 2.5\%$  which is adequate from the process and safety considerations.

The numerical and experimental studies in the search of optimum bypass geometry have been done with a main line size of 254.5 mm and water as flowing fluid. Experiments have been conducted with the model of the optimized geometry and numerical results are validated.

The research work of this thesis is focused on the problems presently faced in pipeline sodium flow measurement in SFRs which needs improvement. They are addressed successfully and redundant, alternative, cost effective, sensitive and accurate flow measurement methods have been selected and detailed studies and analysis are carried out on each one of them.

# LIST OF FIGURES

Page No.

## Chapter-1

Fig. 1.1: Schematic of FBTR.....	2
Fig. 1.2: Schematic of PFBR.....	3
Fig. 1.3: Magnetic flow meter principle.....	9
Fig. 1.4: Permanent magnet flow meter.....	9
Fig. 1.5: Schematic of ECFM .....	13
Fig. 1.6: Schematic of flow meter in core bypass line.....	15
Fig. 1.7: Bypass flow meter at primary pump discharge of BN 600.....	16
Fig. 1.8: Eddy current type flow meter at pump discharge pipe in PFR.....	17
Fig. 1.9: FBTR layout with sodium flow meters.....	21
Fig. 1.10: PFBR layout with sodium flow meters.....	21
Fig. 1.11: Schematic of ECFM in primary pumps .....	22
Fig. 1.12: ECFM sensor made for PFBR primary pump .....	22
Fig. 1.13: CFMM seating on subassembly top during flow measurement in reactor.....	23
Fig. 1.14: 200 NB pipe permanent magnet flow meter .....	24
Fig. 1.15: FFLM flow meter with 3 m long electrode cable.....	25
Fig 1.16: Details of inner and outer pipe of double wall PM flow meter .....	26
Fig. 1.17: 100 NB size double wall PM flow meter.....	26
Fig. 1.18: Bypass flow meter arrangement at PFBR secondary pump suction line.....	27

## Chapter-2

Fig. 2.1: Electrical equivalent circuit of PMFM.....	36
Fig. 2.2: Factor $K_2$ versus the ratio of pole face length to pipe ID.....	37
Fig. 2.3: Grid locations for flux density measurement.....	39

Fig. 2.4:	Locking stud and slot arrangement for flow meter.....	43
Fig. 2.5:	Magnetic field shift due to end shunting effect .....	44
Fig. 2.6:	Electrode positioning in 100 NB PMFM.....	44
Fig. 2.7:	Electrode welding details on pipe.....	45
Fig. 2.8:	Details of PMFM calibration set up.....	47
Fig. 2.9:	Schematic of PMFM calibration set up.....	48
Fig. 2.10:	Flow versus sensitivity for 100 NB Alnico-V flow meter at 200 °C...	52
Fig. 2.11:	Flow versus sensitivity for 100 NB Alnico-V flow meter at 300 °C....	52
Fig. 2.12:	Flow versus sensitivity for 100 NB Alnico-V flow meter at 355 °C....	53
Fig. 2.13:	Sensitivity verses temperature at different flow rate.....	53
Fig. 2.14:	Configuration of PMFM with three pairs of electrodes.....	59
Fig. 2.15:	Cross correlation analysis of signals from electrodes at 15 mm spacing.....	60
Fig. 2.16:	Cross correlation analysis of signals from electrodes at 30 mm spacing.....	62
Fig. 2.17:	Calibration curves obtained by cross correlation for 100 NB PMFM.....	62

**Chapter -3**

Fig. 3.1:	Hard and soft magnetic materials.....	65
Fig. 3.2:	Normal induction hysteresis loop.....	67
Fig. 3.3:	Normal induction and intrinsic induction hysteresis loop.....	67
Fig. 3.4:	100 NB PMFM magnet assembly with pole face dimensions.....	73
Fig. 3.5:	Isometric view of 100 NB PMFM magnet assembly.....	74
Fig. 3.6:	Unit property curves of anisotropic cast Alnico-V.....	76
Fig. 3.7:	Schematic of PMFM magnet assembly magnetization circuit.....	78
Fig. 3.8:	Schematic of PMFM magnet assembly stabilization circuit.....	80
Fig. 3.9:	Magnet assembly selected for stability test.....	82

Fig. 3.10: Alnico-V assembly stabilization process.....	83
Fig. 3.11: Magnetic flux density Vs temperature. ....	84
Fig. 3.12: Normalized magnetic flux density Vs temperature.....	85
Fig. 3.13: Air gap magnetic flux density Vs temperature.....	86
Fig. 3.14: Flux density Vs temperature for endurance tested magnet assembly..	86
Fig. 3.15: Flux density Vs temperature for non endurance tested magnet assembly.....	87

**Chapter- 4**

Fig. 4.1: Dimensions of Sm-Co magnet assembly for 100 NB pipe PMFM...	94
Fig. 4.2: Three dimensional view of 100 NB pipe Sm-Co PMFM.....	95
Fig. 4.3: Operating point of PMFM on the demagnetization curve of $Sm_2Co_{17}$ .....	98
Fig. 4.4: BH curve for soft iron parts of Sm-Co magnet assembly.....	99
Fig. 4.5: 3D model for 100 NB flow meter.....	99
Fig. 4.6: Velocity profile for flow rate of $14\ m^3/h$ .....	100
Fig. 4.7: Velocity profile for flow rate of $146\ m^3/h$ .....	100
Fig. 4.8: Magnetic flux density (T) in the magnetic circuit Sm-Co flow meter.....	101
Fig 4.9: Relative permeability in magnetic circuit of flow meter.....	101
Fig. 4.10: Vector plot of magnetic field in the PMFM assembly.....	102
Fig. 4.11: Magnetic flux density (T) distribution in pipe.....	102
Fig. 4.12: Voltage signals across the electrodes at the center line of pole....	103
Fig. 4.13: Output voltage verses flow based on COMSOL analysis.....	103
Fig. 4.14: Predicted sensitivity variation with temperature from COMSOL analysis.....	104
Fig. 4.15: Output voltage trace during calibration at a sodium flow rate of $133\ m^3/h$ .....	105
Fig. 4.16: Sm-Co PMFM sensitivity verses flow rate at $250\ ^\circ C$ .....	106
Fig. 4.17: Sm-Co PMFM sensitivity verses flow rate at $350\ ^\circ C$ .....	106
Fig. 4.18: Sm-Co PMFM sensitivity verses flow rate at $450\ ^\circ C$ .....	107

Fig. 4.19: Non linearity in sensitivity due to flow at 140 m <sup>3</sup> /h.....	107
Fig. 4.20: Sensitivity variation with temperature.....	107
Fig. 4.21: Experimental voltage of Sm-Co at 350 °C.....	108
Fig. 4.22: Comparison between experimental and computed sensitivity for different flow rates.....	109
Fig. 4.23: Comparison between experimental and computed sensitivity for different flow rates.....	110
Fig. 4.24: Error between the experimental and predicted voltage with flow rate.....	110
Fig. 4.25: Magnet assemblies selected or stability test.....	111
Fig. 4.26: Stability test data for Sm-Co magnet assembly at 200°C.....	112
Fig. 4.27: Magnetic flux density variation with temperature.....	113

**Chapter -5**

Fig. 5.1: Cross sectional and side view of SWFM.....	118
Fig. 5.2: Three dimensional view of SWFM.....	118
Fig. 5.3: 100 NB SWFM assembly.....	119
Fig. 5.4: Three dimensional model of side wall flow meter.....	122
Fig. 5.5: Magnetic flux density (T) in SWFM pipe cross section.....	123
Fig. 5.6: Sodium flow profile across the pipe cross section.....	124
Fig. 5.7: Electric field distribution within the pipe of SWFM.....	124
Fig. 5.8: Output voltage trace during calibration of SWFM.....	125
Fig. 5.9: SWFM voltage verses flow for electrodes 60° apart.....	126
Fig. 5.10: SWFM voltage verses flow with electrodes 120° angle apart.....	126
Fig. 5.11: SWFM voltage verses sodium temperature.....	127
Fig. 5.12: SWFM sensitivity verses sodium flow rate at 250 °C.....	127
Fig. 5.13: SWFM sensitivity verses sodium flow rate at 350 °C.....	127
Fig. 5.14: SWFM sensitivity verses sodium flow rate at 450 °C.....	128
Fig. 5.15: SWFM flow meter output Vs flow rate.....	130
Fig. 5.16: Variation of SWFM voltage with electrode position.....	131

## Chapter-6

Fig. 6.1: Bypass flow meter geometry for PFBR secondary sodium flow measurement.....	134
Fig. 6.2: Scale down model of PFBR bypass circuit.....	136
Fig. 6.3: Main flow versus bypass flow for the scale down model of PFBR bypass configuration.....	137
Fig. 6.4: Relation between the measured sodium flow through bypass line and total sodium flow through the main line for PFBR geometry....	138
Fig. 6.5: Model for optimized bypass loop for experimental and numerical studies.....	142
Fig. 6.6: Schematic of velocity vector profile in optimized bypass geometry (m/s).....	142
Fig. 6.7: Schematic of pressure contour profile in optimized bypass geometry (Pa).....	143
Fig. 6.8: Comparison of volumetric flow rate through bypass line and main line between PFBR and optimized configuration.....	143
Fig. 6.9: Optimized bypass configuration for new reactor designs.....	144
Fig. 6.10: Variation of $F_m$ with respect to $Re$ for optimized bypass configuration.....	145
Fig. 6.11: Relation between sodium flow through bypass main line for optimized geometry.....	145

## LIST OF TABLES

Page No.

### Chapter-1

Table 1.1: Physical properties of sodium.....	4
Table 1.2: Primary sodium flow measurement in pool type reactors.....	18
Table 1.3: Sodium flow measurement in reactor circuits.....	19
Table 1.4: Weight and sensitivity of flow meters with Alnico-V magnet assembly.....	29

### Chapter-2

Table 2.1: Specifications of Alnico-V based 100 NB PMFM.....	35
Table 2.2: Results of flow rate estimation from electrodes at 15 mm gap.....	61
Table 2.3: Results of flow rate estimation from electrodes at 30 mm gap.....	61

### Chapter-4

Table 4.1 : Design features for 100 NB flow meter.....	91
Table 4.2 : Comparison of magnetic properties.....	92
Table 4.3 : Comparison Sm-Co and Alnico-V PMFM.....	110

### Chapter-7

Table 7.1 : Sodium flow measurement in Indian SFRs.....	149
---	-----

## NOMENCLATURE

$A_g$	-	Area of air gap in the magnetic circuit, $m^2$
$A_m$	-	Area of permanent magnet blocks, $m^2$
$a$	-	Dimension of part a, m
$B$	-	Magnetic flux density, Tesla
$B_m$	-	Value of flux density at operating point of the demagnetization curve, Tesla
$B_g$	-	Flux density in the air gap, Tesla
$B_r$	-	Residual induction, Tesla
$BH_{max}$	-	Peak energy product, $kJ/m^3$
$b$	-	Dimension of part b, m
$b^1$	-	Dimension of part $b^1$ , m
$C$	-	Calibration constant for bypass flow meter
$C_1$	-	Proportionality constant for bypass PMFM
$C_2$	-	Proportionality constant for bypass flow meter system
$D_m$	-	Diameter of main line, m
$D_o$	-	Pipe outer diameter, m
$d$	-	Pipe internal diameter, m
$d_b$	-	Inside diameter of bypass line, m
$d_e$	-	Distance between the two electrodes, m.
$E$	-	Electric field intensity, Volts/m
$E_v$	-	Induced voltage, mV
$E_{trans}$	-	Voltage due to transformer action, Volts
$E_{motion}$	-	Voltage due to fluid motion, Volts
$F_m$	-	Volumetric flow ratio
$H$	-	Magnetizing force, AT/m
$H_c$	-	Coercivity, AT/m
$H_{ci}$	-	Intrinsic coercivity, AT/m
$H_m$	-	Magnetic field at operating point of the demagnetization curve, AT/m
$J$	-	Current density, $A/m^2$

$K$	- Overall correction factor
$K_1$	- Pipe shunting factor
$K_2$	- End shunting factor
$K_3$	- Factor which takes into account flux change due to temperature
$k_m$	- Resistance loss coefficient for friction in main line
$k_{fri}$	- Resistance loss coefficient for friction in bypass line
$k_e$	- Resistance loss coefficient at entry and exit of pipe
$k_{be}$	- Resistance loss coefficient due to bends in bypass pipe
$k_{red}$	- Resistance loss coefficient due to reducers
$k$	- Sample number
$L_m$	- Total length of permanent magnet blocks, m
$L_g$	- Total length of air gap in the magnetic circuit, m
$L F$	- Leakage Factor
$M$	- Magnetization vector, A/m
$M$	Correlation delay range
$N$	- Record length of samples
$p$	- Pressure, Pa
$Q$	- Sodium flow through the PMFM, $m^3/s$ .
$Q_m$	- Volumetric flow rate in main line, $m^3/h$
$Q_{SV}$	- Volume of sodium vessel drained, $m^3$
$Q_c$	- Flow rate estimated using cross correlation, $m^3/h$
$Q_r$	- Flow rate calculated from DC voltage of PMFM, $m^3/h$
$q_b$	- Volumetric flow rate in bypass line, $m^3h^{-1}$
$RF$	- Reluctance factor
$Re$	- Reynolds number
$R_m$	- Magnetic Reynolds number
$S$	- Sensitivity $mV/m^3/h$
$S_1$	- Primary coil
$S_2$	- Secondary coil
$T$	- Integration time, s
$T_m$	- Magnet temperature, $^{\circ}C$
$T_c$	- Curie temperature, $^{\circ}C$
$t$	- Time taken for complete draining of sodium vessel, s

$U_a$	-	Perimeter of cross section of different parts a in the assembly, m
$U_b^1$	-	Perimeter of cross section of different parts b <sup>1</sup> and in the assembly, m
$U_c$	-	Perimeter of cross section of different parts c in the assembly, m.
$V$	-	Electric scalar potential, Volts
$v$	-	Mean velocity of sodium in pipe, m/s
$v$	-	Milli volt output from the flow meter in every second, mV
$v_b$	-	Velocity of sodium in bypass line, m/s
$v_u$	-	Mean velocity of sodium at unit flow rate, m/s

### Greek Symbols

$\rho$	-	Density, kg/m <sup>3</sup>
$\rho_f$	-	Electrical resistivity of fluid, $\mu \Omega \text{ cm}$
$\rho_w$	-	Electrical resistivity of pipe material, $\mu \Omega \text{ cm}$
$\mu$	-	Permeability of sodium, N/A <sup>2</sup>
$\mu_0$	-	Permeability of vacuum, N/A <sup>2</sup>
$\sigma$	-	Electric conductivity of sodium, S/m
$\eta$	-	Dynamic viscosity, N.s/m <sup>2</sup>
$\tau$	-	Transit time, s
$\Delta p_f$	-	Pressure drop in main line due to frictional losses, Pa
$\Delta p_{fo}$	-	Pressure drop in bypass line due to form losses, Pa
$\Delta p_{fri}$	-	Pressure drop in bypass line due to frictional losses, Pa
$\Delta p_k$	-	Pressure drop in main line due to loss of kinetic head, Pa
$\Delta p_m$	-	Total pressure drop in main line, Pa
$\Delta p_s$	-	Pressure drop in main line at the exit of bypass line due to suction, Pa
$\Delta S$	-	Error in sensitivity, m <sup>3</sup> /h/mV
$\Delta v$	-	Error in mV out put, mV
$\Delta t$	-	Error in time, s
$\Delta Q_{SV}$	-	Error in sodium vessel volume, m <sup>3</sup>
$\Delta t$	-	Sampling interval, s
$\chi_m$	-	Magnetic susceptibility of the material

## Abbreviations

ANL	-	Argonne National Laboratory
AC	-	Alternate Current
CDFR	-	Commercial Demonstration Fast Reactor
CFD	-	Computational Fluid Dynamics
CFMM	-	Core Flow Monitoring Mechanism
DC	-	Direct Current
DW	-	Double Wall
ECFM	-	Eddy Current Flow Meter
EFR	-	European Fast Reactor
FBTR	-	Fast Breeder Test Reactor
EP	-	Electrode Pair
EM	-	Electro Magnetic
FEM	-	Finite Element Method
FFLM	-	Failed Fuel Location Module
FFTF	-	Fast Flux Test Facility
GAAA	-	Groupement Atomique Alsacienne Atlantique
GEC	-	General Electric Company
GIF	-	Generation IV International Forum
GHC	-	Gradual Heating and Cooling cycle
LCTR	-	Large Component Test Rig
IHX	-	Intermediate Heat Exchanger
IGCAR	-	Indira Gandhi Centre for Atomic research
MMPA	-	Magnet Materials Producers Association
NB	-	Nominal Bore
PDV	-	Pneumatic Dump Valve
PFBR	-	Prototype Fast Breeder Reactor
PFR	-	Prototype Fast Reactor
PI	-	Plugging Indicator
PMFM	-	Permanent Magnet Flow Meter

PNC	-	Power Reactor and Nuclear Fuel Development Corporation, Japan
RHC	-	Rapid Heating and Cooling Cycle
SCRAM	-	Safety Control Rod Actuated Movement
SFR	-	Sodium Cooled Fast Reactor
SGDHR	-	Safety Grade Decay Heat Removal system
SPX-1	-	Super Phenix
SW	-	Single Wall
SWFM	-	Side Wall Flow Meter
SWG	-	Standard Wire Gage
SV	-	Sodium Vessel

# CONTENTS

No	Titles	Page No.
<b>CHAPTER-1 INTRODUCTION.....</b>		<b>1</b>
1.1	Sodium Cooled Fast Breeder Reactors.....	1
1.2	Sodium as a Fast Reactor Coolant.....	3
1.3	Parameters to be Measured in SFRs.....	4
1.4	Challenges in Sodium Flow Measurement.....	5
1.5	Need for Core Flow Measurement.....	5
1.5.1	Operational functions .....	5
1.5.2	Protective functions.....	5
1.6	Need for Circuit Flow Measurement.....	6
1.7	Electromagnetic Flow Meters .....	7
1.7.1	EM flow meters based on induced voltage .....	8
1.7.1.1	Advantages of EM flow meters.....	10
1.7.1.2	Additional advantages of PMFM .....	11
1.7.1.3	Disadvantages of EM flow meters .....	11
1.7.1.4	Disadvantages specific to saddle coil type EM flow meter .....	12
1.7.1.5	Disadvantages specific to permanent magnet flow meters .....	12
1.7.2	EM flow meters based on magnetic field distortion .....	12
1.8	International Experience on Sodium Flow Measurement in SFRs .....	14
1.8.1	Core flow measurement in pool type reactors.....	14
1.8.2	Flow measurement in SFR circuits .....	19
1.9	Sodium Flow Measurement in FBTR .....	20
1.10	Sodium Flow Measurement in PFBR.....	21
1.10.1	Primary pump flow measurement .....	22
1.10.2	Subassembly flow measurement .....	23
1.10.3	Flow measurement in single wall pipelines .....	24
1.10.4	Flow measurement in FFLM.....	24
1.10.5	Flow measurement in double wall pipes .....	25

No	Titles	Page No.
1.10.6	Flow measurement in PFBR secondary main circuit .....	27
1.11	Advancements in Sodium Flow Measurement .....	28
1.12	Thesis Organization.....	30
<b>CHAPTER-2 ALNICO –V BASED PERMANENT MAGNET</b>		
	<b>FLOWMETERS .....</b>	<b>32</b>
2.1	Introduction .....	32
2.2	Sodium Flow Measurement .....	32
2.3	Definition of Sensitivity of PMFM.....	34
2.4	Analytical Estimate of Sensitivity.....	34
2.4.1	Pipe wall correction factor ( $K_1$ ).....	35
2.4.2	End effect correction factor ( $K_2$ ).....	37
2.4.3	Factor which takes into account flux change due to temperature ( $K_3$ ) ..	38
2.4.4	Correction on pipe diameter.....	39
2.4.5	Average flux density estimate .....	39
2.4.6	Estimation of sensitivity.....	40
2.5	Factors Affecting Sensitivity of PMFM.....	40
2.5.1	Magnet and sodium temperature .....	40
2.5.2	Velocity profile in pipe .....	41
2.5.3	Non uniform magnetic field in the pipe .....	41
2.5.4	Magnetic effects .....	41
2.5.5	External magnetic field and exclusion zone.....	42
2.5.6	Wetting of pipes .....	42
2.5.7	Orientation of the pipe .....	42
2.5.8	Flow meter electrodes .....	43
2.5.9	Sodium purity.....	45
2.5.10	Upstream and downstream straight pipe requirement .....	45
2.6	Response Time of PMFM .....	46
2.7	Sodium Calibration of 100 NB PMFM .....	46
2.7.1	Calibration setup .....	46
2.7.2	Instrument specifications.....	48

No	Titles	Page No.
2.7.3	Calibration procedure .....	50
2.7.4	Sensitivity estimate .....	50
2.7.4.1	Thermal offset voltage correction .....	50
2.7.4.2	Sensitivity calculation .....	51
2.7.4.3	Trend of sensitivity .....	51
2.8	Analysis on Error in Sensitivity .....	54
2.8.1	Error in milli volt measurement .....	54
2.8.2	Error in time measurement.....	55
2.8.3	Error in sodium volume measurement .....	56
2.8.4	Total error in sensitivity estimate.....	56
2.9	In-Situ Calibration of Permanent Magnet Flow Meters .....	57
2.9.1	Cross correlation technique .....	57
2.9.2	Experimental details.....	59
2.10	Closure .....	63
<b>CHAPTER-3 STABILITY STUDIES ON ALNICO-V BASED PERMANENT MAGNET FLOWMETERS .....</b>		<b>64</b>
3.1	Introduction .....	64
3.2	Ferro Magnetism .....	64
3.3	Soft and Hard Magnetic Materials .....	65
3.4	Permanent Magnets.....	66
3.5	Magnetic Properties.....	68
3.6	Alnico Magnets .....	69
3.7	Properties of Alnico-V .....	70
3.7.1	Magnetic properties of Alnico-V .....	70
3.7.2	Physical and mechanical properties of Alnico-V .....	70
3.7.3	Chemical composition of Alnico-V .....	70
3.8	Alnico-V Magnet Assembly.....	71
3.9	Design of Magnetic Circuit for 100 NB PMFM .....	71
3.10	Magnetization of Magnet Assembly .....	77
3.11	Permanent Magnet Stability .....	78

No	Titles	Page No.
3.12	Losses in Magnetic Field.....	78
3.12.1	Reversible losses .....	78
3.12.2	Irreversible but recoverable losses .....	79
3.12.3	Irreversible and unrecoverable losses .....	79
3.13	Stabilization of Magnet Assembly .....	79
3.13.1	Magnet stabilization by AC knockdown.....	80
3.13.2	Temperature stabilization of magnet assembly.....	80
3.14	Stabilization and Stability Testing .....	81
3.15	Endurance Testing of Magnet Assembly at Higher Temperatures .....	84
3.16	Reversible Temperature Coefficient .....	85
3.17	Closure .....	87

#### **CHAPTER-4 SIDE WALL TYPE PERMANENT MAGNET**

##### **FLOW METER FOR SODIUM FLOW**

##### **MEASUREMENT IN LARGE PIPELINES OF SFRS..... 89**

4.1	Introduction .....	89
4.2	Flow Measurement Methods in Large Pipes .....	90
4.3	Description of Side Wall Flow Meter .....	92
4.4	Sensitivity of SWFM.....	96
4.5	FEM Analysis of Side Wall Flow Meter.....	97
4.5.1	Magnetic circuit simulation of SWFM.....	98
4.5.2	Sodium Flow Simulation .....	99
4.5.3	Flow meter signal estimation .....	100
4.6	Testing and Calibration of PM Based SWFM for Sodium Flow Measurement .....	104
4.7	Error in Estimated Sensitivity of SWFM .....	108
4.8	Comparison of Experimental and FEM Results.....	109
4.9	Comparison of Sm-Co PMFM with Alnico-V .....	110
4.10	Stability Test on Sm-Co Magnet Assembly.....	111
4.11	Estimation of Temperature Coefficient of Reversible Losses .....	112
4.12	Closure .....	113

**CHAPTER-5 SIDE WALL TYPE PERMANENT MAGNET**

**FLOW METER FOR SODIUM FLOW**

**MEASUREMENT IN LARGE PIPELINES OF SFRS ..... 115**

5.1	Introduction .....	115
5.2	Flow Measurement Methods in Large Pipes.....	116
5.3	Description of Side Wall Flow Meter .....	117
5.4	Sensitivity of SWFM.....	119
5.5	FEM Analysis of Side Wall Flow Meter.....	121
5.5.1	Magnetic circuit simulation of SWFM.....	121
5.5.2	Sodium Flow Simulation .....	123
5.5.3	Flow meter signal estimation .....	124
5.6	Testing and Calibration of PM Based SWFM for Sodium Flow Measurement .....	125
5.7	Error in Estimated Sensitivity of SWFM .....	128
5.8	Comparison of Experimental and FEM Results.....	130
5.	Closure .....	131

**CHAPTER-6 BYPASS TYPE FLOW METERS FOR FLOW**

**MEASUREMENT IN LARGE SFR PIPELINES..... 133**

6.1	Introduction .....	133
6.2	Bypass Type Flow Meter .....	133
6.2.1	Description of bypass flow meter.....	134
6.2.2	Bypass flow meter for secondary main line flow measurement in PFBR.....	135
6.2.3	Optimization of bypass circuit geometry .....	138
6.2.4	Numerical estimation of flow multiplication factor .....	144
6.3	Closure .....	146

No	Titles	Page No.
	<b>CHAPTER-7 CONCLUSIONS AND SCOPE FOR FUTURE WORKS</b>	147
7.1	Conclusions .....	147
7.2	Scope for future Research .....	150
7.2.1	Alnico-V based PMFM .....	150
7.2.2	Sm-Co flow meter for large 200 NB pipe .....	150
7.2.3	SWFM for large pipes .....	150
7.2.4	In-situ calibration methods .....	151
7.2.5	Development of flow straightners .....	151
7.2.6	PMFM heavy liquid metals .....	151
	<b>REFERENCES .....</b>	<b>152</b>

# CHAPTER 1

## INTRODUCTION

Sodium cooled Fast breeder Reactors (SFR) have primary, secondary and auxiliary circuits with liquid sodium as the coolant. The safe and economic operation of the fast breeder reactor systems depends on the successful monitoring of flow and other process parameters accurately in different circuits. The specific focus of the research topic is on the advancements in flow measurement techniques in the pipelines of primary, secondary and auxiliary sodium circuits of fast reactors.

### 1.1 Sodium Cooled Fast Breeder Reactors

Development of sustainable energy resources with minimum environmental impact is very much essential for future generation. Along with other sustainable energy sources, nuclear power is an inevitable option for producing electricity without carbon dioxide emission. Electricity from commercial nuclear power plants is a significant contributor towards meeting the energy needs throughout the world. Around 11 % of the electrical energy generated in the world today is from nuclear reactors [1]. To harness energy from abundantly available fertile isotopes, fast neutron reactors with closed fuel cycle are being deployed. Fast neutron reactors, when fueled with plutonium, have the potential for breeding new fuel by neutron capture in uranium-238 isotope which forms 99.3% of natural uranium and Thorium-232. In the Indian context, development of fast breeder reactor technology, which is capable to convert the large resources of fertile Thorium available in the country to fissile Uranium-233 isotope, is essential.

Breeding ratio is an important parameter in fast breeder reactors and is defined as the ratio of fissile isotopes produced to the fissile isotopes consumed. A breeding ratio of upto 1.2 can be achieved by selecting suitable combination of

fuel, coolant, structural materials and core configurations. Power generated per unit volume in fast reactor is high and hence liquid metal is the preferred coolant. The Generation IV International Forum (GIF) with thirteen countries as members has a co-operative international endeavor to carry out research and development (R&D) needed to establish the feasibility and performance capabilities of the next generation nuclear energy systems [2]. GIF selected six reactor technologies for further research and development, which include SFR. This shows the international importance of SFR. SFRs are generally classified into two types. They are loop type and pool type. Figure 1.1 gives schematic Fast breeder test reactor (FBTR) which is a loop type SFR of 40 MWt and 15 MWe [3]. In the loop type design of SFR, the reactor vessel, primary sodium pumps and intermediate heat exchangers (IHX) are installed separately and connected by double wall piping. The heat generated by fission reaction in the reactor core is transferred to liquid sodium circulated through the core by the primary centrifugal sodium pumps. Hot radioactive sodium coming out of the reactor vessel is passed through the IHXs, where it transfers heat to the secondary non radioactive sodium passing through the tube side of IHXs. Non radioactive, hot secondary sodium is admitted to sodium heated steam generators, where water in the tube side is heated and superheated steam is produced. The superheated steam is admitted to the turbine which is coupled to the alternator to produce electricity.

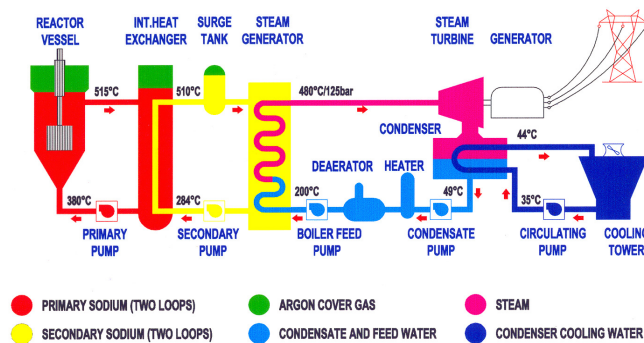


**Fig. 1.1: Schematic of FBTR [3]**

Figure 1.2 is the schematic of Prototype fast breeder reactor (PFBR) which is a pool type reactor of 1250 MWth and 500 MWe capacity [4]. In the pool

type design, primary sodium pumps, intermediate heat exchangers and the reactor core are inside the sodium pool within reactor main vessel. An inner vessel inside the reactor separates the cold and hot sodium pools. Sodium from the cold pool is sucked by the centrifugal sodium pumps and discharged through the pump discharge pipe and admitted to a high pressure header known as the grid plate on which fuel subassemblies are vertically positioned. The hot sodium coming out of the reactor core is admitted to the IHXs where heat is transferred to the non radioactive secondary sodium passing through the tube side of IHXs. Hot non radioactive secondary sodium coming out of IHXs is admitted to steam generator, where water in the tube side is heated and superheated steam is produced for electricity generation.

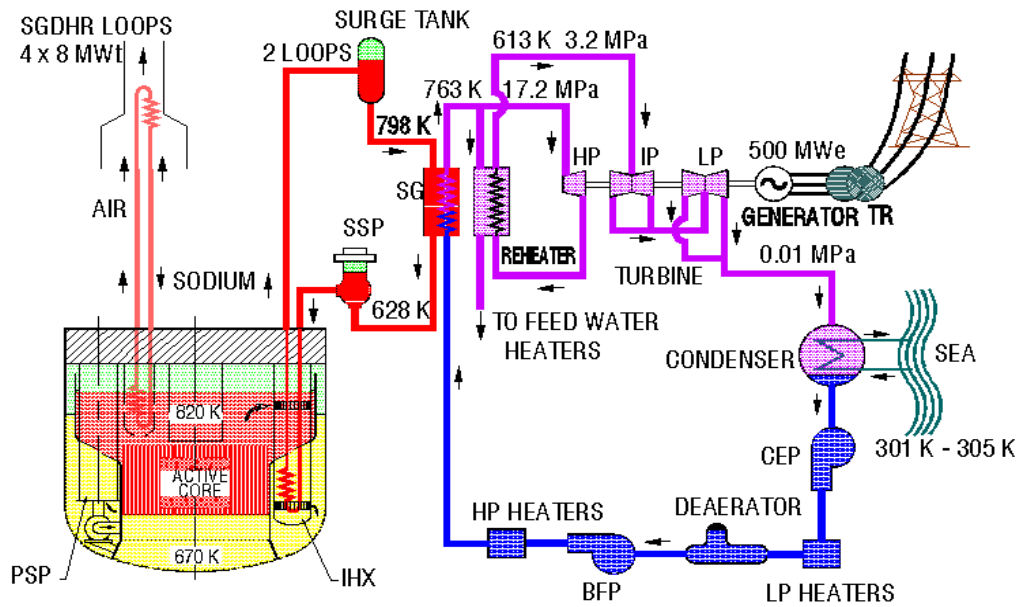


**Fig. 1.2: Schematic of PFBR [4]**

## 1.2 Sodium as a Fast Reactor Coolant

Liquid sodium is used as the coolant in sodium cooled fast reactors due to its favorable nuclear properties and excellent heat transfer properties. Sodium cooling allows the reactor to be at atmospheric pressure even at high temperature. Physical properties of sodium are given in Table 1.2.

**Table 1.1: Physical properties of sodium**

Sl. No	Property	Value
1.	Atomic number	11
2.	Melting point (760 mm Hg)	97.8 °C
3.	Boiling point (760 mm Hg)	883 °C
4.	Volume change on melting	2.7 %
5.	Heat of fusion at 97.8 °C	113.3 kJ/kg
6.	Heat of vaporization at 883 °C	3,750 kJ/kg
7.	Density of solid at 20 °C	0.968 g/cc
	Density of liquid at 100 °C	0.927 g/cc
8.	Viscosity at 100 °C	0.670 cps
	Viscosity at 400 °C	0.281 cps
9.	Surface tension at 100 °C	192 dynes/cm
10.	Vapor pressure at 600 °C	24.6 Hg
11.	Specific heat of solid at 25 °C	1.22 kJ/kg/°C
12.	Specific heat of liquid at 100 °C	1.38 kJ/kg/°C
13.	Thermal conductivity at 300 °C	76 W/m/°C
	a. Electrical resistivity at 20 °C	$4.88 \times 10^{-8} \Omega \text{ m}$
	b. Electrical resistivity at 100 °C	$9.67 \times 10^{-8} \Omega \text{ m}$
	c. Electrical resistivity at 555 °C	$30 \times 10^{-8} \Omega \text{ m}$

### 1.3 Parameters to be Measured in SFRs

Sodium temperature, flow rate, level, purity and leakage are the important process parameters to be measured/detected in SFRs. The chemically reactive nature of sodium and the all welded construction approach followed to eliminate the possibility of sodium leak, prevent conventional methods of process instrumentation for their direct use in sodium systems. In addition, the high operating temperature of 550 °C and the nuclear radiation environment make the measurement of process parameters in SFR a complex and challenging task.

## **1.4 Challenges in Sodium Flow Measurement**

Sodium, which is chemically reactive with air and water, requires special sensors for measurement of process parameters such as flow. Sodium is chemically reactive to many conventional materials used in process sensors. The sensors for SFRs are to be operated normally up to 550 °C and in transient conditions the temperature may go up to 600 °C. In the primary sodium system of SFR, sodium is radioactive and the sensors should be able to withstand radiation without degradation of the characteristics of the sensors. The sensors deployed are designed for a life of 40 years. Provision should be available for easy removal for maintenance and replacement. Non invasive sensors are desirable to meet these requirements. Sodium as a metal is a good conductor of electricity and this property is effectively utilized for developing process sensors for SFRs.

## **1.5 Need for Core Flow Measurement**

Information on the flow rate of sodium through SFR core is an important parameter for monitoring core cooling. It has both operational and protective (safety) functions, as given below:

### **1.5.1 Operational functions**

- a) Flow monitoring is required to check the performance of the primary sodium pumps and intermediate heat exchangers.
- b) After a reactor scram, core flow is reduced rapidly to mitigate avoid thermal shocks on the components. For this, flow rate is required to be known and controlled.

### **1.5.2 Protective functions**

The flow rates are continuously monitored for initiating safety related actions for the following events:

- a) Primary pump trip

- b) Primary pump seizure
- c) Transient over-power during low power operation/startup
- d) Transient over-power during power operation
- e) Off-site power failure
- f) Rupture of the pipe joining the primary pump to the grid plate
- g) Changes in the speed of the pump

The ratio of the neutronic power (P) to the flow through the core (Q), P/Q is one of the parameters used to initiate reactor shutdown (SCRAM), as it provides protection against both transient over-power and under cooling. Core temperature signals also initiate safety actions in case of insufficient core cooling. But, due to the large time constant ( $6\pm 2$ s) of the thermocouples, there is some time delay in initiating the safety actions [5]. Flow monitoring serves as a fast and diverse signal for core monitoring and reactor protection during such events.

## **1.6 Need for Circuit Flow Measurement**

In secondary circuits of SFR, the performance of the mechanical type sodium pump in the main secondary circuit is assessed based on flow measurement in large single wall secondary pipes. In the safety grade decay heat removal (SGDHR) circuits, the effectiveness of natural convection for decay heat removal is also to be confirmed by measuring sodium flow in the circuit. Auxiliary circuits of primary and secondary sodium systems such as sodium purification circuit and steam generator leak detection circuit in SFR, need flow measurement to assess the system performance. For the radioactive primary main and auxiliary circuits in the case of loop type reactor and in the radioactive primary auxiliary circuits in the case of pool type reactors, double wall pipelines with inert nitrogen gas in the annular space is used to mitigate the effects of sodium leak if any from the inner pipe. The pipeline flow meters required for sodium flow measurement in these circuits also must be of double wall type to ensure continuity of the inert nitrogen system.

## 1.7 Electromagnetic Flow Meters

Electrically conducting material moving in a magnetic field experiences an electromotive force acting in a direction perpendicular both to the motion and to the magnetic field. This discovery is one of the foundations of electromagnetism. The fact that it would happen even when the material is fluid did not escape the attention of early investigators such as Faraday, who reported to the Royal Society of London in 1832, how he had tried vainly to measure the voltage induced across the river Thames by the motion of the water in the vertical component of the earth's magnetic field [12]. The measurement is made between large electrodes, lowered into the river from Waterloo bridge. The signals he had detected are found to be spurious due to electro chemical and thermoelectric effects, two factors which can still trouble, when the principle of electromagnetic induction is applied for measuring a fluid velocity or flow rate. Faraday's experiments failed mainly because, the river bed short-circuited much of the signal. Later, electromagnetic flow meters are well developed and found wide applications in many types of industries [12]. For measuring instantaneous blood flow in arteries, electromagnetic flow measurement principle provided an attractive solution [12]. The great advantage of an electromagnetic flow meter is its response, which is rapid enough to indicate the details of blood-flow pulsations.

There have been proposals to use AC rather than DC fields in EM flow meters. The main reason for this was to avoid polarization at the electrodes and DC potentials due to thermoelectric and electrochemical effects.

With liquid metals, these troubles do not occur significantly and DC fields are usually employed. With electrolytic conductors, AC operation is essential. For example, it is a standard practice among physiologists to use AC flow meters to measure the flow of blood [12]. There are other advantages for AC as distinct from DC operation. An important one is the readiness with which AC signals may be amplified. AC flow meters have been used very successfully to measure remarkably small flow rates and also the flow of very weakly conducting liquids.

Electromagnetic (EM) flow meters used for sodium flow measurements in sodium cooled fast reactors are classified into different categories based on the methods by which a signal indicative of sodium flow rate is derived from a flow meter. Electromagnetic flow meters are broadly classified into two different categories:

- a) EM flow meters based on induced voltage
- b) EM flow meters based on magnetic field distortion

### **1.7.1 EM flow meters based on induced voltage**

An electromagnetic flow meter based on induced voltage basically consists of a pipe made of a non-magnetic material (SS) mounted in the transverse magnetic field between the two poles of a permanent magnet or electromagnet structure. In electromagnet type flow meter, the field can be generated by an electromagnet or a permanent magnet. If the field is produced by coils embedded on the pipeline with suitable structures and powered with DC power supply, it is called saddle coil type EM flow meter. If the field is generated by a permanent magnet structure, it is called permanent magnet flow meter (PMFM). Both these types work on the principle of DC generator and are based on the Faraday's law of electromagnetic induction. Electrical contacts (electrodes) positioned diametrically opposite to each other are welded to the outer surface of the pipe, with their central axis oriented normal to the direction of the lines of magnetic field and sodium flow. A small DC voltage is developed across the electrodes as conductive liquid metal (sodium) flows through perpendicular magnetic field. The magnitude of DC voltage depends on velocity profile of the liquid metal and magnetic field profile in the pipe and the polarity is determined by the direction of liquid flow. Figure 1.3 is the schematic of a typical EM flow meter. An isometric view of a typical PMFM is shown in Fig. 1.4. The magnetic field established by permanent magnet is perpendicular to the direction of sodium flow in the pipeline. The induced electro motive force (EMF) is the signal output and is in the direction mutually perpendicular to both flow and magnetic field, as shown in Figs. 1.3 and 1.4.

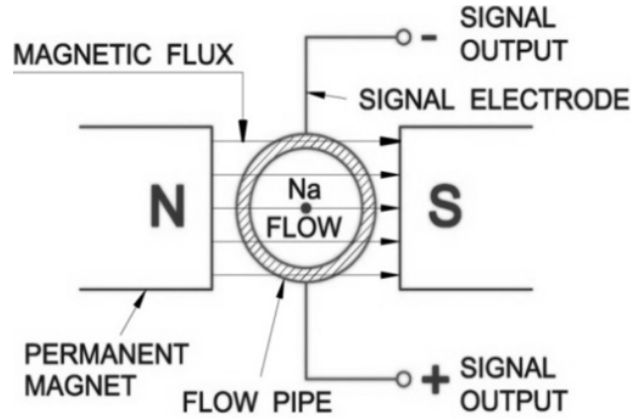


**Fig. 1.3: Magnetic flow meter principle**

PMFM is a non-invasive and passive device for sodium flow measurement [6]. Critical part of the PMFM is the permanent magnet assembly to produce required magnetic field, as shown in Fig. 1.4. Cast Alnico-V, is used as permanent magnet material due to its superior magnetic properties like high remanance, coercive force, curie temperature and high temperature stability. Maximum sodium temperature during normal operation is 550 °C. As the sodium pipe is thermally insulated, maximum temperature of the magnet during operation of flow meter is less than 100 °C in most of the cases. Permanent magnet based flow meters do not require any active power supply for producing magnetic field and is a passive device. A few limitations arise in permanent magnet based flow meters due to increase in size and weight of the magnet assembly for larger pipes.

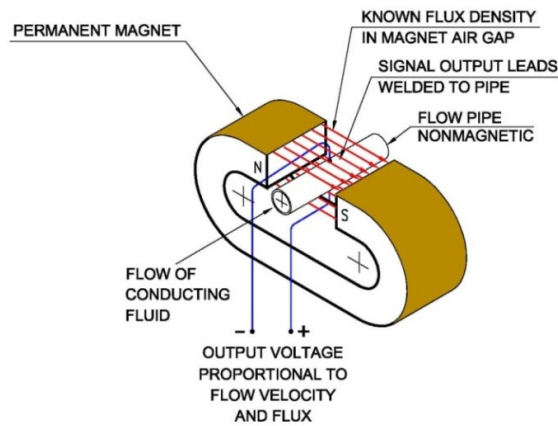


**Fig. 1.4: Permanent magnet flow meter [6]**

### 1.7.1.1 Advantages of EM flow meters

The following are the advantages of the electro magnetic flow meters [6, 7]

- a) All welded construction requirement is easily attainable
- b) No additional piping is required
- c) It is non invasive, without any penetrations or contact with sodium
- d) Has no moving parts
- e) Very little maintenance only is required
- f) Size and weight are low for small diameter pipes
- g) Introduces negligible pressure drop in the system
- h) It can withstand high temperature
- i) Simple DC milli volt indicator is only required as external device
- j) It has wide dynamic range
- k) Fast response
- l) Linear output with flow
- m) Reasonable level of DC output and easy transmission of the signal
- n) Multiple signal output is possible from the same sensor
- o) Inherent reliability of flow indication is high
- p) High accuracy can be achieved
- q) Accuracy of calibration from theoretical and by numerical modeling is high
- r) Internal impedance is low and is comparable with thermocouples
- s) In-situ calibration is possible by signal analysis techniques

All the advantages of EM flow meters are applicable to permanent magnet flow meters also.

### **1.7.1.2 Additional advantages of PMFM**

The following are the additional advantages of PMFM over saddle coil flow meters

- a) Improved reliability.
- b) Passive in nature as it does not require power supply.
- c) Enhanced long term stability can be achieved by proper stabilization of magnet assembly.
- d) No operating power costs.
- e) No heat dissipation and cooling requirements.
- f) Less possibility of field interruption.
- g) No electrical insulation required.
- h) Immune to problems of moisture and electrical short circuit.
- i) Magnet can be replaced without replacing the pipe if a C shaped magnet is used.

### **1.7.1.3 Disadvantages of EM flow meters**

- a) The accuracy of flow measurement depends on precise measurement of flux density.
- b) The presence of magnetic field or magnetic material affects the sensitivity.
- c) Output depends on wetting of the sodium to pipe wall.
- d) The output varies with the electrical resistivity of pipe and fluid.
- e) Pipe should have high resistivity compared to fluid to minimize pipe shunting effect.
- f) Minimum upstream and downstream straight pipe lengths have to be maintained to achieve axial symmetric velocity profile and thereby accuracy.

#### **1.7.1.4 Disadvantages specific to saddle coil type EM flow meter**

- a) Large saddle coil size and large space requirements
- b) High DC current and reliable power supply requirements
- c) Fluctuations and ripples in DC power supply as it is derived from AC supply
- d) Reliability of power supply
- e) Problems associated with heat dissipation, insulation failure and moisture ingress

#### **1.7.1.5 Disadvantages specific to permanent magnet flow meters**

- a) The instrument is temperature sensitive and hence, the output varies with magnet temperature and fluid temperature.
- b) The output is sensitive to orientation of the magnet assembly to pipe
- c) Difficult to regulate field and clean the magnets.
- d) Long term stability of the magnet to provide stable field. Periodical checking of the magnet flux density is required to confirm flux density.
- e) The magnet assembly is bulky and heavy for large size pipes.

#### **1.7.2 EM flow meters based on magnetic field distortion**

The eddy-current flow meters (ECFM) [8, 9] utilize the distortion of the imposed magnetic field as the means of measuring flow rate. As shown in Fig. 1.5, the ECFM consists of a primary winding energized by an alternating current source. Primary winding is surrounded by two identical secondary windings  $S_1$  and  $S_2$  on either side [10]. When sodium is static, the alternating flux produced by the primary winding induces equal voltages in both the secondary windings due to

transformer action. When sodium flows, motion voltage is produced in both the secondary coils. The motion voltage is subtractive to transformer voltage in upstream coil ( $S_1$ ) and additive to transformer voltage in downstream coil ( $S_2$ ). ECFM output is the voltage difference between the two coils and is proportional to the sodium velocity around the sensor.

When the temperature of the surrounding sodium increases, its electrical resistivity increases resulting in less eddy currents and hence an increase in both  $E_{trans}$  and  $E_{motion}$  voltages [11]. The effect of temperature is compensated by using normalized signal which is a function of velocity only. Thus we have

$$S_2 = E_{trans} + E_{motion}$$

$$S_1 = E_{trans} - E_{motion}$$

$$ECFM \text{ output} = (S_2 - S_1)/(S_1 + S_2) = E_{motion}/E_{trans}$$

Primary winding is made with MgO insulated SS sheathed (MI) cable with copper conductor and secondary winding is made of MI cables with Nichrome conductor. Nichrome conductor has very low temperature coefficient of resistance. Current through secondary coil is negligible during measurement. The coils are wound over a bobbin (pure iron) and the bobbin is encapsulated in a stainless steel (SS) pocket.

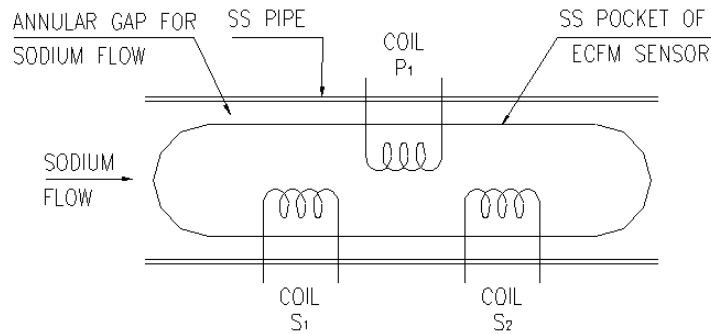


**Fig. 1.5: Schematic of ECFM**

## **1.8 International Experience in Sodium Flow Measurement in SFRs**

Theory for measuring the flow of electrically conducting fluids in pipes is first developed by Shercliff [12]. He developed two dimensional weight functions to represent the contribution of fluid velocity profile to flow meter voltage signal developed across pipe cross sections of different shapes. The short circuiting effect of pipe wall conductivity on flow meter voltage signal and effect of finite length of magnetic field were studied by Hemp and Versteeg [13]. Electromagnetic flow meters used to measure the flow of liquid metals encounter the problem of magnetic field distortion due to currents induced in liquid metals [14].

Invasive and non invasive type flow meters have been used in FBRs. Invasive flow meters such as eddy current flow meters and probe type permanent magnet flow meters have been used in primary sodium circuits [7]. Saddle coil flow meters have been used in PFR [15, 16] and JOYO reactors [17] for pipeline flow measurement. Permanent magnet flow meters which are of non invasive type were used in BN-350, BN-600, FFTF, Phenix, Super-Phenix, SNR-300, KNK and FBTR reactors for pipeline flow measurement [7].

### **1.8.1 Core flow measurement in pool type reactors**

Table 1.3 gives the methods of primary sodium flow monitoring adopted in the pool type fast reactors [7]. In BN 600 reactor, PM flow meters are provided in core bypass line. This line originating from the core inlet plenum is routed out of reactor vessel (RV) and flow meters are provided on roof slab. Figure 1.6 is the schematic of flow meter in the core bypass line. This arrangement needs special shielding and precautions against leakage of radioactive sodium.

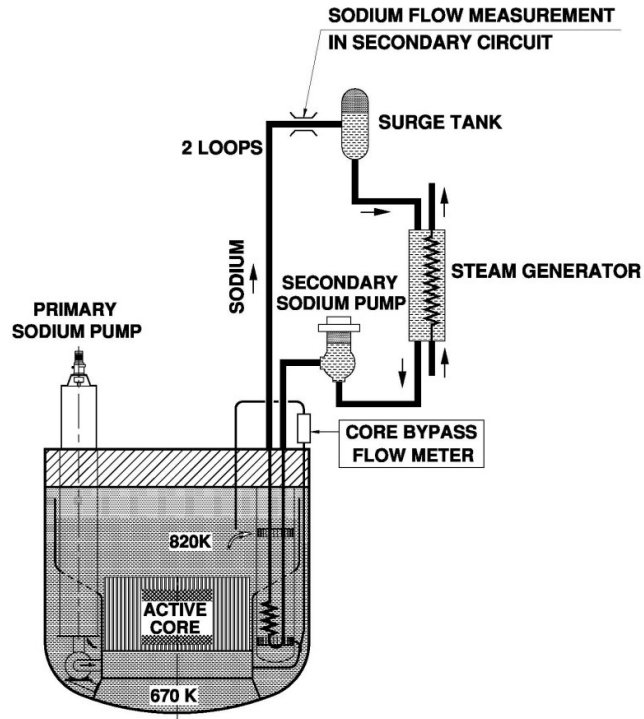


**Fig. 1.6: Schematic of flow meter in core bypass line [4]**

In BN 800 reactor being constructed in Russia, PM flow meters are provided on a bypass line at pump discharge [18], as depicted in Fig. 1.7. A bypass tapping is taken from the pump discharge line and a PMFM is installed in the bypass line. The inlet and outlet of the bypass circuit are configured in such a way that the maximum velocity head is available for establishing flow in the bypass circuit.

In Phenix and Super Phenix reactors, pump discharge flow was monitored using bypass type permanent magnet flow meters at discharge of the pumps. These flow meters have been made as part of the pumps and are removable along with the pumps. In Phenix reactor, for in-situ calibration of the flow meters, a core inlet pressure transducer was provided in the core in the form of a subassembly. Pressure transducers were also provided at the pump discharge [19, 20].

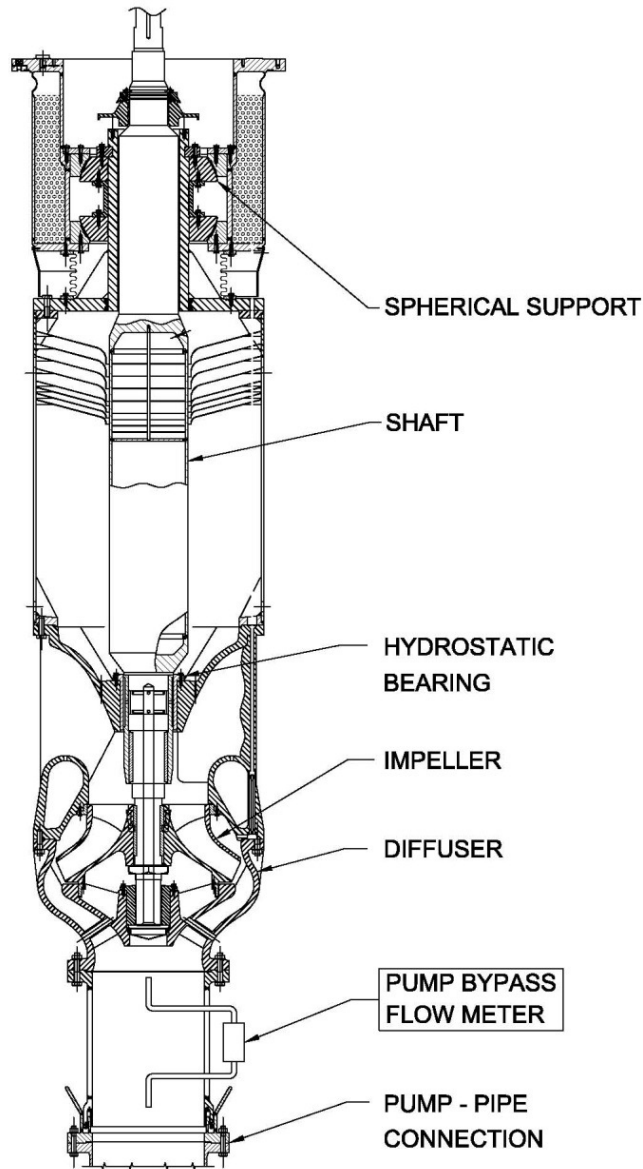


**Fig. 1.7: Bypass flow meter at primary pump discharge of BN 600 [18]**

In EBR II reactor, flow meters working on venturi tube principles and electromagnetic principles were provided on the pump discharge lines and core outlet lines [7]. In PFR reactor, probe type eddy current flow meters were used in the pump discharge ducts [15]. Figure 1.8 is the schematic of the same. ECFM provided in the pipe between pump discharge and core inlet plenum measures the velocity in the pipeline from which the core flow is estimated.

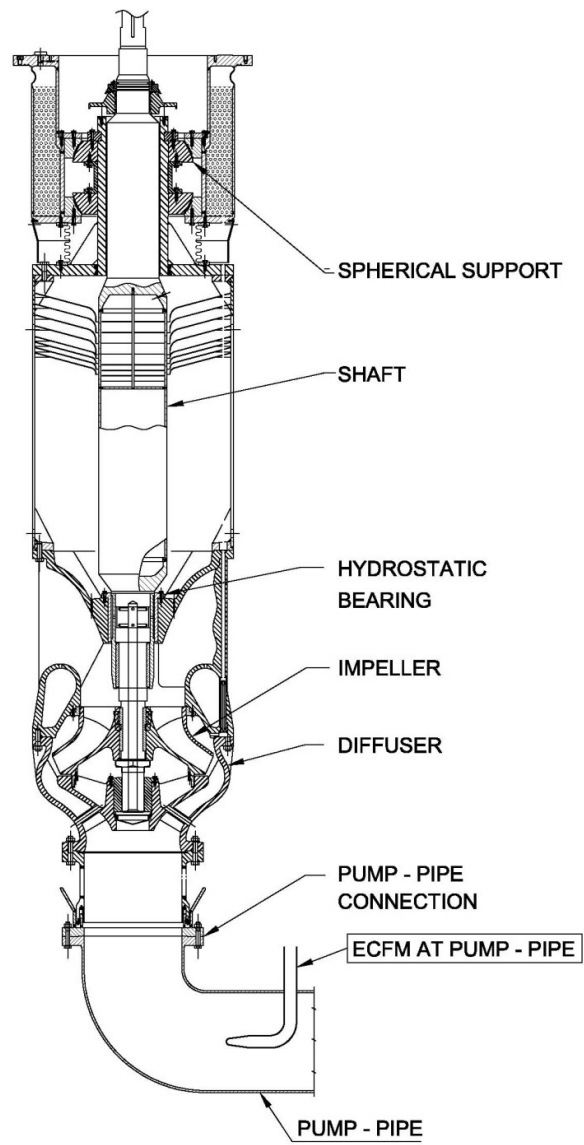


**Fig. 1.8: Eddy current type flow meter at pump discharge pipe in PFR [15]**

**Table 1.2: Primary sodium flow measurement in pool type reactors**

SL.No	Reactor	Type of flow meter	Nos. and Location
1.	EBR II	a) Electromagnetic	5 Nos. (Pump discharge lines + core outlet line)
		b) Venturi tube type	5 Nos. (Pump discharge lines + core outlet line)
		c) Ultrasonic (later addition)	4 Nos. in pump discharge lines (For testing)
		d) Differential pressure type (later addition)	1 No. Core outlet
2.	Phenix	a) Bypass type PM flow meter	1 No. at each pump discharge
3.		b) Pressure transducer	1 No. at each pump discharge
4.	PFR	Probe type Eddy current flow meter	1 No. at each pump discharge
5.	SPX-1	Bypass PM flow meter	1 No. at each pump discharge
6.	CDFR	Probe type Eddy current flow meters	At pump discharge
7.	BN-600	Bypass PM flow meters	4 Nos. In the core bypass line brought out of RV
8.	BN- 800	Bypass PM flow meters	At pump discharge
9.	EFR	a) Eddy current flow meter	Not known
		b) Ultrasonic flow meter	

In CDFR, probe type eddy current flow meters were proposed at pump discharge ducts [7, 21]. In EFR reactor it was proposed to provide probe type eddy current flow meters and ultrasonic flow meters for primary circuit flow monitoring [22]. In USA, EPRI had conducted detailed studies on design of large pool type fast reactors of 1000 MWe capacity. M/s. Rockwell International and M/s. Bechtel Corporation have proposed bypass type PM flow meters at pump discharge and on core bypass line [23]. The flow meters at pump discharge are removable with the pump. The core bypass line originating from the core inlet plenum is to be routed out of reactor vessel and flow meters have to be located in the deck structure. The report submitted by M/s. General Electric Company has proposed flow

measurements by static pressure measurements at reactor inlet plenum and reactor outlet plenum [24]. M/s. General Electric has also proposed that flow through the reactor could be computed from the pump speed, pump outlet pressure, reactor pressure drop and eddy current probes at core outlets [25].

### 1.8.2 Flow measurement in SFR circuits

In loop type of reactor, the core flow has to be measured by measuring flow in the double wall primary system piping. In pool type and loop type concepts, flow in the large single wall pipes of secondary circuit also has to be measured. Auxiliary circuits of primary system need double wall flow meters whereas auxiliary circuits of secondary system need single wall flow meters. Table 1.4 gives the methods used for flow measurement in circuits of different reactors [7, 26, 27].

**Table 1.3: Sodium flow measurement in reactor circuits**

Sl.No	Reactor	Country	Type of flow Meter	Type of reactor
1.	Rapsodie	France	EM & PMFM	Loop
2.	Phenix	France	PMFM on bypass line	Pool
3.	Super Phenix	France	PMFM on bypass line	Pool
4.	PFR	UK	Saddle coil EM flow meter	Pool
5.	CFR	UK	Saddle coil EM flow meter	Pool
6.	KNK	FRG	PMFM	Loop
7.	SNR 300	FRG	PMFM	Loop
8.	Joyo	Japan	Saddle coil EM flow meter	Loop
9.	Monju	Japan	PMFM	Loop
10.	FFTF	US	PMFM	Loop
11.	BN350	Russia	EM & PMFM	Loop
12.	BN800	Russia	PMFM	Pool

International development and production units and laboratories such as ANL, Westinghouse, GAAA, GEC, PNC and INTERATOM have studied

various types of flow measurement techniques for large diameter pipelines. Most of these studies conclude with a need for focused effort towards development of permanent magnet flow meters.

Detailed study on flow measurement methods adopted in FBTR is required to understand the difficulties faced and experience gained. In depth study on sodium flow measurement techniques followed in PFBR, which is in an advanced stage of construction is essential to understand the associated challenges which are to be met, to ensure operating and safety requirements. Moreover, the improvements, new designs and the methods developed as part of this research would find application in future reactors which in an advanced stage of design.

### **1.9 Sodium Flow Measurement in FBTR**

FBTR is a loop type reactor which is in operation at IGCAR Kalpakkam since 1985. FBTR lay out with sodium flow meters is shown in Fig. 1.9 [3]. Permanent magnet type EM flow meters are used for flow measurement in FBTR both in primary and secondary circuits. There are 31 flow meters for pipe sizes ranging from 15 NB to 200 NB. The permanent magnet material used is Ticonel-E which is equivalent to Alnico-V. Primary main circuit is made up of 200 NB double wall pipe. The size of the inner pipe is 200 NB and the size of the outer pipe is 250 NB. Two permanent magnet flow meters each with three pairs of electrodes are provided at the reactor inlet line for core flow measurement. Two flow meters are provided for achieving redundancy. The auxiliary primary circuit such as purification system is also made up of double wall pipes and double wall flow meters are provided in these lines. Main secondary line is provided with 200 NB single wall permanent magnet flow meter. The main primary and secondary pipeline flow meters are calibrated up to a flow rate of 180 m<sup>3</sup>/h to an accuracy of  $\pm 3\%$ . Flow meters of sizes ranging from 80 NB to 15 NB are used in primary and secondary auxiliary circuits and are calibrated to an accuracy of  $\pm 3\%$  over their full range, before their installation in the reactor circuits. The performance of these flow meters is found to be satisfactory.

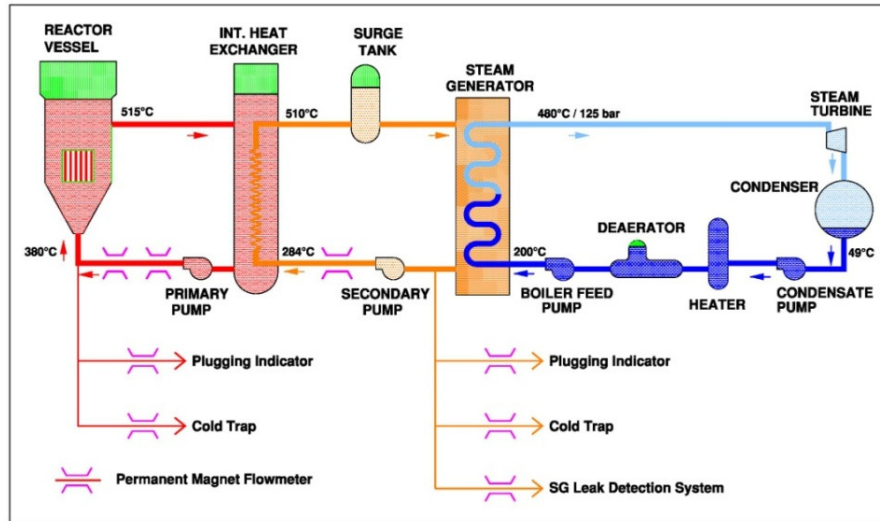


Fig. 1.9: FBTR lay out with sodium flow meters [3]

### 1.10 Sodium Flow Measurement in PFBR

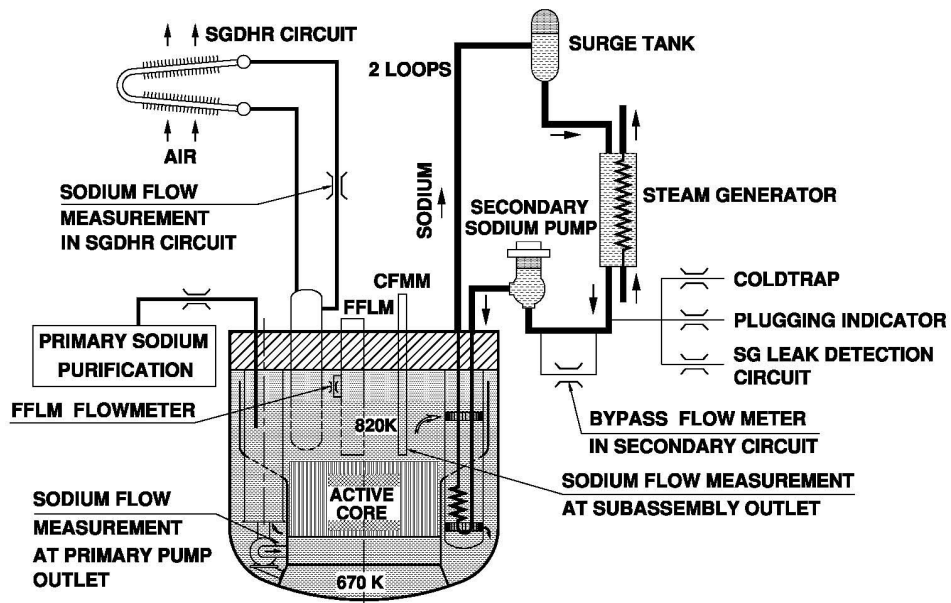


Fig. 1.10: PFBR layout with sodium flow meters

PFBR is a pool type reactor which is in an advanced stage of construction at Kalpakkam, India. Figure 1.10 shows the layout of PFBR with locations of sodium flow meters. The requirements of PFBR are met basically with

two type of flow meters, ECFM and PMFM. These primary flow meters are configured suitably to meet all the requirements.

### 1.10.1 Primary pump flow measurement

Schematic of the ECFM configuration in Primary Sodium Pump (PSP) of PFBR is shown in Fig. 1.11. In PFBR, two vertical primary sodium pumps are used to circulate sodium through the reactor core. The pump outlet is connected to a spherical header. Two discharge lines from the spherical header are connected to the plenum below grid plate, as shown in Fig. 1.11. Sodium flow through the core is measured at the PSP using ECFM, located in a bypass line from the pump discharge to suction. Each pump is provided with two probes and each probe has two ECFM sensors of 14 mm diameter. Overall length of the probe is 9.3 m but the length of the sensor region is only 200 mm. Long length facilitates the installation and removal of the probe from the reactor top. A magnetic shield is used around ECFM to avoid the influence of external flow. Figure 1.12 shows the ECFM sensor made for PFBR pump.

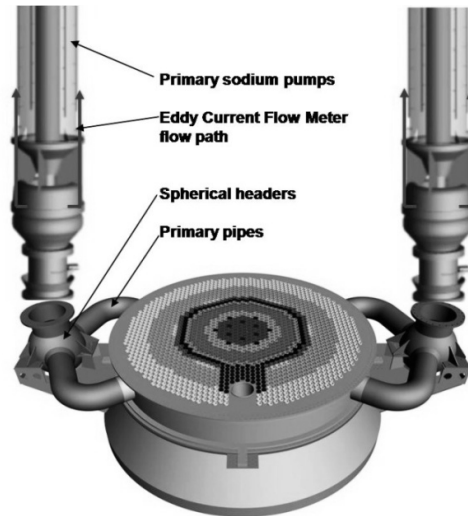


**Fig. 1.11: Schematic of ECFM in primary pumps**



**Fig. 1.12: ECFM sensor made for PFBR primay sodium pump**

### 1.10.2 Subassembly flow measurement

In-core flow measurement before every start-up of the reactor is oriented to ensure that each subassembly receives the required flow, as reduction in sodium flow results in decrease of heat removal from the core of the reactor [28]. This measurement is done by Core Flow Monitoring Mechanisms (CFMM-1 & 2) with ECFM sensors. The CFMM-1 mounted on central canal will be used for fuel subassembly flow measurement and CFMM-2 mounted on observatory canal will be used to measure blanket and storage subassembly flows. The sensors are calibrated in sodium at different temperatures and at different flow rates covering the operating range. During the flow measurement in the reactor, CFMM will be made to seat on the subassembly head as shown in Fig. 1.13 and flow passing around the sensor will be measured by ECFM sensor. Extensive modeling and experimental studies are carried out to assess the leakage flow at the CFMM seat on the subassembly top.

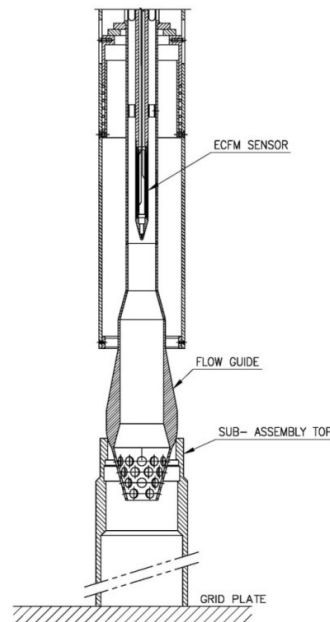


**Fig. 1.13: CFMM seating on subassembly top during flow measurement in reactor**

### 1.10.3 Flow measurement in single wall pipelines

Conventional PMFM with Alnico-V based magnet assemblies are used for flow measurement in PFBR from 15 NB to 200 NB pipe size. Magnet blocks of C shape, U shape and rectangular blocks are used for manufacturing the assemblies for pipe sizes upto 80 NB. For flow meters above 80 NB size, C shaped magnet structure with two parallel magnetic circuits is selected. Two parallel magnetic circuits are required to get the adequate flux density. The pipes of PMFM are of SS316LN, meeting the specification of PFBR pipes. SS sheathed MgO insulated cable is used as electrode. The electrode conductor is made of same material as the pipe to minimize thermal EMF. Flow meters are covered with nonmagnetic SS perforated sheets for ventilation. Thermal insulation is provided between the pipe support and magnet to limit the temperature of magnet during operation. All the assemblies are provided with a reference point near the pole face center to monitor the flux density during service. There are 61 single wall flow meters in PFBR in 12 different pipe sizes. The largest single wall flow meter is of 200 mm size (Fig. 1.14)

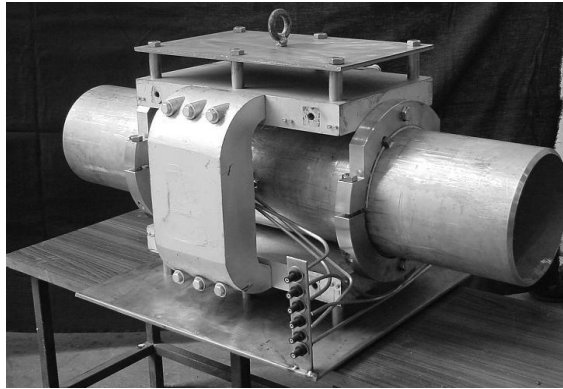


**Fig. 1.14: 200 NB pipe permanent magnet flow meter**

### 1.10.4 Flow measurement in FFLM

Three numbers of Failed Fuel Localization Modules (FFLM) are provided in PFBR to identify the fuel subassembly with failed fuel clad. These modules, suck sodium from each subassembly outlet one by one, using a sodium

submersible DC conduction type electromagnetic pump and circulates through the delayed neutron detector. Sodium flow through the FFLM has to be measured to confirm the performance of the system. A compact special PMFM is developed and manufactured for this application. Small duct of size 10 mm OD/8 mm ID, high ambient temperature of 465 °C, operating in sodium mist atmosphere, two pairs of electrodes and long electrode cable of 3 m length are the specialties of the FFLM flow meter. The magnet assembly is made with a single C shape magnet. The magnet is magnetized, electrically and thermally stabilized at 500°C. The magnet is subjected to endurance test at 465 °C for 10000 hrs and it is confirmed that magnetic flux density is stable at the operating conditions. Sensitivity of the flow meter is estimated to be 11.5 mV/m<sup>3</sup>/h. Figure 1.15 is the photograph of FFLM flow meter assembly with 3 m long electrode cable.

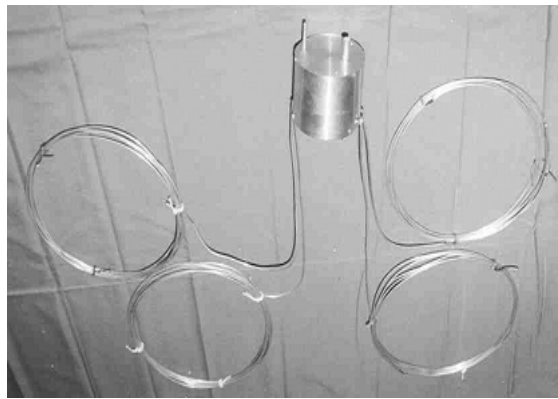


**Fig. 1.15: FFLM flow meter with 3m long electrode cable**

#### **1.10.5 Flow measurement in double wall pipes**

A stream of the primary radioactive sodium is taken out of the reactor vessel for purification and is returned to the reactor vessel through double wall piping. Double wall PMFMs are used for flow measurement in these circuits. The flow meter consists of two concentric pipes, magnet assembly, electrodes and supporting mechanisms. The outer pipe is fabricated in two halves. The magnet assembly is placed over the outer pipe assembly. One end of the inner pipe has fixed support with outer pipe and the other end has a sliding support. The inner pipe carries sodium at 550 °C, whereas the annular space between the inner pipe and

the outer pipe contains nitrogen at relatively lower temperature. Arrangement for supporting the outer and inner pipes, accommodating the differential thermal expansion between them and retaining them as an integral part are the challenges involved in design and development of the double wall flow meters. Three pairs of electrodes are welded to the inner pipe, routed through the annular space penetrating the outer pipe to reach the terminal box. Figure 1.16 is the schematic with details of the inner pipe, outer pipe, supporting arrangement and the electrode routing of double wall flow meters. The electrodes are mineral insulated, SS sheathed, SS conductor cable of 4 mm outer diameter. Photograph of a typical double wall PM flow meter for pipe size 100 NB is depicted in Fig. 1.17.

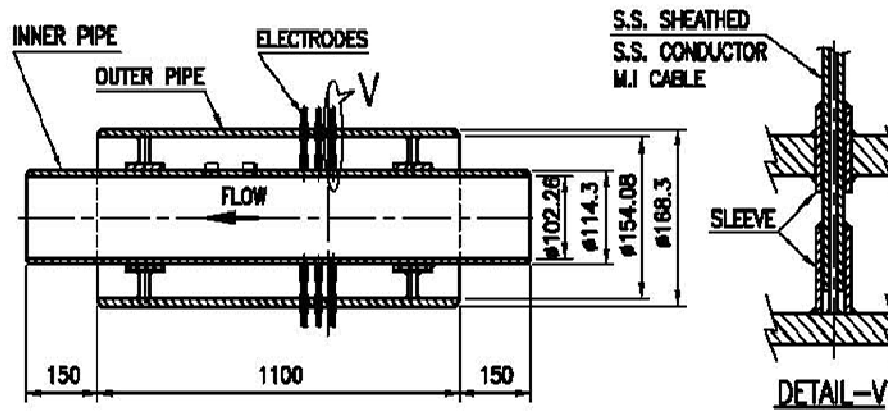


**Fig. 1.16: Details of inner and outer pipe of double wall PM flow meter**

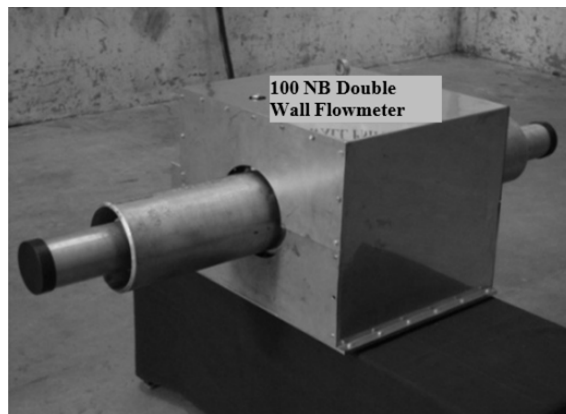


**Fig. 1.17: 100 NB size double wall PM flow meter**

### 1.10.6 Flow measurement in PFBR secondary main circuit

In PFBR secondary main circuit, the largest pipe in which sodium flow is to be measured is of 800 NB and flow in this pipe is measured by means of a bypass flow meter at the secondary pump suction line. A conventional PMFM is used for measuring the flow in the bypass circuit. This flow meter is installed in the vertical suction line of the secondary pump (Fig. 1.18). Main flow can be estimated from the previously determined ratio of main flow to bypass flow. Rated flow in the pump suction line is of the order of  $12700 \text{ m}^3/\text{h}$ . The velocity head available in the main line enables circulation of a flow in the bypass circuit. The rate of bypass flow to main flow was found to be a function of flow rate.

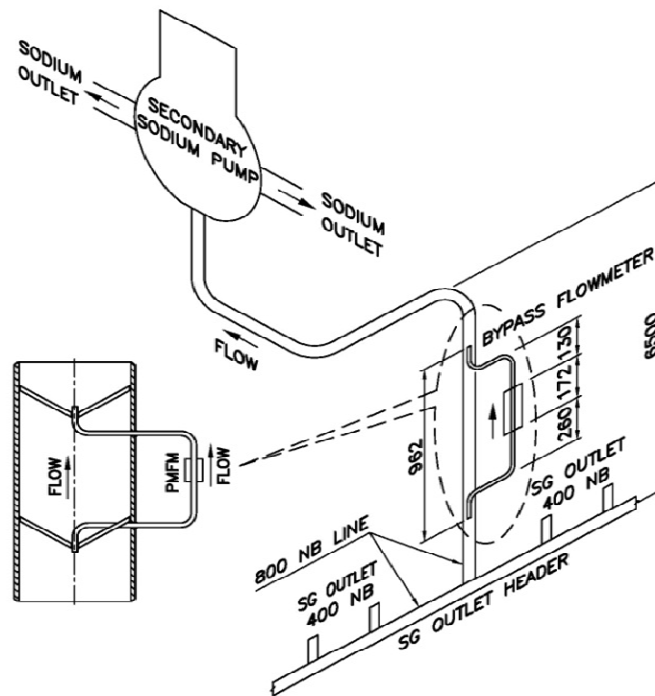


**Fig. 1.18: Bypass flow meter arrangement at PFBR secondary pump suction line**

Based on the literature survey, areas for further experimental and theoretical investigations, including modeling, application of advanced materials, implementation of innovative designs and techniques and optimization of the existing designs are identified as detailed in the next paragraph.

## 1.11 Advancements in Sodium Flow Measurement

The scheme for the measurement of sodium flow in pipelines using electromagnetic flow meters has been established and they have also been put to use for reactor applications. However, the following are a few of the problems currently faced in the pipeline flow meters.

- a) The ability of the Alnico-V magnet assembly to provide stable field is not known
- b) They are bulky and heavy for large size pipes
- c) Their sensitivity is relatively low for large size pipes
- d) Sodium calibration of permanent magnet flow meter (PMFM) is costly and time consuming
- e) Conventional PMFMs are not suitable for large pipe sizes

Improvements are required in sodium flow measurement methods in pipelines to achieve compactness, high sensitivity, better accuracy, stability and economy and they form the objective/goal of the present work.

The weight and sensitivity of the flow meters for single wall (SW) and double wall (DW) pipe sizes varying from 15 nominal bore (NB) to 200 nominal bore (NB), with Alnico-V permanent magnet assembly are given in Table 1.1. From the table, it is clear that the weight of large pipe size (100 NB and above) flow meters are very high and their sensitivity is relatively low.

Cast Alnico-V is currently used in PMFMs due to their superior magnetic properties. From Table 1.1, it is also clear that the flow meter with Alnico-V permanent magnet assembly can be used for smaller pipes (below 100 NB) with relatively low weight, compactness and adequate sensitivity. However, capability of the magnet assembly to provide stable magnetic field at the operating environment over the design life has to be established. The sodium calibration method followed today for accurate sensitivity determination is costly and time

consuming. Modeling and simulation of flow meters to predict the sensitivity and its experimental validation would be a major advancement in this area of work.

**Table 1.4: Weight and sensitivity of flow meters with Alnico-V magnet assembly**

S. No	Title of Flow meter	Total assembly weight (kg)	Sensitivity (mV/m <sup>3</sup> /h)
1	15 NB	14.1	11
2	20 NB	14.5	2.5
3	32 NB	28.6	0.8
4	50 NB	41.3	0.5
5	100 NB Single wall	109.6	0.14
6	100 NB Double wall	255.5	0.174
7	200 NB Single wall	289.1	0.066

The present research is focused to address specific problems currently faced with pipeline flow meters in various circuits of SFR. In addition, advancements and improvements are aimed in design configuration, modeling, analysis and calibration. Alternative methods are developed for flow measurement in large size pipelines. For large pipes, higher weight of the Alnico-V based flow meters is due to usage of large volume of magnetic material along with larger pole face and connecting pieces made of mild steel. PMFM with suitable high energy rare-earth magnets such as Samarium-Cobalt based magnets will provide high magnetic flux density and make the flow meter more sensitive and compact. For large sodium pipes, it is also desirable to develop redundant and diverse flow measurement techniques. Side wall type PMFM is an alternative. For main secondary pipelines, conventional permanent magnet flow meters become inaccurate as the minimum upstream and downstream straight length requirement is difficult to achieve. The bypass flow meter which is in use currently needs optimization to reduce the flow ratio and to get better resolution and accuracy in the flow measurement. Techniques for in-situ calibration of flow meters by noise analysis techniques such as cross correlation will be very useful to confirm consistency

and repeatability of flow meter sensitivity during operation. Hence, these studies have been taken up in this thesis.

The following are the key areas, where research work of the thesis is focused:

- a) Studies on Alnico-V based pipeline flow meters, factors affecting the sensitivity, establishing sodium calibration method and error estimation for the sensitivity determined by calibration method.
- b) Development of in-situ calibration techniques by cross correlation of noise signals from different pairs of electrodes of the same flow meter
- c) Studies on loss of magnetism, stabilization of magnet assemblies of PMFM and stability studies at accelerated conditions.
- d) Analysis, design and development of Samarium Cobalt based PMFM with the objective of compactness and improved sensitivity.
- e) Analysis, design development, and testing of side wall type permanent magnet flow meter for sodium flow measurement in large pipes.
- f) Modeling, design, optimization and validation of bypass flow meters to improve accuracy and resolution specifically for the main secondary circuit flow measurement.

## **1.12 Thesis Organization**

Chapter 2 of the thesis covers the studies carried out on Alnico-V based permanent magnet sodium flow meters. The procedure followed for analytical estimation of the sensitivity and various factors affecting the sensitivity are identified. The setup used for sodium calibration, determination of sensitivity and the calibration procedure are highlighted. The methodology followed for calibration

error analysis is described and the calibration error is estimated. In-situ calibration method developed for PMFM is described. Chapter 3 deals with stability studies carried out on a magnet assembly of Alnico-V based PMFM. Chapter 4 contains details of design, development, analysis and experimental investigation carried out on Samarium Cobalt based permanent magnet flow meters. Chapter 5 describes the design and analysis of compact side wall flow meters, their modelling and validation by calibration experiments. Chapter 6 of the thesis deals with the design, analysis and experimental validation of the bypass type flow meter used for PFBR and the optimisation of the bypass flow meter circuit for future SFRs. Chapter 7 summarizes the advancements and improvements made in the area of sodium flow measurement in pipelines in this thesis and highlights of the research findings and scope for future work.

## CHAPTER 2

### ALNICO-V BASED PERMANENT MAGNET FLOW METERS

#### 2.1 Introduction

As part of the research related to this thesis, a permanent magnet flow meter with Alnico-V magnet assembly suitable for 100 NB pipe is designed and manufactured. The sensitivity of the flow meter is estimated analytically and various factors affecting the sensitivity are identified. The flow meter is calibrated in sodium at various flowrates and at various temperatures and sensitivity is estimated. An error analysis is carried out and the accuracy of calibration is determined. The same flow meter is installed in a sodium facility and further, in-situ calibration of the flow meter is carried out by cross-correlation technique. This chapter describes the R & D studies carried out for Alnico-V based permanent magnet flow meters.

#### 2.2 Sodium Flow Measurement

The conductivity of liquid metal is several orders of magnitude higher than that of non-metallic liquid conductors. One immediate result of this is that the operation of AC flow meters may be complicated by the occurrence of the skin effect. The applied AC field, though uniform in the absence of the fluid, would be no longer uniform inside the fluid and might not penetrate. However, from the early days of practical magnetic flow measuring devices, there have been proposals to use AC rather than DC fields. The main incentive for this has been to avoid polarization at the electrodes and stray DC potentials due to thermoelectric and electrochemical effects. In liquid metal EM flow meters, with DC field, there is no tendency towards polarization at the electrodes. High thermal conductivity of liquid precludes large temperature differences that might have caused troubles by generating DC thermoelectric potentials.

It is therefore a common practice to use DC fields for sodium flow meters [5, 29]. If a permanent magnet is used, stabilized power supply for an electromagnet is no longer required. To investigate the performance of permanent magnet flow meters an Alnico-V based flow meter suitable for 100 NB scheduled 40 pipe is designed and manufactured. Based on the earlier experience and literature survey, various design features as indicated in next paragraph are incorporated in the flow meter for achieving better performance. The specifications of the same are given in Table 2.1 [30].

**Table 2.1: Specifications of Alnico-V based 100 NB PMFM**

S.No	Parameter	100 NB PMFM
1.	Type	Permanent Magnet
2.	Flow rate range	0 ~ 105 m <sup>3</sup> /h
3.	Fluid	Sodium
4.	Maximum operating temperature	550 °C
5.	Maximum operating pressure	10 bar
6.	Sensitivity	0.15mV/m <sup>3</sup> /h
7.	Pipe size	100 NB sch. 40
8.	Pipe length	1050 mm
9.	Number of pairs of electrodes	Three
10.	Distance between each electrode pair	15 mm
11.	Mounting	Horizontal
12.	Magnets assembly	Alnico-V, double circuit.

The following are the new features incorporated in the flow meter:

- a) Parallel magnetic circuit is selected to get higher flux density in the air gap and there by higher sensitivity.
- b) Alnico-V is a brittle material which cannot carry much load. Magnet assembly is made with mild steel connecting blocks, mild steel pole faces and SS bolts, which provided adequate mechanical strength.

- c) The electrical and thermal stabilization of the assembly is carried out as per the procedure established as a part of the research work of this thesis.
- d) Sizing of pole faces and air gap is performed to minimize end shunting factor and to provide adequate thermal insulation to minimize the magnet temperature.
- e) Locking studs and groove arrangement are provided on flow meter pipe to prevent axial movement and rotation of the pipe.
- f) Electrode material is selected to be same as that of pipe material to avoid generation of thermal EMF. The size of the electrode is optimized to be 1.5 mm which reduces the averaging effect.
- g) Three pairs of electrodes are provided for redundancy. These electrode pairs helped in understanding the effect of electrode positioning on sensitivity.
- h) Electrode pairs are shifted to downstream side of flow meter by 10 mm to enhance linearity.

### **2.3 Definition of Sensitivity of PMFM**

Sensitivity of a permanent magnet flow meter at a given temperature is defined as the milli volt output it gives when liquid of one  $\text{m}^3/\text{hour}$  is passed through the flow meter pipe. The commonly used unit of sensitivity is  $\text{mV}/\text{m}^3/\text{h}$ . Sensitivity is also expressed in some cases as  $\text{m}^3/\text{h}/\text{mV}$ .

### **2.4 Analytical Estimate of Sensitivity**

For axi-symmetric velocity profile, transverse PMFM voltage signal is independent of velocity distribution/profile. This is true for any shape of duct or channel. SS pipe with circular cross section is chosen in sodium systems due to mechanical reasons. In SFR applications, the flow meters are positioned in regions

far away from bends, valves etc. where flow is fully developed and hence is axi-symmetric.

Calculation of flow meter sensitivity requires an accurate estimation of air gap flux density surrounding electrode area of the flow meter. For this, flux density is measured from many points in the air gap of the magnet assembly where the sodium flowing duct will be positioned and average air gap flux density is estimated. EMF output from the flow meter is calculated by the formula given below [6, 7].

$$E_v = B_g \times d \times v_u \times K_1 \times K_2 \times K_3 \times 10^3 \text{ mV} \quad (2.1)$$

where

- $E_v$  : The motion induced volatge in, mV
- $B_g$  : Average magntic flux density in the pipe corss section, in Tesla
- $d$  : Inner dia meter of pipe at operating temperature, in m
- $v_u$  : Mean velocity of of sodium in pipe at operating temeprature
- $K_1$  : Pipe wall correction factor
- $K_2$  : End effect correction factor
- $K_3$  : Factor which takes into account flux change due to change in temperature of the magnet

#### 2.4.1 Pipe wall correction factor ( $K_1$ )

Conducting walls can short-circuit some part of the output signal of a flow meter. Since the pipe is also a conductor, which does not move with respect to magnetic field provides a parallel conducting path to the generated E.M.F. The equivalent circuit of a PMFM is shown in Fig. 2.1. A circulating current flows through the sodium and pipe. Because of the circulating current, a part of the voltage generated gets dropped in sodium and the remaining part only is available across the SS pipe for measurement. The correction factor denoted by  $K_1$  accounts for this and it is a fraction of voltage available across the pipe [6, 7] given by

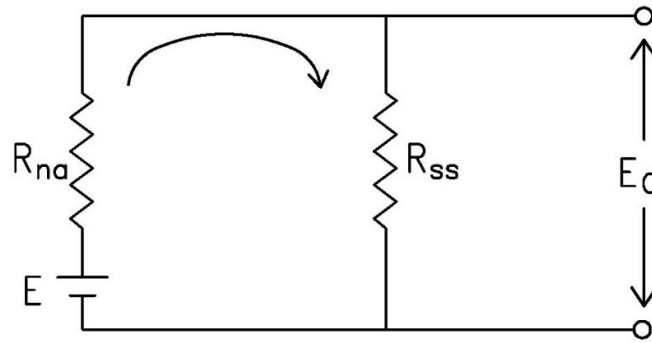


**Fig. 2.1: Electrical equivalent circuit of PMFM**

$$K_1 = \frac{2d/D_o}{\left(1 + \left(d/D_o\right)^2\right) + \left(\rho_f/\rho_w\right)\left(1 - \left(d/D_o\right)^2\right)} \quad (2.2)$$

where

$d$  : inner diameter of pipe

$D_o$  : Outer diameter of pipe

$\rho_f$  : Resistivity of sodium

$\rho_w$  : Resistivity of wall

These values for the 100 NB sch 40 pipe flow meter at 550 °C sodium temperature are

$d$  : 0.1023 m

$D_o$  : 0.1143 m

$\rho_f$  : 19.82  $\mu\Omega$  cm at 350 °C

$\rho_w$  : 96.64  $\mu\Omega$  cm at 350 °C

Substituting the above values in equation (2.2),  $K_1$  is calculated as 0.968. When Sodium temperature increases, pipe wall temperature also increases. The resistivity of both sodium and SS pipe increases with temperature. However, the

ratio of  $\rho_f/\rho_w$  also increases with temperature as the percentage increase of sodium resistivity is high compared to the pipe resistivity. Hence, pipe wall correction factor ( $K_1$ ) reduces with temperature, leading to reduction in sensitivity with increase in temperature. The pipe thickness (pipe ID and pipe OD) also affects the factor  $K_1$  which is also known as pipe shunting effect.

#### 2.4.2 End effect correction factor ( $K_2$ )

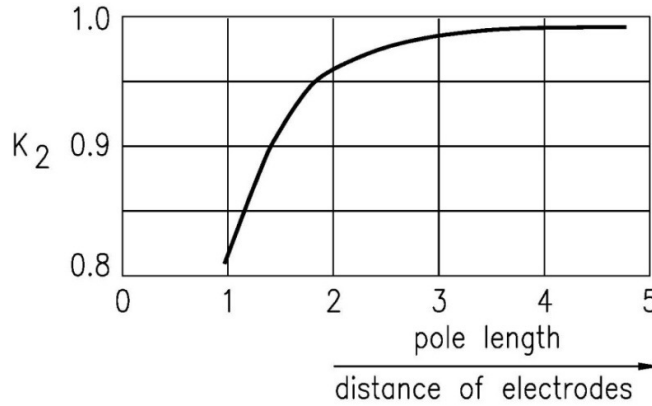


**Fig. 2.2: Factor  $K_2$  versus the ratio of pole face length to pipe ID**

The equation (2.1) is applicable for infinite magnetic field. For any real flow meter, the length of magnetic field is finite and is limited by the length of pole face of the magnet assembly. So, there will be short-circuiting at the ends of the flow meter where the transverse field ends and hence the induced e.m.f. falls to zero. This circulating short circuit current will produce magnetic field which will have cross-magnetizing effect on the imposed magnetic field by permanent magnet assembly. The factor  $K_2$  takes into account the effect of the finite length of pole face. This factor is a function of pole face length to pipe internal diameter ratio. This ratio versus correction factor is plotted in Fig. 2.2 [7].

$$K_2 = f(\text{pole face length/distance between electrodes})$$

The distance between electrodes is the pipe inner diameter and for the 100 NB sch 40 pipe flow meter Pole face length is 0.2 m, pipe ID is 0.1023 m. Hence the ratio is calculated as 1.955.

Correction factor ( $K_2$ ) corresponding to the above ratio (from Fig. 2.2) is 0.96. From Fig. 2.2, it can be seen that the effect can be made negligible if the pole face length is made three times more than pipe ID.

This factor is also called end shunting factor and it depends on sodium velocity and sodium resistivity. When the flow increases, the induced motional voltage increases, and induced currents at the end of the pole face increase, which leads to higher distortion on imposed magnetic causing reduction in sensitivity. At a particular flow rate, if the sodium temperature increases, resistivity increases and the induced currents reduce. This leads to lower distortion of the imposed magnetic field causing increase in sensitivity.

### **2.4.3 Factor which takes into account flux change due to temperature ( $K_3$ )**

When the temperature of the magnet increases, the flux density comes down. For Alnico-V magnet assembly,

$$K_3 = 1 - (T_m - 30) \times 0.0003 \quad (2.3)$$

where the factor 0.0003 is the temperature coefficient of flux density for Alnico-V which is available in the MMPA standard [31].

So the value of  $K_3$  for the flow meter has been calculated as 0.979 for 100 °C magnet temperature. Sodium pipe is thermally insulated and thermal insulation is also provided between the pipe and the flange which is used for fixing the pipe on the magnet assembly. The magnet assembly is exposed to ambient air and the flow meter cover plate is provided with perforations to enhance natural cooling. When the sodium temperature is at 550 °C, the magnet temperature is well below 100 °C. This is based on measurements made during operation of flow meters with sodium temperature at 550 °C. The temperature of the magnet can be monitored and exact correction can be applied.

#### 2.4.4 Correction on pipe diameter

The pipe internal diameter has to be measured at different points circumferentially and average value has to be taken for sensitivity estimate. Depending on the temperature of operation, the pipe internal diameter will increase and the velocity per unit flow also will change. Suitable correction is applied to take this into consideration.

#### 2.4.5 Average flux density estimate

The flux density has been measured at many points in the air gap of the magnet assembly where the sodium flowing pipe will be positioned and average air gap flux density is used for sensitivity estimation. Hall probe type Gauss meter has been used for flux density measurement. The accuracy of the instrument used is better than  $\pm 1\%$ . A zero chamber made of magnetic shielding material was used for setting zero of the measuring instrument along with a and a reference magnet for checking the correctness of the reading.

Average flux density in the air gap of the magnet assembly which interacts with flowing sodium to produce milli volt output has been measured for the magnet assembly. Flux density readings were taken at 25 different points as indicated in Fig. 2.3 in three XY planes. Readings were averaged to get the mean air gap flux density.

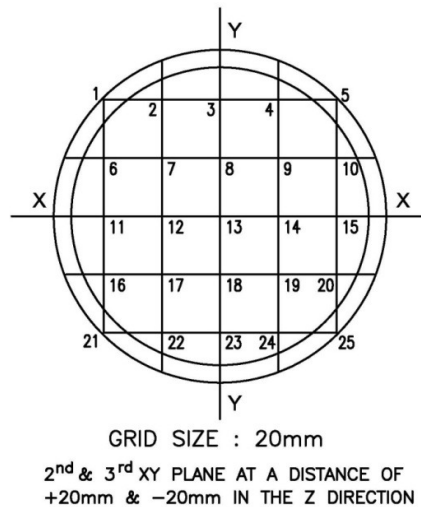


**Fig. 2.3: Grid locations for flux density measurement**

#### 2.4.6 Estimation of sensitivity

EMF output from the flow meter is given by the formula (2.1)

$$E_v = B_g \times d \times v_u \times K_1 \times K_2 \times K_3 \times 10^3 \text{ mV}$$

where  $B_g$  : 0.0495 Tesla; average value of 100 NB pipe flow meter assembly

$d$  : 0.1023 m, pipe ID for 100 NB pipe, to be corrected for operating temperature

$Q$  : 1 m<sup>3</sup>/s, unit flow

$A$  :  $\pi d^2/4$  ;  $d=0.1023$ , and to be corrected for operating temperature

: 8.219 x 10<sup>-3</sup> m<sup>2</sup>

$v_u$  :  $Q/\text{Area of cross section}$

: 0.0338 m/s

$K_1$  : 0.968

$K_2$  : 0.96

$K_3$  : 0.979

Substituting the above values in equation (2.1), E.M.F. output of the flow meter has been estimated as 0.1557 mV/m<sup>3</sup>/h. The voltage output at rated flow of 105 m<sup>3</sup>/h flow is 16.34 mV.

### 2.5 Factors Affecting Sensitivity of PMFM

As part of the research work a detailed study on the factors affecting sensitivity of PMFM has been carried out.

#### 2.5.1 Magnet and sodium temperature

As mentioned in sections 2.4.1 to 2.4.4, magnet temperature and sodium temperature affect the sensitivity of the flow meter.  $K_1$  and  $K_3$  vary with temperature.  $K_2$  compensates the effect of limited length of the magnetic field. For a

given length of the magnetic field, sodium temperature variation changes the end shunting effect, which is not accounted for in the factor  $K_2$ .

### **2.5.2 Velocity profile in pipe**

The sensitivity estimation by equation (2.1) is based on uniform average velocity in the pipe, However, the actual velocity profile will be different at various flow rates. Velocity profile is parabolic in laminar flow regime but close to rectangular when the flow is in turbulent region. This velocity distribution has an effect on the motion induced voltage. However, if the velocity profile is axially symmetric, considering the average velocity for sensitivity estimate is reported to be accurate [12].

### **2.5.3 Non uniform magnetic field in the pipe**

The sensitivity estimation by equation (2.1) assumes uniform magnetic flux density in the flowing pipe of the flow meter. But the actual magnetic flux density is non uniform with higher values near the pole face of the magnet assembly. This leads to an error in the analytical method of sensitivity estimation.

### **2.5.4 Magnetic effects**

A dimensionless group  $\mu\sigma vd$  is defined as magnetic Reynolds number  $R_m$ , where

$\mu$  : Permeability of sodium

$\sigma$  : Electrically conductivity of sodium

$v$  : velocity of sodium

$d$  : Inner diameter of pipe

$R_m$ , measures the severity of the perturbation of the imposed field by the induced currents. For large sodium flow meters, as the imposed field is low, distortion of the imposed field may indeed be appreciable [14].

### **2.5.5 External magnetic field and exclusion zone**

The magnetic field produced by the permanent magnet assembly should remain constant to provide same sensitivity for the flow meters. An external magnetic field or a magnetic material near the magnet assembly changes the magnetic flux density. External magnetic field affects the air gap flux density. Magnetic materials will provide a bypass path for the flux and reduce the flux density in the flow meter pipe section. Hence, care has been taken while installing the flow meter such that no magnetic material is present close to the flow meter. The presence of magnetic materials within 5 times the air gap length of magnet assembly has been completely avoided.

### **2.5.6 Wetting of pipes**

Passivated stainless steel pipe internal surface will have chromium oxide layer initially. The liquid sodium at low temperature will not wet the stainless steel pipe and the contact electrical resistance will be high. This high resistance will partially block the output voltage and the sensitivity can be low during the initial period of flow meter operation at low temperatures. By increasing the temperature to 350 to 400 °C and by purifying the sodium by continuous cold trapping, the oxide layer gets dissolved in sodium, and good electrical contact gets established ensuring wetting. Once wet, the pipe will remain wet even after lowering the temperature. High surface tension of the liquid sodium at low temperature also is a factor which avoids wetting of stainless steel pipe [7].

### **2.5.7 Orientation of the pipe**

The pipe electrode axis was made perpendicular to the flow direction and the magnetic field direction. A provision was made in the assembly and maintain the position under all conditions of operation. This was achieved by providing two locking studs on pipe and a matching slot on the fixing flange, as shown in Fig. 2.4. This arrangement avoids rotation and axial movement of the pipe with respect to its axis.

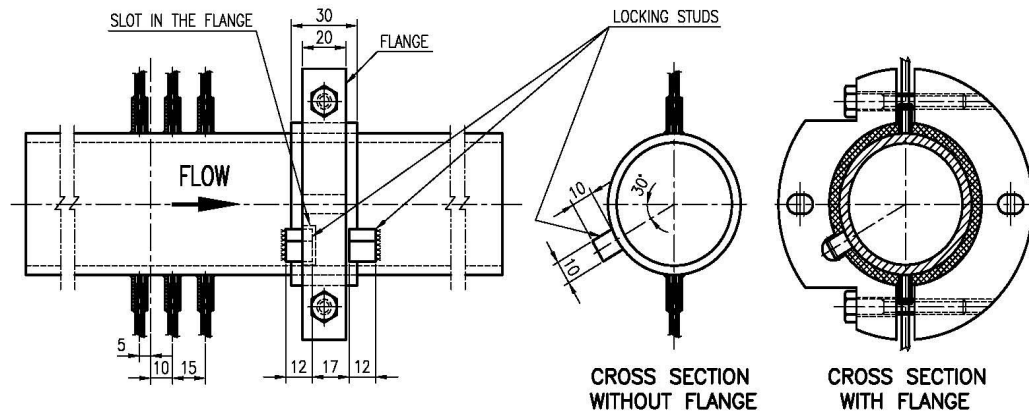


**Fig. 2.4: Locking stud and slot arrangement for flow meter**

### 2.5.8 Flow meter electrodes

Multiple pairs of electrodes are provided for the flow meters to achieve redundancy in measurement. When flow increases, the induced voltage produces circulating currents at both sides of the magnetic field, as shown in Fig. 2.5a. The amplitude of magnetic field provided by the magnet assembly without sodium flow in the pipe is shown in dotted lines in Fig. 2.5b. This field produced by the circulating current has demagnetizing effect on the upstream side and a magnetizing effect on the downstream side. Due to this, when flow increases, the resultant effect is that the magnetic field gets shifted from pole face centre to downstream direction, as shown by continuous line in Fig. 2.5b. Hence, the magnetic flux density in the vicinity of upstream electrode pair reduces but the same in the downstream electrodes pair does not get affected. To achieve linearity with respect to flow, it is essential to shift all pairs of electrodes in the downstream direction with respect to pole face centre. Hence, for the 100 NB PMFM, three pairs of electrodes are provided and the electrode axis is shifted by 10 mm downstream with respect to the pole face centre, as shown in Fig. 2.6. This arrangement improves the linearity for the flow meter with respect to flow.

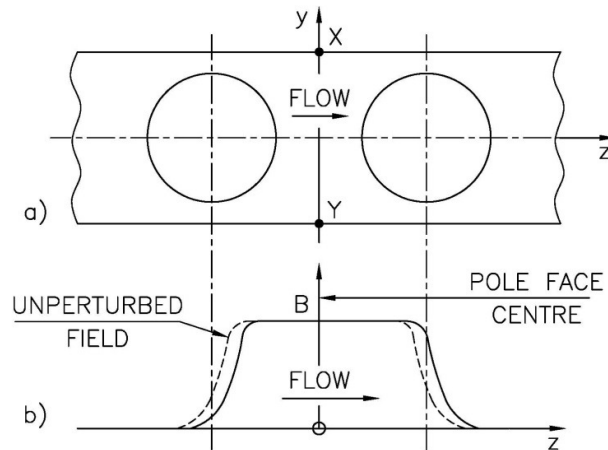


**Fig. 2.5: Magnetic field shift due to end shunting effect**

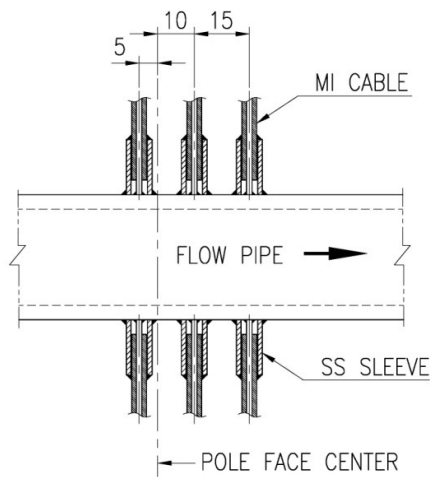


**Fig. 2.6: Electrode spacing in 100 NB PMFM**

Electrodes should be of the same material as that of the pipe to avoid thermal EMF. The electrode size should be as small as possible but should be able to be welded to the pipe. Large size electrode will average out the output voltage in the contact region. SS sheathed mineral insulated SS conductor is used as electrode cable. The 316 LN SS is the conductor and sheath material for reactor applications. The diameter of the cable is of 4 mm with conductor of diameter 1.5 mm. The conductor will be welded to the pipe and for mechanical strength, a sleeve is introduced and welded to the pipe and cable sheath, as shown in Fig. 2.7.

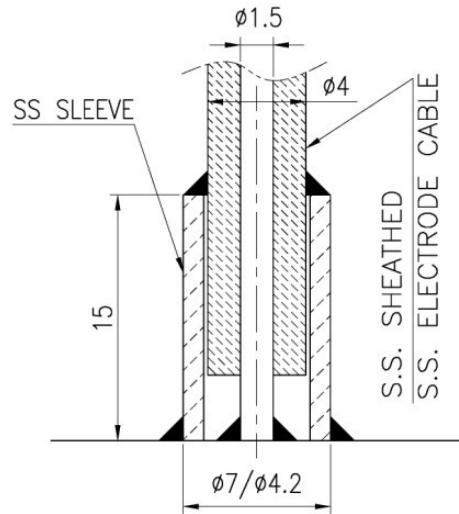


**Fig. 2.7: Electrode welding details on pipe**

### **2.5.9 Sodium purity**

Purity level of sodium in SFR circuits will be 99.95% during normal operating conditions. Presence of ppm level of non metallic impurities such as oxygen and hydrogen does not affect the overall conductivity of sodium and hence, performance of the flow meter is not affected by normal range of impurities in sodium. The effect of dissolved conducting metallic impurities will also be negligible as they are limited to ppm level.

### **2.5.10 Upstream and downstream straight pipe requirement**

The sensitivity of the flow meter depends on the average velocity of sodium in the pipe. However, this is applicable only when the velocity profile is axially symmetric. Presence of bends, valves and other devices causing change in hydraulic characteristic of the system can alter the velocity profile. This can cause serious error in flow measurement, and in some cases even up to 100%. To avoid such errors, straight distances of five times the internal diameter of the pipe on the upstream side and two times the internal diameter of the pipe on the downstream side of the flow meter have been provided.

## 2.6 Response Time of PMFM

Magnetic flow meters will have potentially the fastest response in comparison to any other type flow meter because of their direct electrical sensing of fluid velocity. No experimental attempt has been made so far to measure response time of a permanent magnet flow meter since it is generally agreed that the sensors which would be required to make such measurements, would have higher response time than that of a PMFM. An indication of rapid response of the PMFM is the high frequency content of the output signal. A theoretical study conducted by Miyazawa [32] shows that the response time of a PMFM is proportional to  $\mu\sigma D_o^2$ , where

$\mu$  : permeability of sodium

$\sigma$  : conductivity of sodium

$D_o$  : pipe outer diameter

Response time of a 300 mm saddle coil flow meter is estimated as 35 millisecond at 230°C. This indicates that the response time of 100 NB PMFM will be of the order of 4 milliseconds.

## 2.7 Calibration of 100 NB PMFM for Liquid Sodium Flow

To determine the actual sensitivity of the 100 NB PMFM, sodium calibration of flow meter has been carried out in a sodium facility [33].

### 2.7.1 Calibration Setup

Calibration set up consists of a sodium vessel (SV) of known volume located at a high elevation and a sodium storage tank (SST) positioned at a lower elevation. The sodium vessel is connected to the sodium storage tank by a 100 NB pipeline with a flow control valve. Sodium flow in the pipe was achieved by gravity draining of sodium from SV to SST. Calibration of the Alnico-V based PMFM has been carried out by absolute constant volume method [34-36]. The total sodium hold up in the storage tanks is 40 tonnes. The volume of the sodium vessel up to high level, which is used for flow meter calibration purpose is 15.454

m<sup>3</sup> at room temperature. The PMFM was installed in the line between vessel and storage tank to calibrate it in sodium. Details of the calibration set up is given in Fig. 2.8. Installation of the PMFM at this location of pipeline, provides more than 10 D and 5 D straight lengths at upstream and downstream of the flow meter respectively. When the flow control valve in the line is opened, sodium in the sodium vessel flows to the sodium storage tank by gravity. The sodium flow was gradually reduced due to head reduction during sodium draining and reduction in the flow due to head variation was around 20%.

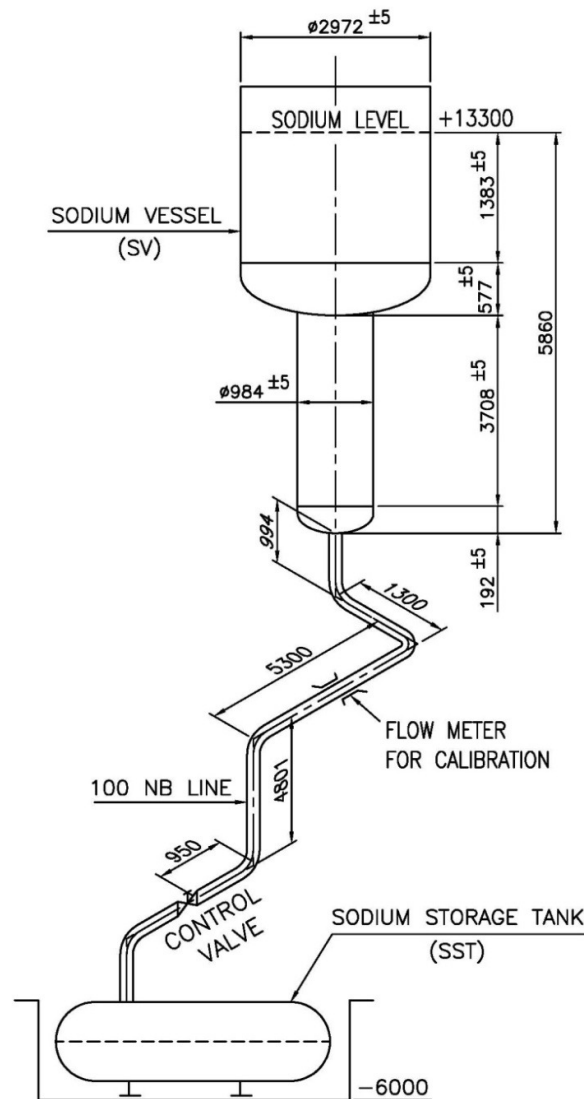


**Fig. 2.8: Details of PMFM calibration set up**

A data acquisition system with an HP make data logger and a personal computer (PC) with a suitable software was used for acquiring data during calibration. The three pairs of electrodes of flow meter were connected to three channels of the data acquisition system. The data acquisition system is such that it reads milli volt output from PMFM electrodes using the software. The scan interval of each channel is set as one second. While draining sodium from the sodium vessel to the sodium storage tank, milli volt output from all the three pairs of electrodes were acquired at every second and stored in the PC. The schematic of the calibration set up is shown in Fig. 2.9.

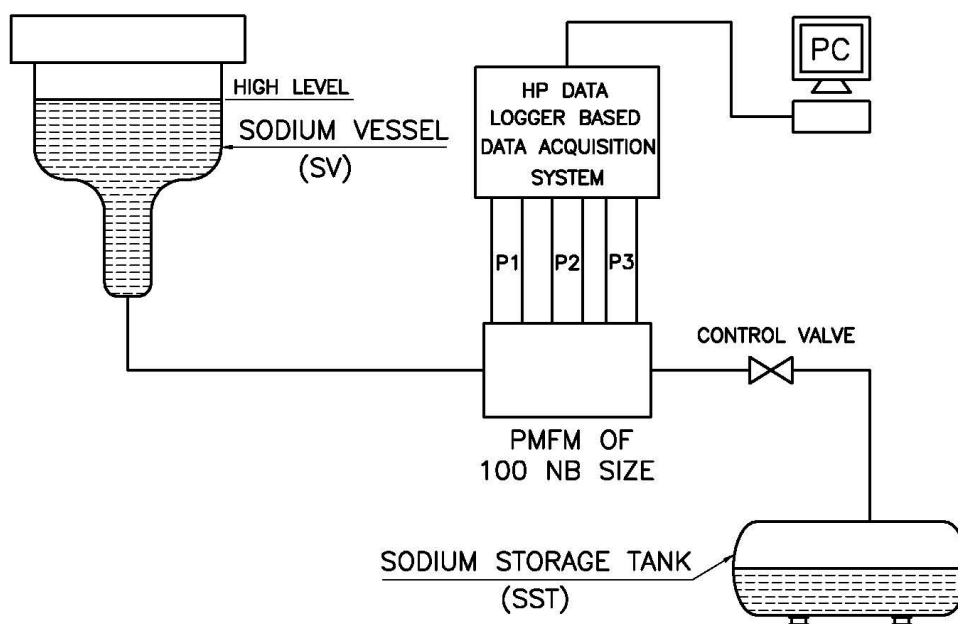


**Fig. 2.9: Schematic of PMFM calibration set up**

### 2.7.2 Instrument specifications

HP make data logger consists of a switch unit of model number 34970A and a 22 channel plug in module of model number 34901A. This instrument was used along with a PC. The following are the specifications of data logger and plug-in module.

### HP data logger specifications

DAS system	Hewlett Packard data acquisition/switch unit, Model – HP 34970A, with provision for using 3 plug-in modules at a time
Plug-in modules	One module of type HP 34901A with 22 channels
Power supply	230 V
Power line frequency	50 Hz
Power consumption	12 W
Operating environment	Full accuracy for 0 to 55 °C, Full accuracy upto 80% R.H. at 40 °C
Resolution	6½ Digits (22 bits)
Accuracy	0.005% of the reading, 0.004 % of the range selected
Temperature coefficient	0.0005% of the reading, 0.0005 % of the range selected

### HP plug-in module specifications

Model description	HP 34901A, 20+2 channel multiplexer
Type	2-wire armature (4-wire selectable)
Scanning speed	60 channels/second
Open/Close speed	120 channels/second
Maximum volts (dc, ac rms)	300 V
Maximum ampere (dc, ac rms)	1 A
Maximum power	50 W
Offset voltage	<3 Micro V
Initial closed channel R	<1 Ohm
Isolation (ch-ch, ch-earth)	>10 G Ohms
Capacitance HI to LO	<50 pF
Capacitance HI to EARTH	<80 pF
Band width	10 MHz
Operating temperature	0 to 55 °C
Humidity	80% RH at 40 °C

### **2.7.3 Calibration procedure**

The sodium vessel has been filled with purified sodium just above the high level of the vessel which corresponds to  $15.632 \text{ m}^3$  at  $200 \text{ }^\circ\text{C}$  as per procedure. For the first calibration run, sodium temperature has been raised to  $350 \text{ }^\circ\text{C}$ . Then the sodium in the vessel has been drained so that high level indication just vanishes. Then the data acquisition system has been put in scan mode and the instrument is allowed to scan for 10 seconds without sodium flow so that thermal offset voltage value can be calculated from the initial ten readings for each channel. By fully opening the flow control valve, flow was set to the maximum value and the sodium is allowed to drain completely through the PMFM by gravity. Sodium flow was confirmed by observing the milli volt display in data acquisition system. The milli volt outputs of the three pairs of electrodes as a function of time with time were simultaneously displayed and stored in PC at every one second. After observing zero flow in the data logger, the instrument was allowed to scan for ten more seconds and then the scan is stopped. Calibration trials were repeated at various flow rates viz., 20, 40, 70, 140 and  $147 \text{ m}^3/\text{h}$ .

Calibration trials were also repeated at various sodium temperatures of 200, 300 and  $355^\circ\text{C}$ . The deviation between the analytically estimated sensitivity and sensitivity obtained from sodium calibration is around 10% higher. This large variation is due to cumulative effect of all factors described in section 2.5.

### **2.7.4 Sensitivity estimate**

From the calibrations reading, the sensitivity at each flow rate and temperature has been calculated as follows.

#### **2.7.4.1 Thermal offset voltage correction**

All the channels of data acquisition system do not give zero value just before sodium draining. Before draining, flow meter pipeline is filled with sodium at a particular temperature. Hence, there is a thermal voltage in micro volt level across each pair of electrodes. This was treated as an error in each channel. For calculating the thermal voltage in each channel, the data acquisition system has been put in scan

mode 10 seconds before sodium draining. The set of ten readings from each channel was averaged and was treated as thermal offset voltage. This average thermal offset voltage was subtracted from milli volt output of each channel for correction.

#### 2.7.4.2 Sensitivity calculation

Based on the high level position of sodium vessel, volume of sodium drained from the vessel has been calculated. The total milli volt seconds (mV.s) obtained and the quantity of sodium drained are equated to obtain milli volt output per one cubic meter per hour flow.

Volume of sodium drained	: $Q_{SV} \text{ m}^3$
Milli volt output from the flow meter	: $v \text{ mV}$
Time taken for complete draining of TV-3 sodium	: $t \text{ s}$
Total milli volt seconds calculated	: $v \times t \text{ m.Vs}$

Sensitivity of the flow meter is the milli volt output corresponds to one  $\text{m}^3/\text{h}$  flow.

$$\begin{aligned} \text{Sensitivity } S &= (v \times t) / (Q_{SV}) \text{ mVs/m}^3 \\ &= (v \times t) / (Q_{SV} \times 3600) \text{ mV/m}^3/\text{h} \end{aligned} \quad (2.4)$$

#### 2.7.4.3 Trend of sensitivity

The three pairs of electrodes have given almost uniform milli volt output. Flow versus sensitivity plot for three different pairs of electrodes at 200, 300 and 350 °C is depicted in Figs. 2.10- 2.12 respectively. As the flow increases, sensitivity of the flow meter decreases marginally. This reduction is due to increase in end shunting effect with respect to flow as explained in section 2.4.2. The maximum reduction with respect to flow is observed in the down-stream pair of electrodes and is only 2.5%. This reduction is small because of the higher value of pole face length provided in the design (ratio of pole face length to pipe ID is 2.2, refer section 2.4.2) and thereby reducing the end shunting effect.

It is found that, upstream side electrode pairs (EP-1) are more sensitive than other pairs of electrodes as the peak flux density occurs at the pole face centre and the upstream electrode pair is positioned close to the pole face centre. Moreover, the upstream pair is least affected by the end shunting effect. Sensitivity reduces as electrodes are shifted to downstream. The trend observed in the results of sodium calibration is in the expected lines. However, the deviations are minimum and within  $\pm 3\%$  as various measures are taken in the design, to minimize the effects and improve the performance.

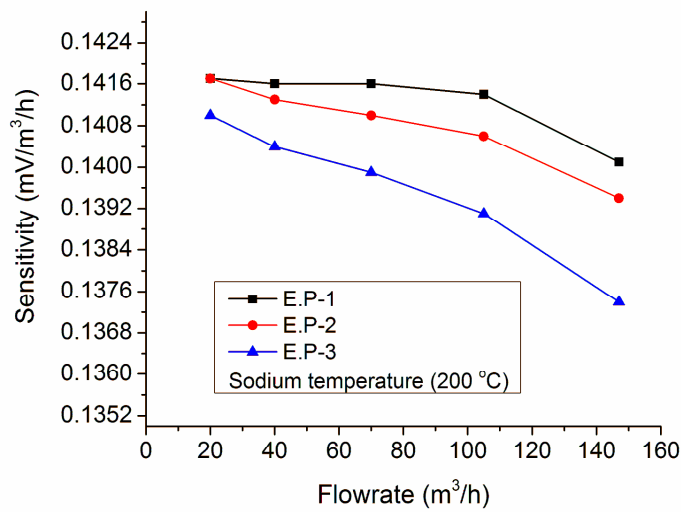


**Fig. 2.10: Flow versus sensitivity for 100 NB Alnico-V flow meter at 200 °C**

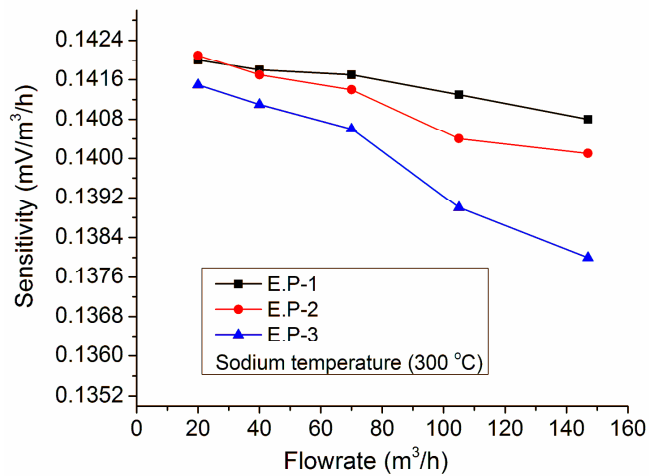


**Fig. 2.11: Flow versus sensitivity for 100 NB Alnico-V flow meter at 300 °C**

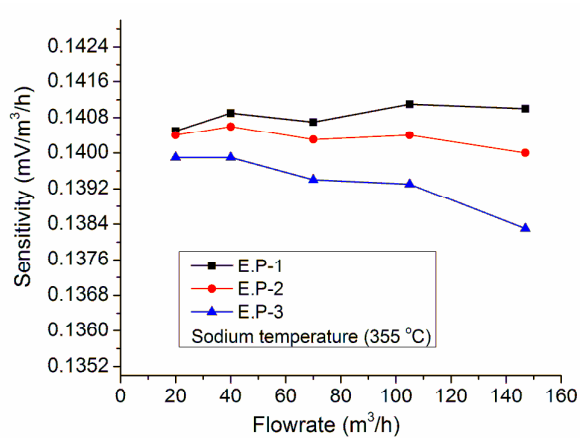


**Fig. 2.12: Flow versus sensitivity for 100 NB Alnico-V flow meter at 355 °C**

Sensitivity versus temperature for downstream pair electrodes at various flow rates is shown in Fig. 2.13. As explained in the previous paragraph, sensitivity reduces when flow increases. At a constant flow rate when temperature increases, the pipe shunting effect increases and reduces the sensitivity, whereas end shunting effect decreases and increases the sensitivity. The trend of resultant effect is shown in Fig. 2.13 and the variation is found to be very marginal. Similar trend was observed for other two pairs of electrodes also.

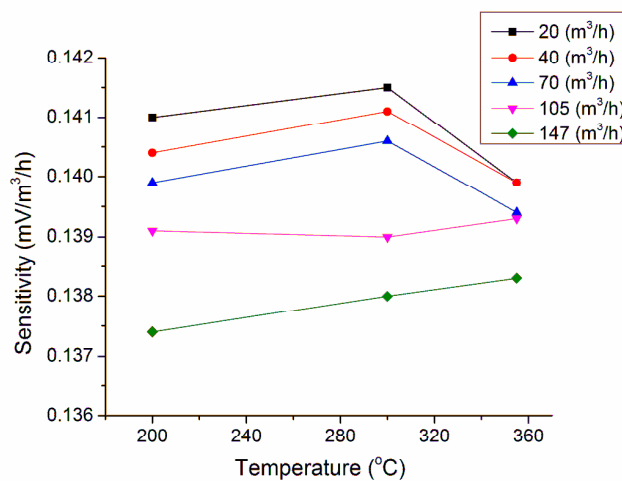


**Fig.2.13: Sensitivity versus temperature at different flow rate**

## 2.8 Analysis on Error in Sensitivity

$$\text{Sensitivity } S = (v \times t) / (Q_{SV} \times 3600)$$

From the errors in the measurement of voltage, volume and time, the overall error in the sensitivity of the flow meter has been calculated using the formula below [37].

$$\Delta S = \left| \frac{\partial(S)}{\partial v} \times \Delta v \right| + \left| \frac{\partial(S)}{\partial t} \times \Delta t \right| + \left| \frac{\partial(S)}{\partial Q_{SV}} \times \Delta Q_{SV} \right| \quad (2.5)$$

$$\frac{\partial(S)}{\partial v} = \frac{t}{3600} \times Q_{SV} \quad (2.6)$$

$$\frac{\partial(S)}{\partial t} = \frac{v}{3600} \times Q_{SV} \quad (2.7)$$

$$\frac{\partial(S)}{\partial Q_{SV}} = \frac{-vt}{3600} \times Q_{SV}^{-2} \quad (2.8)$$

Average voltage output at maximum flow rate for the 100 NB flow meter is  $v = 20$  mV. For the maximum flow drain time of 420 s and sodium volume of  $15.717 \text{ m}^3$  the sensitivity is computed to be  $0.14057 \text{ mV} / \text{m}^3/\text{h}$ .

### 2.8.1 Error in milli volt measurement

HP 34970A data acquisition/switch unit with 34901, 22 channel multiplexer module was used for flow meter output measurement. In the 100 mV range used for measurement, accuracy is 0.005 % of reading + 0.004% of range, i.e., 0.005 mV. The specifications include the initial calibration errors plus the internal digital multi meter long term drift errors. These long term accuracy specifications of the instrument are valid for  $23 \pm 5^\circ\text{C}$  temperature range. Additional temperature coefficient errors must be added to the accuracy specification, when the instrument operates outside the specified range. Temperature coefficient is 0.0005% of reading + 0.0005 % of range per  $^\circ\text{C}$ . When the meter is operating at  $38^\circ\text{C}$ , the error due to temperature is 0.0075 mV. So, the total measurement error is 0.0126

mV or 12.6 micro volts. The thermal voltage induced is measured during each calibration run before establishing the flow and the average value is calculated and appropriate correction applied. The measured thermal voltage is around 15 micro volts at low flow condition. During calibration run the flow varies and temperature distribution in sodium pipe electrode junction changes. Based on this, an error of 10 micro volts is considered in the thermal voltage measurement and correction. The voltage induced due to noise pickup to the signal cables and flow fluctuation is taken as 30 micro volts. These values were taken based on actual observations made during calibration. Hence, the total error in voltage measurement (RMS value) of the above two value is 34 micro volts.

$$\frac{\partial(S)}{\partial v} = \frac{t}{3600} \times Q_{sv} \quad (\text{refer equation 2.6})$$

$$\frac{\partial(S)}{\partial v} \times \Delta v = \left( \frac{v}{3600} \times Q_{sv} \right) \Delta v = \left( \frac{420}{3600} \times 15.717 \right) \times 0.034$$

$$\left| \frac{\partial(S)}{\partial v} \times \Delta v \right| = 0.00025$$

### 2.8.2 Error in time measurement

$\Delta t$  is the error in time measurement in the data acquisition unit. As such, the time measurement will be very accurate but an error of 1 sec is assumed.

$$\frac{\partial(S)}{\partial t} = \frac{v}{3600} \times Q_{sv} \quad (\text{refer equation 2.7})$$

$$\frac{\partial(S)}{\partial t} \times \Delta t = \left( \frac{v}{3600} \times Q_{sv} \right) \times 1$$

$$= \left( \frac{v}{3600} \times Q_{sv} \right) \times 1$$

$$= \left( \frac{20}{3600} \times 15.717 \right) = 0.00035$$

$$\left| \frac{\partial(S)}{\partial t} \times \Delta t \right| = 0.00035$$

### 2.8.3 Error in sodium volume measurement

Sodium volume has been calculated based on dimensional measurements of the sodium vessel. There can be an error in the dimension measurements and was assumed as 5 mm in the measurement of all the dimensions. An error of 5 mm was also assumed in the level measurement. Volume at 350 °C was calculated as 15.717 m<sup>3</sup>. Error in volume corresponding to 5 mm error in dimensional measurement and level measurement was calculated as 0.1158 m<sup>3</sup>.

$\Delta Q_{SV}$  is the error in volume of sodium and is 0.1158 m<sup>3</sup>

$$\frac{\partial(S)}{\partial Q_{SV}} = \frac{-vt}{3600} \times Q_{SV}^{-2} \quad (\text{refer equation 2.8})$$

$$\begin{aligned} \frac{\partial(S)}{\partial Q_{SV}} \cdot \Delta Q_{SV} &= \left( \frac{-vt}{3600} \times Q_{SV}^{-2} \right) \times \Delta Q_{SV} \\ &= \left( \frac{-20 \times 420}{3600} \times 15.717^2 \right) \times 0.1158 = -0.00109 \end{aligned}$$

$$\left| \frac{\partial(S)}{\partial Q_{SV}} \cdot \Delta Q_{SV} \right| = 0.00109$$

### 2.8.4 Total error in sensitivity estimate

$$\Delta S = \left| \frac{\partial(S)}{\partial v} \times \Delta v \right| + \left| \frac{\partial(S)}{\partial t} \times \Delta t \right| + \left| \frac{\partial(S)}{\partial Q_{SV}} \times \Delta Q_{SV} \right|$$

$$\Delta S = 0.00109 + 0.00025 + 0.00035 = 0.00169$$

$$\% \text{ Error} = (\Delta S/S) \times 100 = (0.00169/0.14057) \times 100 = \pm 1.204\% = 1.2\%$$

The error in sensitivity estimated by calibration in sodium facility is 1.2% and is within the acceptable limit.

## **2.9 In-Situ Calibration of Permanent Magnet Flow Meters**

The performance of PMFM can degrade with respect to time due to various reasons. This degradation results in reduction in output voltage affecting the flow meter stability and repeatability. Further, the performance of the flow meter is also affected by mechanical shocks, magnet temperature, external magnetic field, presence of magnetic material close to the flow meter and change of reluctance within the magnetic circuit. It was found essential to calibrate the PMFM at periodic intervals for ensuring accuracy and stability. It is very difficult to calibrate flow meters once installed in the system under actual flow conditions in a sodium loop. Therefore, it is desirable to calibrate the flow meter in-situ without disturbing its normal operating conditions [38, 39]. The PMFM is installed in a sodium facility for actual use. Based on literature survey and our earlier experience a procedure has been developed for in-situ calibration of the same using cross correlation of the signals from different pairs electrodes. In this method of calibration, the voltage fluctuations from two sets of electrode pairs in the PMFM are cross correlated and the transit time of fluctuation between the two electrode pairs, caused by flow turbulence, is found from the peak value of the cross correlation function. As the spacing between the electrode pairs is known, velocity of sodium and the flow rate can be calculated. The advantage of cross correlation technique is that it can be used to calibrate flow meters that are inaccessible and large enough, not to be calibrated in sodium loops [40, 41]. Experiments have been carried out in various sodium loops with permanent magnet flow meters of different sizes and different electrode distances to develop the in-situ calibration procedure. The deviation of the flow rate estimated using cross-correlation technique is found to be within  $\pm 5.5\%$ . In this section the proposed in-situ calibration of the PMFM by cross-correlation technique is described.

### **2.9.1 Cross correlation technique**

The voltage output of permanent magnet flow meter used in the turbulent flow conditions consists of a DC signal (proportional to mean sodium velocity) over which a fluctuating component (noise signal) is superimposed [42, 43]. This

fluctuation is due to the turbulent conditions existing in the region of the magnetic field. The fluctuating component occurring at any instant at the upstream electrodes pair of flow meter takes a finite time to reach the downstream electrodes pair of flow meter. Once the transit time is found, flow rate is estimated given the distance between the electrodes pair and pipe diameter. The advantage of this noise analysis techniques is that flow rate estimated using this method is independent of electrodes absolute voltage signal. This transit time is obtained by cross correlating the noise signals from the two pairs of electrodes of PMFM. Therefore, cross-correlation technique is a promising tool for in-situ calibration of PMFMs in SFRs.

Consider  $x(t)$  and  $y(t)$  as the upstream and downstream random disturbance signals (noise signals) of PMFM electrode pairs that differ by an unknown transit time. The transit time can be found from the maximum of the cross correlation function of the two electrode pair signals  $x(t)$  and  $y(t)$  using the following equation [43].

$$R_{xy}(\tau) = \frac{1}{T} \int_0^T x(t)y(t+\tau)dt \quad (2.9)$$

where  $T$  is the integration time and  $R_{xy}(\tau)$  is obtained by shifting the  $y(t)$  along the time axis and calculating the integral of the product of  $x(t)$  and  $y(t)$  at each position. When  $y(t)$  is equal to  $x(t)$  after a time shift  $\tau$ , the product gives large contribution to integral and the peak value of cross correlation function corresponds to the delay of  $y(t)$  with respect to  $x(t)$ .

For discrete time signals, Equation (2.9) can be written as

$$R_{xy}(j) = \frac{1}{N} \sum_{i=1}^N x(i)y(i+j) \quad j=0,1,2,\dots,M \quad (2.10)$$

where  $N$  is the record length,  $M$  is the correlation delay range,  $x(i)$  is the sampled data sequence of one pair of electrodes signal and  $y(i)$  is the sampled data sequence of the other pair of electrode signal. The cross correlation calculation is carried out, using Equation (2.10), to obtain the cross correlation function. Maximum correlation

reading is obtained at the delayed sample number  $k$ . By multiplying this delayed sample number  $k$  with the sample interval  $\Delta t$ , the time delay between the two pairs of electrodes signals, i.e.,  $k\Delta t$  is obtained.

### 2.9.2 Experimental details

Experiments have been carried out initially with permanent magnet flow meters in different sodium systems and in reactor sodium circuit. Three pairs of electrodes as shown in Fig. 2.14 are provided in the PMFM to record output signals. The axial distances between the electrode pairs  $a_1$ - $a_2$  &  $b_1$ - $b_2$  or  $b_1$ - $b_2$  &  $c_1$ - $c_2$  are 15 mm. The distance between the electrodes pairs  $a_1$ - $a_2$  &  $c_1$ - $c_2$  is 30 mm. The voltage fluctuations from the two pairs of electrodes of the PMFM are acquired with a sampling frequency of 10 kHz for estimating the cross correlation function and the voltage output from the third pair is connected to flow indicator at control room. The flow meter voltage output is filtered using a band pass filter (0.1-30 Hz) to remove DC signal (0 Hz) as well as power line frequency (50 Hz).

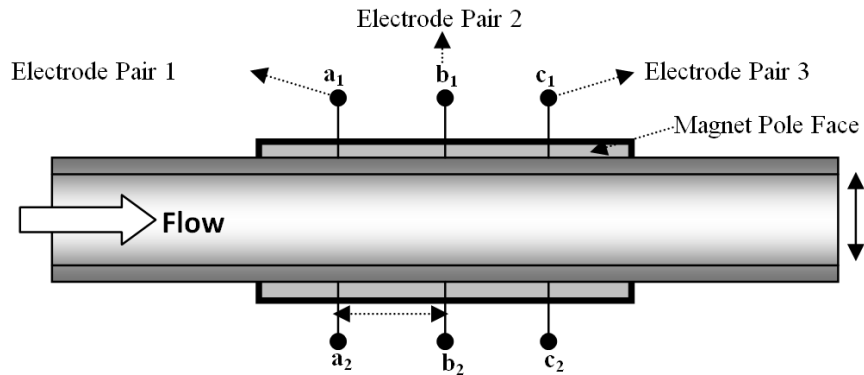


**Fig. 2.14: Configuration of PMFM with three pairs of electrodes**

The sodium temperature in the system is maintained at 330 °C and sodium flow is varied from 25 m<sup>3</sup>/h to 105 m<sup>3</sup>/h by varying the applied voltage to the electromagnetic pump in the system. During the experiment the voltage fluctuations from the two pairs of electrodes of the PMFM are acquired for analysis. In this analysis, the normalized cross correlation function is obtained from the average of ten cross correlation functions with each cross correlation function

computed for 10000 samples. The analysis is done in time domain using Lab VIEW software. Fig. 2.15 shows the typical time domain signals (after filtering) acquired from the 100 NB PMFM between  $b_1$ - $b_2$  &  $c_1$ - $c_2$  and the cross correlation function calculated at sodium flow of  $35.59 \text{ m}^3/\text{h}$ . Figures 2.16 shows similar analysis carried out with the voltage signals from  $a_1$ - $a_2$  &  $c_1$ - $c_2$ .

The time shift that corresponds to the peak value in the cross correlation function is the transit time for the fluid (sodium) to pass between the two pairs of electrodes. The transit time is calculated from the cross-correlation function for various sodium flow rates and the flow rate of the sodium is estimated as below:

$$v_u = d_e / \tau;$$

where

$v_u$  : mean velocity of sodium flow through PMFM at operating temperature in m/s

$d_e$  : distance between electrodes, in m

$\tau$  : Transit time obtained from cross correlation function

$Q_c = v_u \text{ (m/s)} \times \text{Area of pipe cross section (m}^2\text{)}$ , where  $Q$  is the volumetric flow rate in  $\text{m}^3/\text{h}$ .

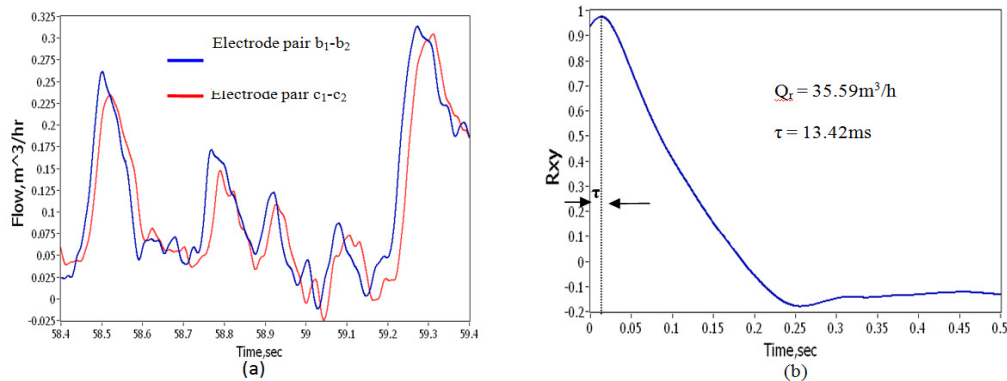


**Fig. 2.15: Cross correlation analysis of signals from electrodes at 15 mm spacing**  
a) PMFM signal after band pass filtering (0.1-30Hz) b) Cross Correlation function of signals from electrode pairs  $b_1$ - $b_2$  &  $c_1$ - $c_2$

Flow rate estimated using cross correlation technique ( $Q_c$ ) is compared with that of flow rate calculated from DC voltage of PMFM ( $Q_r$ ) and given in Tables 2.2 and 2.3 for 15 mm and 30 mm electrode distances respectively. It can be observed from the Table 2.2 that the error is positive in all flow rates except in one case, i.e., the flow rate calculated using cross correlation techniques is higher as compared to that from DC voltage of PMFM and the maximum error is 3.91%. In case of 30 mm electrode distance, (Table 2.3), the error is negative in all flow rates, i.e., flow rate calculated using cross correlation techniques is lower as compared to that from DC voltage of PMFM and the maximum error is 5.5%.

**Table 2.2: Results of flow rate estimation from electrodes at 15 mm gap**  
(15 mm gap electrode pair  $b_1$ - $b_2$  &  $c_1$ - $c_2$  )

S.No	$Q_r$ ( $m^3/h$ )	Re $\times 10^5$	$\tau$ (ms)	$Q_c$ ( $m^3/h$ )	Error %
1	28.06	2.57	17.48	28.39	1.18
2	35.59	3.26	13.42	36.98	3.91
3	46.9	4.29	10.19	48.70	3.84
4	55.00	5.03	8.83	56.18	2.15
5	65.08	5.96	7.56	65.66	0.89
6	74.98	6.86	6.57	75.52	0.72
7	85.12	7.79	5.93	83.62	-1.76
8	95.12	8.79	5.17	95.90	0.82
9	104.95	9.61	4.61	107.65	2.57

**Table 2.3: Results of flow rate estimation from electrodes at 30 mm gap**  
(30 mm gap electrode pair  $a_1$ - $a_2$  &  $c_1$ - $c_2$ )

S.No	$Q_r$ ( $m^3/h$ )	Re No $\times 10^5$	$\tau$ (ms)	$Q_c$ ( $m^3/h$ )	Error %
1	25.59	2.28	39.81	24.94	-2.54
2	35.24	3.15	28.81	34.46	-2.21
3	45.25	4.04	23.22	42.76	-5.50
4	55.55	4.96	18.82	52.76	-5.02
5	65.45	5.85	15.42	64.36	-1.67
6	75.25	6.72	13.73	72.31	-3.91
7	85.16	7.61	12.03	82.52	-3.10
8	95.30	8.52	10.56	93.96	-1.41
9	104.95	9.38	9.55	103.92	-0.98

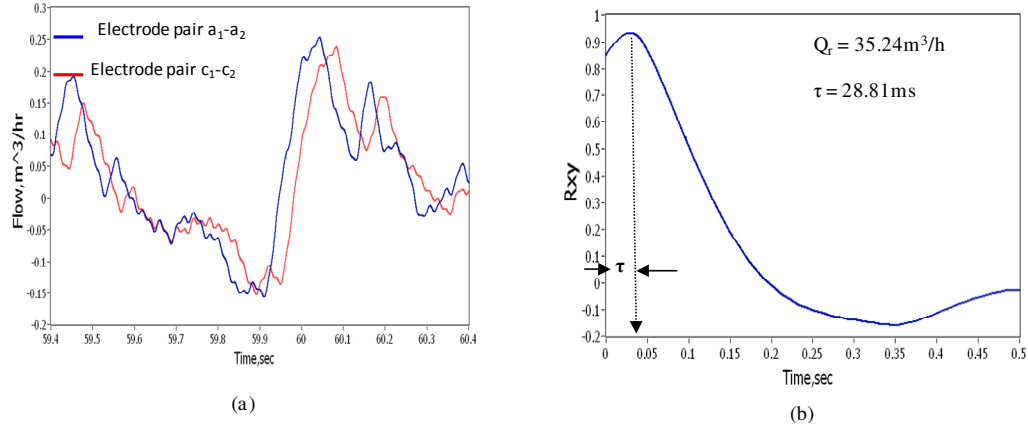


**Fig. 2.16: Cross correlation analysis of signals from electrodes of 30 mm spacing**

a) PMFM Signal after band pass filtering (0.1-30Hz) b) Cross Correlation function of signals from  $a_1-a_2$  and  $c_1-c_2$  electrode pairs.

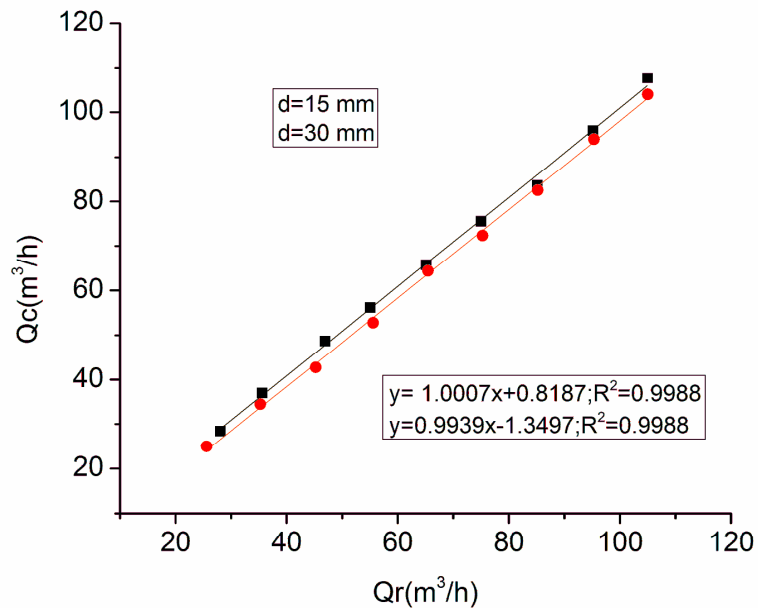


**Fig. 2.17: Calibration curves obtained by cross correlation for 100 NB PMFM**

Figure 2.17 shows the calibration curves obtained using cross correlation technique for the 100 NB PMFM with 15 mm and 30 mm electrode distances. The linear fit of the experimental data is given in the graph. Deviation of the flow rate estimated using cross-correlation technique is found to be within  $\pm 5.5\%$ .

## 2.10 Closure

Basics of electromagnetic flow measurement, sensitivity of PMFM, the methodology followed for analytical estimation of sensitivity and factors affecting sensitivity are described. A PMFM suitable for 100 NB sch 40 pipe was designed and manufactured and its sensitivity has been estimated analytically. A sodium setup was made ready for calibration of flow meters by constant volume method and the 100 NB flow meter has been calibrated in the setup by constant volume method. The error in the sensitivity was determined as 1.2%. In-situ calibration of the same flow meter, installed in a system for use, was carried out by cross correlation technique. Flow rate estimated using cross correlation function was compared with that of measured by PMFM and the deviation of the flow rate estimated using cross correlation technique was found to be within  $\pm 5.5\%$ . The cross correlation technique is found to be very promising and can be used for in-situ calibration of permanent magnet flow meters in SFR circuits. The stability of the Alnico-V magnet assembly to provide constant magnetic field throughout the life of the reactor is to be established. Next chapter covers stability studies carried out on Alnico-V based PMFM. The weight of the 100 NB Alnico-V based PMFM is around 110 kg, which is very high for a flow sensor and leads to handling and installation difficulties compounded with a low sensitivity. Further research taken up to address these issues are presented in chapters 3 and 4.

## **CHAPTER 3**

### **STABILITY STUDIES ON ALNICO-V BASED PERMANENT MAGNET FLOW METERS**

#### **3.1 Introduction**

The critical part of a permanent magnet flow meter is found to be the permanent magnet assembly. The permanent magnet assembly is normally made of Alnico-V magnet blocks, mild steel assembling pieces and mild steel pole faces. They are assembled with non magnetic SS bolts to form the magnetic circuit. The magnet assembly provides required flux density in the air gap where the flow meter pipe is positioned. The performance of the flow meter mainly depends on the performance of the magnet assembly under various operating conditions and the hostile environment that exists in the SFR circuits. This chapter deals with ferromagnetism, magnetic materials, magnetic properties, design of magnetic circuit and the experimental investigation carried out to evaluate the long term stability of Alnico-V magnet assemblies used in permanent magnet flow meters.

#### **3.2 Ferromagnetism**

Ferromagnetism normally appears only in solid crystallized substances. For ferromagnetism to appear in materials, the following three conditions must be met simultaneously:

- a) There must be an unfilled inner electron shell within the atom.
- b) There must be uncompensated electronic spins in its unfilled inner shell.
- c) The ions of the atoms must form a crystal lattice having lattice constant at least three times the radius of the unfilled electron shell.

All the spins of a ferromagnetic body are not spontaneously aligned as a whole but the alignment normally spreads over a limited number of spins. Such mutually aligned spin groups are called ‘elementary domains’, ‘Weiss domains’ or simply domains. Within a domain, the materials is magnetized to saturation spontaneously without any external field. In a poly crystalline magnetic body, the domains are in general randomly oriented so in toto all lines of flux are locally closed and no field is detectable externally. On applying a magnetic field, elementary magnets are brought into parallelism, so as to form poles at the free end of a rod like specimen [44].

### 3.3 Soft and Hard Magnetic Materials

It is known that there are two categories of ferromagnetic materials and they are hard and soft magnetic materials. A material in magnetic sense is termed soft if the magnetization process is nearly reversible and hard if there is considerable hysteresis in the magnetization process. Soft magnetic materials are easily magnetized and demagnetized. They will have high magnetic saturation,  $M_s$ , low coercivity  $H_c$ , high permeability, low magneto crystalline anisotropy, low core loss and high resistivity. Hard magnetic materials are difficult to magnetize and difficult to demagnetize. They are permanent magnets, having high saturation magnetization, coercivity, magneto crystalline anisotropy and maximum energy product. Figure 3.1 shows the hysteresis loops of soft magnetic material and hard magnetic material.

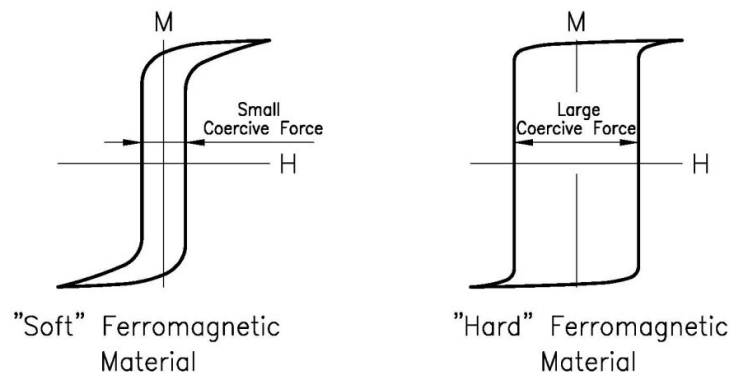


**Fig. 3.1: Hard and soft magnetic materials**

### 3.4 Permanent Magnets

One of the distinguishing features of ferromagnetic materials is the nonlinear relationship between the observed induction  $B$  and the magnetizing field  $H$ . For most engineering applications, the measured induction  $B$  is plotted against magnetic field strength  $H$ . Sometimes it is necessary to use the curve of the intrinsic induction  $B_i$  plotted against field strength  $H$ . The intrinsic induction is that component of the normal induction which is due alone to the presence of ferromagnetic material. These two representations differ by the fact that the intrinsic induction  $B_i$  approaches a saturation limiting value  $B_{is}$  with increasing positive field, whereas the increase in normal induction depends on the applied field. Total induction of a magnetic material is made up of two components. The magnetizing field  $H$  and intensity of magnetization  $M$ . The induction is the vectorial sum of the two components  $B = H + M$  or  $B = B_i + H$ .

The magnetizing force  $H$  may be of the same or opposite sign as the induction and is the effective magnetizing force usually measured on ring specimens. The value of magnetizing force  $H_s$  required for saturation is also the field strength which must be employed in the magnetization process to obtain maximum utilization of a permanent magnet in service [31, 44]. It is reported that, the field strength required for saturation is five to six times the value of intrinsic coercive force  $H_{ci}$ . After reaching saturation, if we steadily reduce the magnetizing field to zero, the induction will not follow the initial magnetization curve, but will lag behind the magnetizing force, a phenomenon referred to as hysteresis as shown Figure 3.2. The subsequent application of a steadily increasing field of opposite direction will eventually saturate the specimen with magnetizing direction reversed. Fig. 3.2 shows normal induction hysteresis loop of a permanent magnet material and Fig. 3.3 shows normal induction and intrinsic induction hysteresis loop of a permanent magnet material.

In a permanent magnet, the field strength measured at the magnet surface has a direction opposite to that of the induction inside the magnet. With positive induction, the field strength is negative. The operating range of a permanent

magnet therefore is a portion of the second quadrant of the major hysteresis called demagnetization curve. This is in contrast to the electromagnet in which both the induction and magnetizing force have the same direction. Hence, the operating range of an electromagnet is in the first quadrant.

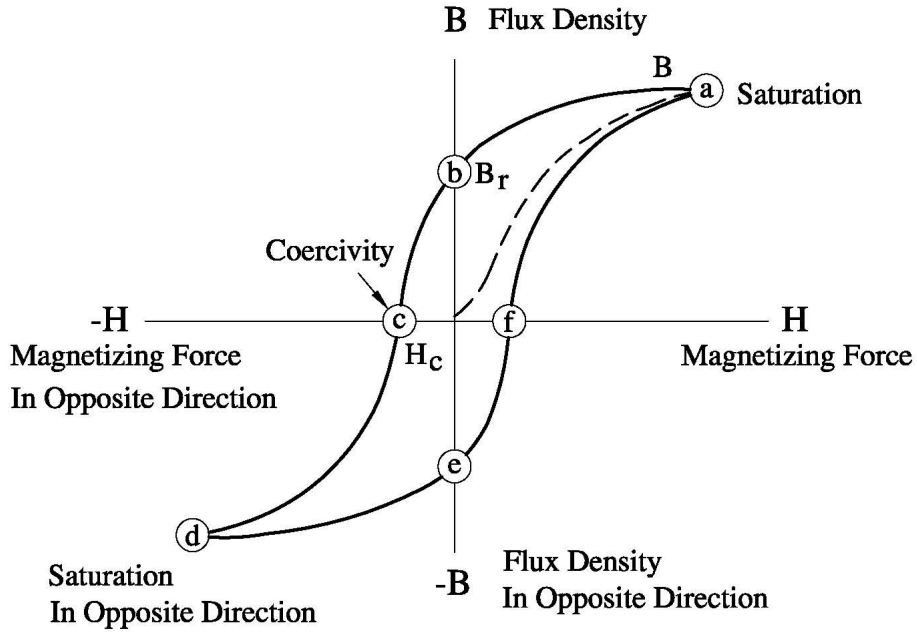


Fig. 3.2: Normal induction hysteresis loop

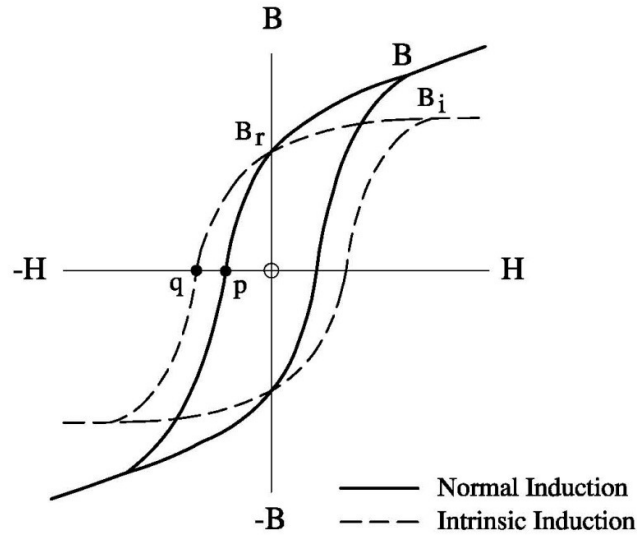


Fig. 3.3: Normal induction and intrinsic induction hysteresis loop

### 3.5 Magnetic Properties [31]

**$(BH)_{\text{Max}}$ :** Maximum product of  $(B_dH_d)$  which can be obtained from the demagnetization curve, indicates the energy that a magnetic material can supply to an external magnetic circuit when operates at any point on its demagnetization curve.

**Coercive force ( $H_c$ ):** The magnetizing force that must be applied to a magnetic material in a direction opposite to the residual induction to reduce the induction to zero (Point c in Fig 3.2 and point p in Fig. 3.3).

**Coercive force intrinsic ( $H_{ci}$ ):** The magnetizing force that must be applied to a magnetic material in a direction opposite to the residual induction to reduce the intrinsic induction to zero (Point q in Fig 3.3),

**Induction Intrinsic ( $B_i$ ):** The excess of the induction in a magnetic material over the induction in vacuum for a given value of magnetizing force. The equation for intrinsic induction is  $B_i = B - \mu_0 H$  (Refer Fig. 3.3).

**Residual induction ( $B_r$ ):** The magnetic induction corresponding to zero magnetizing force in a magnetic material (Refer Fig. 3.2 and 3.3).

**Reversible temperature coefficient:** A number which describes the change in a magnetic property with change in temperature. It is usually expressed as the percentage change per unit temperature for both  $B_r$  and  $H_c$ .

A good permanent magnet should produce a high magnetic field with low mass and should be stable against the influences which would demagnetize it. The desirable properties of such magnets are typically stated in terms of the remanance ( $B_r$ ) and coercivity ( $H_c$ ) of the magnet materials.

### 3.6 Alnico Magnets

A tremendous advance in technology and use of permanent magnets started with the announcement in 1932 by Mishima of the excellent magnetic properties found in an aluminum- nickel-iron alloy [44]. Many investigators later examined this alloy system and contributed to many improvements. From the efforts of these investigators, a whole series of alloys generally known as Alnico possessing a wide range of magnetic properties have come into existence. Alnico alloys basically consist of aluminum, nickel, cobalt, copper, iron and titanium. In some grades, cobalt and/or titanium are omitted. The physical properties of Alnico alloys are rather poor. The state of high coercivity is closely accompanied by extreme hardness and brittleness. Castings are prone to shrinkage and porosity. On cooling the magnet from an elevated temperature through the region of its curie point, under the influence of a magnetic field, it is found that the preferred axis of magnetization, parallel to the axis of the magnetic field is developed in the magnet. When magnetized along this preferred axis, even up to five fold increase in available energy is observed. The Alnico alloys are formed by casting or powder metallurgical processes. Induction melting furnace is universally used to prepare Alnico alloys. The ingredients are rapidly melted and poured off into bake sand molds. Speed is essential in this operation to prevent excessive oxidation losses and elemental segregation.

An elongated particle would exhibit an enhanced coercivity along its major axis, and this phenomenon is known as shape anisotropy. This is the dominant mechanism in Alnico magnets in which elongated magnetic particles are precipitated throughout the matrix of Al Ni Fe Co alloy. There are many variations on the constituents of this alloy, which produce different magnet characteristics [44].

There are ten varieties of cast Alnico alloys as per magnetic materials producers association (MMPA) standard. Alnico I to Alnico III are isotropic. Different grades of Alnico-V, different grades of Alnico-VIII, Alnico-VI and Alnico-IX are anisotropic in nature. The magnetic properties and thermal properties

are varied by changing the chemical composition and heat treatment process. Sintered Alnico magnets are inferior in their magnetic properties compared to cast alnico magnets. Cast Alnico-V provides maximum residual induction ( $B_r$ ). Cast Alnico-VIII provides maximum coercive force ( $H_c$ ) but residual induction is low. Curie temperature (880 °C) is the same for both but maximum service temperature is 525 °C for Alnico-V and 550 °C for Alnico-VIII. The high operating temperature of Alnico-VIII is due to its high coercivity which is 2.5 times higher than Alnico-V. Because of the high coercivity, magnet has more resistance to demagnetizing forces due to temperature.

### 3.7 Properties of Alnico-V

#### 3.7.1 Magnetic properties of Alnico-V

Peak energy product( $BH_{max}$ )	: 43.8 kJ/m <sup>3</sup>
Remanance ( $B_r$ )	: 1.28 Tesla
Coercivity ( $H_c$ )	: 51,700 A/ m
Curie point ( $T_c$ )	: 880°C

#### 3.7.2 Physical and mechanical properties of Alnico-V

Density	: 7300 kg/m <sup>3</sup>
Tensile Strength	: 97 x 10 <sup>6</sup> Pa
Transverse Modulus of Rupture	: 28 x10 <sup>6</sup> Pa
Hardness (Rockwell C)	: 45
Coefficient of Thermal Expansion 10 <sup>-6</sup> per °C	: 12.6
Electrical Resistivity Ohm-cm x 10 <sup>-6</sup> (at 20 °C)	: 75

#### 3.7.3 Chemical composition of Alnico-V

Composition (mass %) for Alnico-V is given below.

Cobalt: 24%, Nickel: 14%, Aluminium: 8 %, Copper: 3%, Iron: 51%

### **3.8 Alnico-V Magnet Assembly**

Design and manufacture of Alnico-V based permanent magnet assembly is the first part of PMFM manufacture. It is desirable to have a pole face length equal to or more than three times the pipe internal diameter to minimize the effect of end shunting factor  $K_2$ . However, to reduce the size of the PM assembly, lower pole face length also is adopted for pipes above 50 NB size. The width of the pole face should be more than the pipe OD, to get magnetic flux density over full cross section of the flow pipe. The air gap between the pole faces should be large enough to accommodate the pipe with adequate thickness of insulation. To get the required sensitivity for the flow meter, the flux density requirement in the air gap has to be arrived at. The magnet assembly has to be designed by providing adequate margin. For flow meters up to 50 NB, single circuit magnet assembly will be able to provide required flux density. For large pipes above 50 NB, the air gap flux density requirement can be achieved only by providing double circuit arrangement. The assembly can be made with specifically manufactured magnets or standard block magnets. Mild steel assembling pieces are used for making the assembly. Non magnetic SS fasteners are used for assembling, to prevent attraction and, make them easy to remove during disassembly. The mating faces are ground finish smooth, to get good physical contact.

### **3.9 Design of Magnetic Circuit for 100 NB PMFM**

Design of a magnet assembly or magnetic circuit, to provide adequate signal output by the PMFM, is an important aspect in the PMFM design. The target sensitivity of the PMFM is fixed based on rated flow and the output desired at the rated flow. Then the flux density required to achieve target sensitivity is calculated using the basic flow meter output equation (2.1). Varying the volume of magnet, iterative calculations are made to get the required flux density. To describe the design procedure followed, an example of 100 NB PMFM magnet assembly design is selected. Double circuit design is followed as shown in Fig. 3.4. Alnico-V rectangular magnet block of 35x100x72 mm size is used.

The following two equations control the various parameters involved in the design of magnetic circuits with air gap [44].

$$B_m \times A_m = L.F \times B_g \times A_g \quad (3.1)$$

$$H_m \times L_m = R.F \times H_g \times L_g \quad (3.2)$$

where  $A_m$  and  $L_m$  are area and total length of permanent magnet blocks, respectively,

$A_g$  and  $L_g$  are area and total length of air gap in the magnetic circuit, respectively

$B_m$  and  $H_m$  are values at operating point on the demagnetization curve for the permanent magnet material.

***L.F*** : Leakage Factor is defined as ratio of total magnetic flux at magnet neutral zone to useful air gap flux.

***R.F*** : Reluctance factor defined as ratio of total magneto motive force required for magnetic circuit to m.m.f required for the air gap based on physical dimensions.

As per equation (3.1) magnetic flux at any cross section of the assembly will be equal. This is analogous to Kirchhoff's current law in an electric circuit. Similarly as per equation (3.2) the magneto motive force across the magnet is equal to the magneto motive force across the air gap in magnet assembly. This analogous to Kirchhoff's voltage law in electric circuits. Since the basic properties of the magnetic material and the dimensions of the magnet assembly are related in these equations, they control the various parameters involved in the design.

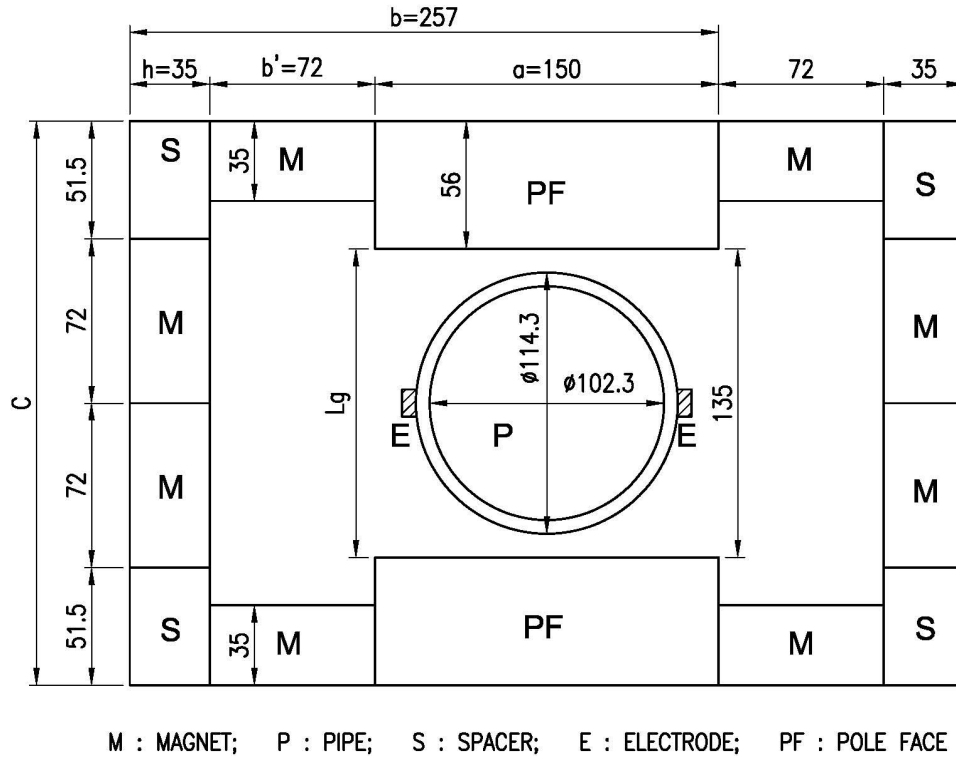
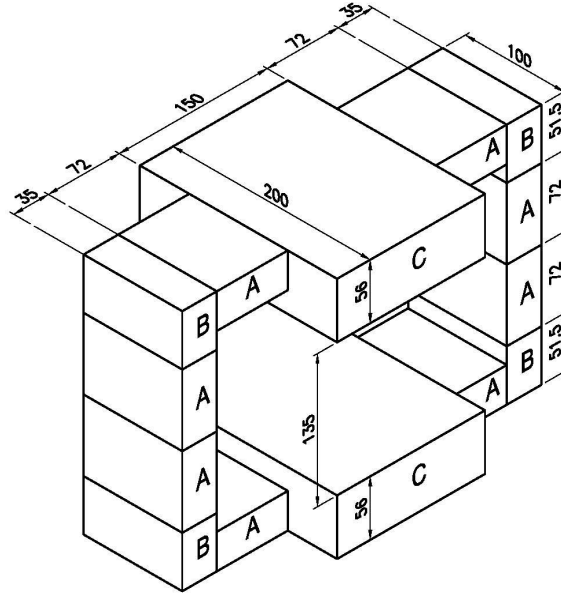


**Fig. 3.4: 100 NB PMFM magnet assembly with pole face dimensions**

Figures 3.4 and 3.5 show a double circuit magnet assembly used for sodium flow meter of pipe size 100 NB. Anisotropic magnet blocks with grain orientation in 72 mm direction, which is the direction of flux lines in the assembly is selected, to maximize the flux density in the air gap. Suitably machined mild steel blocks are used as intermediate pieces to complete the assembly. SS bolts are used for fastening the parts in the assembly. The following are the pole face and air gap dimensions:

- Pole face length : 200 mm, almost double the pipe OD, so that  $K_2$  is nearly 2
- Pole face height : 150 mm, more than pipe OD, so that full pipe cross section is covered
- Air gap length : 135 mm, more than pipe OD, adequate insulation thickness can be provided



PART A : MAGNET – ALNICO V; PART B : SPACER – MILD STEEL; PART C : POLE FACE – MILD STEEL

**Fig. 3.5: Isometric view of 100 NB PMFM magnet assembly**

Figures 3.4 and 3.5 also show the dimensions of the magnet assembly. For this type of assembly, reluctance factor ( $RF$ ) varies from 1.1 to 1.5 assembly. Average value of 1.3 is assumed as  $RF$  [45].

For estimating leakage factor ( $LF$ ), [45]

$$L.F = 1 + \frac{L_g}{A_g} \left[ 1.7U_a \frac{a}{a + L_g} + 1.4 \frac{\sqrt{U_c}}{\sqrt{b}} (h + 0.45b^1) + \frac{0.67cU_b^1}{2(b^1 + 2h)} + 0.67U_c \right] \quad (3.3)$$

where

$U_a, U_b^1, U_c$  : Perimeter of cross section of different parts a, b and c in the assembly.

$a, b, c, b^1, h$  : Dimensions of parts in the assembly.

The leakage factor and the air gap flux density can be calculated only by making certain assumptions, since the above formula is not directly applicable to the parallel circuit configuration considered in the present case.

The magnet circuit is assumed to have only one circuit with four magnets on one side of the assembly. The entire pole face is considered as part of this simplified circuit. The air gap flux density is then calculated by substituting double the magnet cross section area to consider the contribution of the four magnets, on the other side of the assembly.

For the magnet assembly depicted in Figs. 3.4 and 3.5, different dimensions are :

$$L_g : 0.135 \text{ m}$$

$$A_g : 0.030 \text{ m}^2$$

$$a : 0.150 \text{ m}$$

$$b : 0.257 \text{ m}$$

$$c : 0.247 \text{ m}$$

$$b^l : 0.072 \text{ m}$$

$$h : 0.035 \text{ m}$$

$$U_a : 0.512 \text{ m}$$

$$U_b^l : 0.270 \text{ m}$$

$$U_c : 0.270 \text{ m}$$

By substituting the above values in equation (3.3), the  $LF$  is calculated as 5.02. Further

$$\frac{B_m}{H_m} = \frac{L.F \times B_g \times A_g \times L_m}{R.F \times H_g \times L_g \times A_m} \quad (3.4)$$

$$LF : 5.02$$

$$RF : 1.30$$

$$A_g : 0.03 \text{ m}^2$$

$$L_g : 0.135 \text{ m}$$

$$L_m : 0.288 \text{ m}$$

$$A_m : 7 \times 10^{-3} \text{ m}^2$$

$B_g = H_g =$  Air gap flux density Substituting the above values in equation (3.4),  $B_m/H_m$  is estimated as 34. Referring to the demagnetization curve for Alnico-V in Fig. 3.6, the value of  $B_m$  corresponding to this  $B_m/H_m$  is found out.

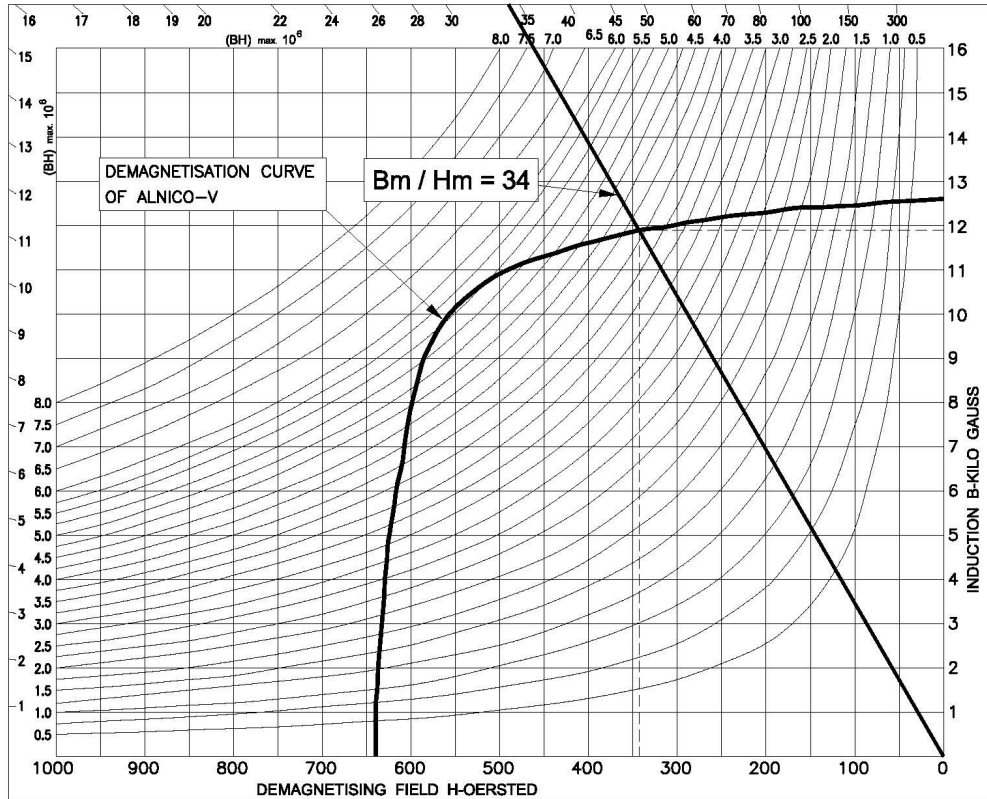


**Fig. 3.6: Unit property curves of anisotropic cast Alnico-V [44]**

From B-H curve,  $B_m$  is found to be 1.18 Tesla. Again substituting this value of  $B_m$  in equation (3.1), the air gap flux density is  $B_g$  is calculated as 0.548 Tesla. When the assembly was manufactured, the air gap flux density was measured to be 0.05 Tesla.

### 3.10 Magnetization of Magnet Assembly

To get maximum flux density in the air gap, it is necessary to magnetize the assembly as a whole to saturation with a mild steel keeper in the air gap [44]. This mild steel keeper is used to complete the magnetic path during the magnetization. To magnetize the assembly to saturation, magnetizing force in ampere turns equal to or more than six times the coercive force has to be applied. When the magnetizing force is applied, the magnetic domains in the material align in the direction of the force. The energy required for alignment of domains is absorbed from the current source. The energy required to magnetize unit volume is estimated from the area under the curve in the first quadrant of the hysteresis loop of the magnetic material. For Alnico-V, this value is estimated as  $76,000 \text{ J/m}^3$ .

Magnetizing coil made up with 16 SWG enameled copper wire is wound with 25 turns/cm over the magnet length to ensure magnetization. Mild steel keeper occupying full volume of air gap is introduced to close the magnetic circuit. Magnetizing coils are connected in series to get magnetic field in the same direction by all the coils. Coils are connected to the magnetization set up consisting of capacitors connected in parallel to form the capacitor bank. It is known that the energy stored in the capacitor bank should be higher than the energy required for the magnet volume of the assembly. The rated voltage of the capacitor bank should also be sufficient to provide required ampere turns. Capacitor is charged to the rated DC voltage of 250 Volts and then discharged through the magnetizing coils. This charging and discharging operation is repeated minimum three times. After removing the keeper, the flux density at the geometric centre of the air gap is measured and compared with the expected value. The schematic of PMFM magnet assembly magnetization circuit is shown in Fig. 3.7. All the measurements are done with Hall probe type Gauss meter. Accuracy of the gauss meter is  $\pm 1\%$ . Gauss meter is checked before each measurement with zero chamber and magnet. The resolution of measurement is one gauss. The readings are repeated for a minimum of three times and consistency is observed.

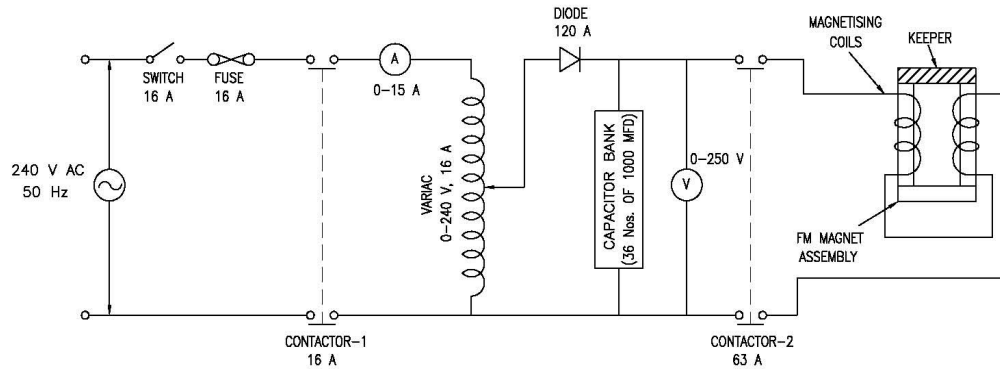


**Fig. 3.7: Schematic of PMFM magnet assembly magnetization circuit**

### 3.11 Permanent Magnet Stability

Main factors affecting the magnet stability include time, temperature, reluctance changes and adverse fields. The effect of time on modern permanent magnets is reported to be minimal. Studies have shown that permanent magnets will see changes immediately after magnetization. These changes occur as, less stable domains are affected by fluctuations in thermal or magnetic energy, even in a thermally stable environment. This variation is reduced as the number of unstable domains decreases. Long-term flux versus time studies have shown that a newly magnetized magnet will lose a minor percent of its flux with ageing. Over the years, these losses are less than 3% for Alnico-V materials at low permeance coefficients ( $B_m/H_m$ ) [46].

### 3.12 Losses in Magnetic Field

#### 3.12.1 Reversible losses

These losses are recovered when magnet returns to original temperature and they cannot be eliminated by stabilization. It is described by reversible temperature coefficient ( $T_c$ ). Reversible temperature coefficient is expressed as % per degree centigrade. It depends on the material and the operating point of magnet assembly on demagnetization curve. In PMFM the magnet assemblies operate at temperatures around 100 °C and the actual magnet temperature depends on sodium

temperature. So the temperature of the magnet assembly has to be measured and correction has to be applied on room temperature flux density value.

### **3.12.2 Irreversible but recoverable losses**

Changes that persist even after the cause has been removed are termed as irreversible losses. The principal cause of irreversible change in the demagnetization curve is thermal fluctuations. Higher thermal energy can activate reversals of some of the magnetic domains. The irreversible loss in the magnet energy can only be recovered by full re-magnetization after temperature returns to its original value. Irreversible changes can be almost completely eliminated by cycling the magnet through a slightly greater temperature than it will experience in service. This cycling is called temperature stabilization.

### **3.12.3 Irreversible and unrecoverable losses**

Metallurgical changes occur in magnets exposed to high temperatures and are not recoverable by magnetization. In the case of Alnico-V, magnets undergo critical phase segregation during their heat treatment between 550 and 650°C. If these magnets are exposed to operating temperature above 550°C then the phase composition will be altered, and the original demagnetization curve cannot be regained even by full re-magnetization. Recasting under magnetic field is the only solution [44].

## **3.13 Stabilization of Magnet Assembly**

A magnet assembly should be stabilized against all factors affecting stability such as adverse magnetic fields, temperature, reluctance changes, vibration and time. Magnet assembly is made with MS pole faces and Alnico-V magnet blocks and is bolted with nonmagnetic SS bolts which avoid any reluctance variation during service [47]. Vibration and mechanical shock to the magnet assembly are avoided during operation. All magnet assemblies are magnetically and thermally stabilized before using them for flow meters.

### 3.13.1 Magnet stabilization by AC knockdown

Magnetizing coils used for magnetization should be connected to the stabilizing circuit. The keeper in the air gap should be removed. Stabilizing circuit consists of an AC power supply of 20 A capacity with provision for varying the current through the coils gradually. Two auto transformers are connected in series to control the current. AC current at 50 Hz through the coil is gradually increased and simultaneously the flux density at the air gap centre is monitored. As the current through the coil increases, the air gap flux density is expected to come down. When flux density reaches approximately 95% of the original value, the current should gradually be reduced to zero. Now the magnet is electrically stabilized by AC knockdown. Any demagnetizing or magnetizing field during the operation of the flow meter will have only reversible effect on the magnetic flux density now. Otherwise irreversible losses due to any adverse demagnetizing magnetic field are deliberately allowed to take place during the process of stabilization by AC knockdown. Schematic of PMFM magnet assembly stabilization circuit with AC knockdown method adopted in present study is shown in Fig. 3.8.

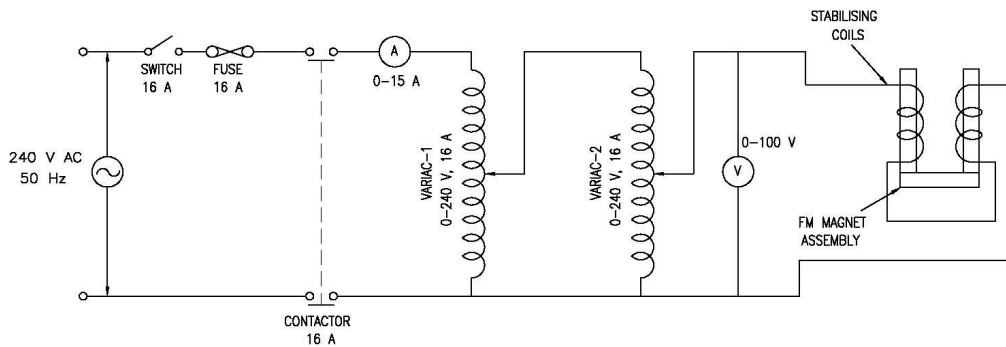


**Fig. 3.8: Schematic of PMFM magnet assembly stabilization circuit**

### 3.13.2 Temperature stabilization of magnet assembly

To get a stable flux density at the operating temperature of the magnet in the air gap, it is necessary to carry out temperature stabilization of the magnet assembly [46]. The procedure for temperature stabilization have been established

based on literature survey and in house experience. This is done by subjecting the magnet assembly to rapid heating and cooling cycles (RHC) and gradual heating and cooling cycles (GHC) at a temperature 50° C above the operating temperature.

Rapid heating and cooling cycles on the 100 NB PMFM magnet assembly, shown Fig. 3.5 is carried out as follows: Magnet assembly is heated in a pre-heated furnace to a temperature of 150 °C and it is soaked for two hours at this temperature. It is then removed from the furnace and allowed to cool to room temperature in air. Flux density value is measured at the geometric centre of the air gap. The above operation is repeated until a stable flux density value is obtained.

Gradual heating and cooling cycles is carried out as follows: Magnet assembly is placed in the furnace and gradually the furnace temperature is raised to 150 °C. The magnet is soaked for two hours at 150 °C. The furnace is then switched off and the magnet is allowed to cool slowly to room temperature in the furnace. The magnet assembly is taken out of the furnace and value of the flux density at the reference point is measured. The above operation is repeated until a stable value of flux density is obtained.

After GHC and RHC, the assembly is endurance tested at the operating temperature of 100 °C for 1000 hours and stable value of flux density in the air gap is confirmed. This completes the temperature stabilization process.

### **3.14 Stabilization and Stability Testing**

The flow meter assembly used for a 32 NB pipe flow meters is selected for stability testing studies. The assembly was made of 72 mm × 35 mm × 100 mm size block magnet and mild steel assembling blocks and pole faces. The assembly was done by SS bolting. The magnet assembly used for stability testing is shown in Fig. 3.9.



The stability of magnet with respect to time at around 100 °C is the main concern. But endurance test at 100 °C for 5000 hours has not shown any variation in the flux density. If the magnet is heated upto 550 °C, the process of demagnetization is same; that is the realignment of weakly aligned magnetic domain due to thermal energy. Above 550 °C, metallurgical and structural changes take place and the process of demagnetization is different. Hence to simulate the long term operation of permanent magnet at low temperature of 100 °C, it was decided to conduct the stability test of magnet at high temperatures but below 550 °C for shorter duration. This accelerated endurance has been conducted on the same assembly at four different temperatures after stabilizing the magnet assembly at temperatures around 50 °C above the endurance test. Accelerated test was selected based on the basic understanding on domain re-alignment process in permanent magnet materials. The process followed for stabilization and flux density variation are shown in Fig. 3.10. The stabilization process involves three RHCs followed by three GHCs. Permanent magnet assembly shown in Fig. 3.9 was initially stabilized at 300 °C. The variation in flux density observed during thermal stabilization process at 300 °C is shown in Fig. 3.10. After ageing for 5000 hours at 50 °C below the stabilization temperature, the assembly was stabilized again at the next higher temperature. Figure. 3.10 indicates the reduction in magnetic flux density during stabilization at each temperature.

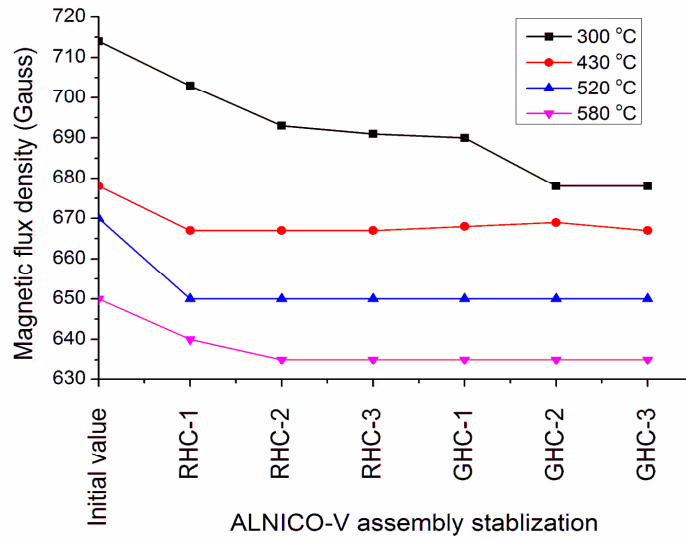


**Fig. 3.10: Alnico-V assembly stabilization process**

### 3.15 Endurance Testing of Magnet Assembly at Higher Temperatures

The magnet assembly after stabilization at 300° C has been subjected to endurance testing for 5000 hours at 250° C. Flux density values at reference point were measured after every 1000 hrs. The flux density measurements were made at room temperature after taking out the assembly from the furnace, and hence the recoverable losses are not taken into account. Evolution of magnetic flux density values with time at various temperatures are shown in Fig. 3.11. It can be seen that stabilized permanent magnet assembly shows a maximum drop of 1.2% in magnetic flux density during endurance testing at 250 °C. Plot of normalized values of magnetic flux density with time is shown in Fig. 3.12. The above experiment was repeated at three different temperatures of 380 °C, 480 °C and 530 °C after temperature stabilization of the assembly at 430 °C, 530 °C and 580 °C respectively. The flux density was monitored after every 1000 hours and the variation is plotted in the same Fig. 3.11. The reduction in flux density observed after endurance test at 250 °C, 380 °C, 480 °C and 530 °C is only 1.2%, -0.3 %, 1.5 % and 1.6 % respectively. It may be noted that the stabilization was done at 580 °C and the endurance test was done only at 530 °C.

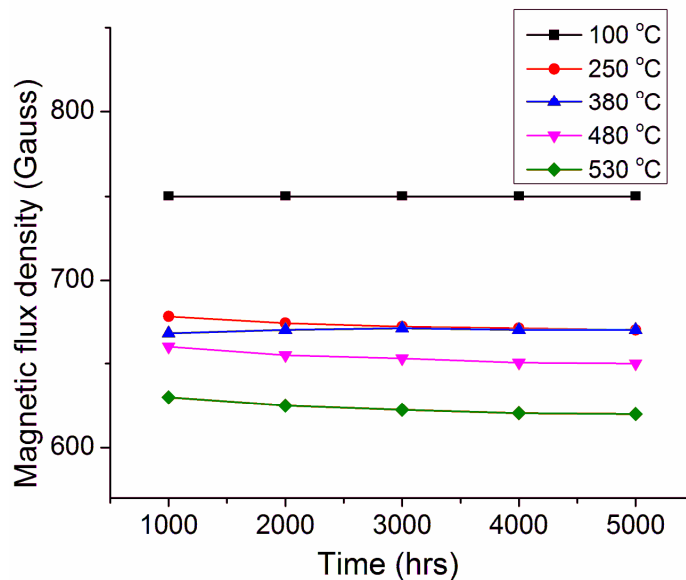
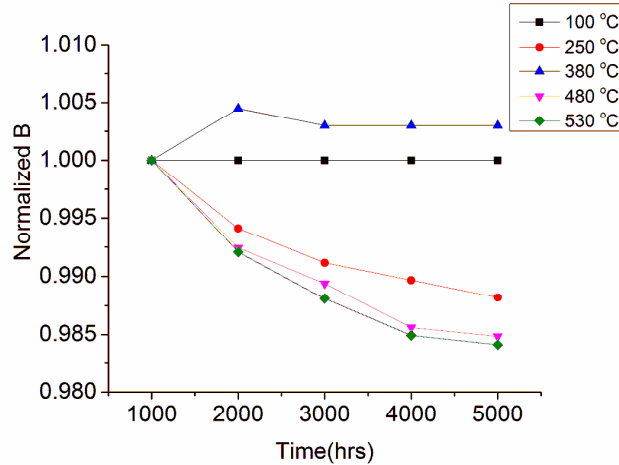


Fig. 3.11: Magnetic flux density Vs temperature



**Fig. 3.12: Normalized magnetic flux density Vs temperature**

Even in the accelerated test, the variation is found to be minimum. At 380 °C, a trend of recovery is noticed even though the absolute value is very small. This type of initial weak rise of field strength is noticed by earlier researchers at 550 °C and 600 °C and the reason attributed by them is precipitation hardening [48].

### 3.16 Reversible Temperature Coefficient

Permanent magnet flow meter for liquid metal flow measurement should have accuracy of minimum  $\pm 5\%$ . Recoverable losses in permanent magnets affect the sensitivity of flow meters at different temperatures. To measure the recoverable losses in indigenous Alnico-V material, the magnet assembly shown in Fig. 3.9 was stabilized at 580 °C and tested at different temperatures. The magnet assembly was provided with tape type of electric surface heater, thermocouples and thermal insulation. Hall probe was positioned in the air-gap and air cooling was provided to limit its temperature below 50 °C. Measured magnetic flux density at various temperatures is shown in Fig. 3.13. Total reduction in magnetic flux density of when magnet temperatures are changed from 30 °C to 550 °C is found to be 12.8 % as shown Fig. 3.13. This corresponds to a value of  $-0.0272 \text{ \%}/\text{°C}$ . Standard specifications for permanent magnet materials [31] gives the reversible temperature coefficient near  $B_r$  and  $BH_{\max}$  of demagnetization curve as  $-0.02 \text{ \%}/\text{°C}$  and  $-0.015 \text{ \%}/\text{°C}$  respectively. When the assembly is cooled to room temperature, the original value is regained. The magnet assembly stabilized at 580 °C is heated to 700 °C to simulate a thermal shock on permanent magnet flow meter. Magnetic flux density values during

30–700–30 °C cycle are shown in Fig. 3.14. Percentage reduction in magnetic flux density values at 30 °C after the cycle is found to be 3.2%, as show in Fig. 3.14.

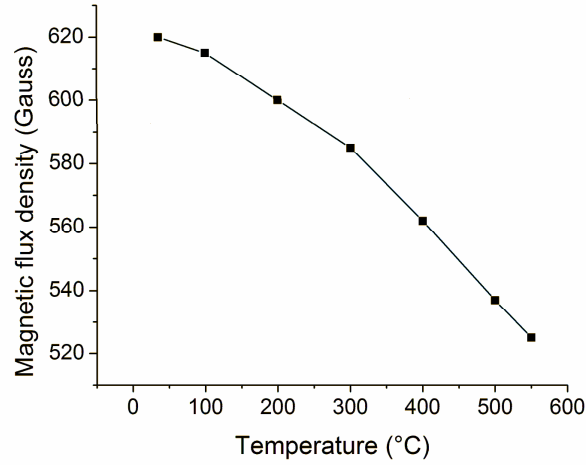


**Fig. 3.13: Air gap magnetic flux density Vs temperature**

Thermal shock testing was also done on a permanent magnet assembly which was magnetically stabilized by AC knockdown and thermally stabilized at 580 °C but not endurance tested. The percentage reduction in magnetic flux density values at 30 °C for not endurance tested permanent magnet assembly after 30 -700 - 30 °C was found to be 7%, indicating better recovery in the thermally stabilized and endurance tested assembly, as shown in Fig. 3.15.

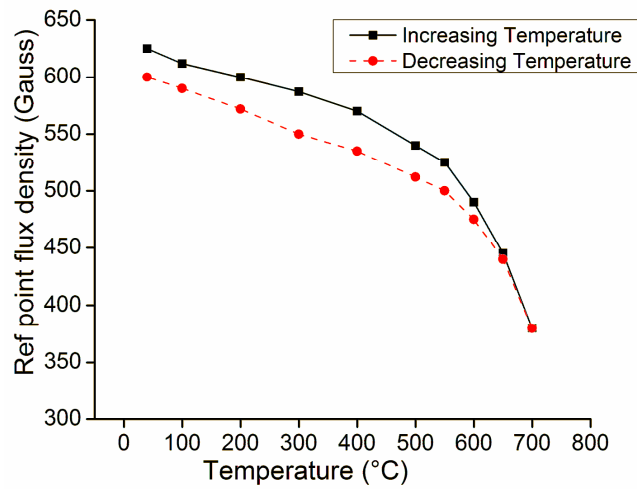


**Fig. 3.14: Flux density Vs temperature for endurance tested magnet assembly**

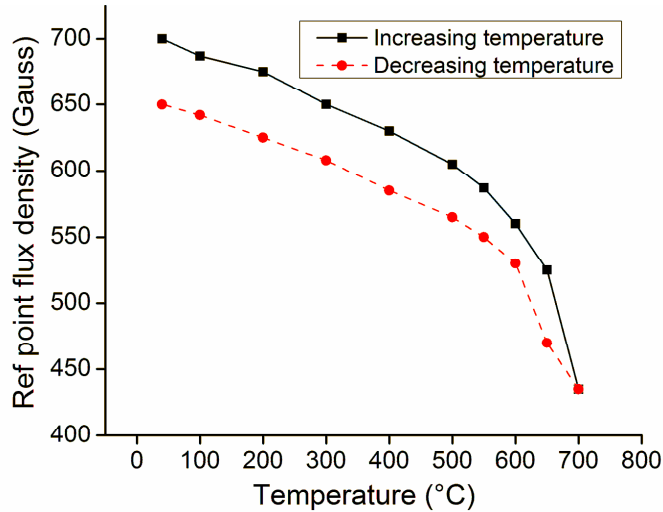


**Fig. 3.15: Flux density Vs temperature thermally for non endurance tested magnet assembly**

### 3.17 Closure

The design methodology of permanent magnet assembly is covered in this chapter. Studies on different types of magnetic field losses in magnet assembly carried out are summarized. Procedures for magnetization, electrical stabilization and thermal stabilization of PMFM magnet assembly have been developed, and validated. Stability tests have been carried out at the operating temperature of the magnet assembly as well as at accelerated conditions. Experimental results show that the air gap flux density is relatively stable during operating conditions of the flow meter. The reversible loss coefficient of flux density has been estimated as  $0.0279\%/^{\circ}\text{C}$  for a typical magnet assembly used in flow meter which matches with the values reported for Alnico-V in the literature. When magnet assemblies are stabilized at  $550^{\circ}\text{C}$  and subjected to a thermal shock of  $700^{\circ}\text{C}$ , the reduction in magnetic flux density value is found to be only 3.2%.

The investigations carried out in this chapter confirm that PMFM based on Alnico-V magnet assembly are stable throughout the life [49]. For low pipe size, these flow meters are compact and they provide adequate sensitivity. So, Alnico-V based PMFM appears to be the best choice for small auxiliary circuits with

pipelines less than 100 NB. However, the weight of the 100 NB Alnico-V based PMFM is around 110 kg, which is very high for a flow sensor, and leads to handling and installation difficulties. The sensitivity is also relatively low. This problem can be addressed by developing alternate design and by use of suitable rare-earth magnets. The next chapter describes the research work taken up to design and develop a compact high sensitive Sm-Co magnet based PMFM suitable for pipe size greater than 100 NB and above.

## CHAPTER 4

### DESIGN AND DEVELOPMENT OF SAMARIUM COBALT BASED PERMANENT MAGNET FLOW METER FOR 100 NB PIPE

#### 4.1 Introduction

In SFRs all over the world, Alnico-V based permanent magnet flow meters are used for flow measurement in pipes. Alnico-V based PMFMs become bulky and heavy, when used for large pipes of diameter 100 NB and above. As the sensitivity of these flow meters is low for higher pipe sizes, it leads to lower resolution in flow measurement. For future reactors, PMFM with Alnico-V magnet assembly is the choice for small pipes below 100 NB size [47]. For sodium flow measurement in pipelines of 100 NB and above, a few other alternate methods are considered [8, 9, 50, 51]. PMFMs with high energy magnetic materials and side wall flow meters (SWFM) are the main options available. The properties of different permanent magnet materials were studied, to assess their suitability to use for liquid sodium flow measurement in SFR circuits. For the operating conditions of SFR sodium circuits, magnet assemblies made of  $\text{Sm}_2\text{Co}_{17}$  are found to be suitable and selected as the magnetic material for the new design of flow meter. As part of the research work, a flow meter for 100 NB pipe with Sm-Co magnet assembly has been analyzed, designed, fabricated and tested in a sodium system and the feasibility is established. Overall weight and sensitivity of this new design of flow meter is compared with Alnico-V based flow meters. Three dimensional finite element modeling (FEM) has been carried out to establish modeling as an alternate method for design and calibration of Sm-Co based PMFMs. In the computational simulation, magnetic field distribution across the flow meter pipe and its effect on the flow meter voltage signal have been analyzed. Effect of sodium temperature on the flow meter voltage signal and its change, with variation in sodium flow rate have been predicted with modeling and compared with the

experimental results. This chapter describes the research and development activities carried out towards development and evaluation of 100 NB pipe size Sm-Co based PMFM.

## 4.2 Compact Flow Meter Development

It was essential to design and develop compact PMFMs due to inherent problems in Alnico-V flow meters. Weight of the flow meters for all pipe sizes has to be reduced, however, it is very essential for pipe size above 100 NB. Weight of the 100 NB pipe Alnico-V based PFBR flow meter is around 110 kg and the sensitivity is  $0.141 \text{ mV/m}^3/\text{h}$ . Research on compact flow meter development was initiated earlier, and a Sm-Co based PMFM suitable for 20 NB pipe was manufactured and tested [51,52]. For flow measurement in pipe size from 100 to 200 NB, side wall flow meter (SWFM) and PMFM with Sm-Co based magnet assembly are the options selected for further research based on initial studies.

SWFM is a passive, non invasive, permanent magnet based flow meter which does not require any special welding or penetration in the pipe. SWFM also possesses the inherent advantage of PMFM, that it does not need a power supply. As the Alnico-V permanent magnet block is positioned on one side of the flow meter pipe side wall flow meter does not have symmetric magnetic flux density in SS pipe. Hence, the correction factors of the pipeline flow meters cannot be used directly for predicting its sensitivity. The studies carried out on SWFM as part of the research are described in detail in the next chapter.

Design, manufacture and testing of a 100 NB  $\text{Sm}_2\text{Co}_{17}$  flow meter in sodium system has been carried out to establish the feasibility. A 100 NB size flow meter has been selected for design and development as various parameters can be compared with the Alnico-V flow meter of same size already manufactured and tested. The following points are identified as the targets of compact flow meter design and development.

- a) The pole face width and length of the Sm-Co magnet assembly should be same as Alnico-V magnet assembly.

- b) Length of the air gap should be same or more than Alnico-V PMFM.
- c) Overall weight should be brought down significantly (by around 40%) in comparison to the Alnico-V PMFM of 110 kg weight.
- d) The sensitivity of the flow meter should be substantially increased. It shall be double that of the Alnico-V based PMFM, which is 0.141 mV/m<sup>3</sup>/h..
- e) Flow meter should be suitable for use upto 550°C sodium temperature.
- f) Stability of PMFM sensitivity with respect to time, temperature and other demagnetizing effects should be ensured.

Earlier studies revealed that these targets can be achieved by optimizing the design and by using suitable rare-earth magnets such as samarium cobalt (Sm<sub>2</sub>Co<sub>17</sub>) [31]. Design features of the 100 NB Sm-Co PMFM are given in Table 4.1.

**Table 4.1: Design features for 100 NB flow meter**

Description	Values for Alnico-V PMFM	Values for Sm-Co PMFM
Pipe size OD/ID	114.3/102.3 mm	114.3/102.3 mm
Pipe length	1000 mm	1000 mm
Mounting	Horizontal	Horizontal
Weight	110 kg	66 kg
Pairs of Electrode	3	3
Internal pressure	4 bars	4 bars
Sodium Temperature	550° C	550° C
Flow range	0 - 150 m <sup>3</sup> /h	0 - 150 m <sup>3</sup> /h
Principal Signal	20 mV	>40 mV
Sensitivity	0.141 mV/m <sup>3</sup> /h	>0.28 mV/m <sup>3</sup> /h

### 4.3 Magnetic Circuit Design

The rare earth magnet alloys are usually formed by powder metallurgical process. The magnetic performance of all the grades of the rare-earth magnets is optimized by applying a magnetic field during the pressing operation, thus producing a preferred direction of magnetization. Pressing and aligning techniques can substantially vary the degree of orientation and the residual induction ( $B_r$ ) of the finished magnet.

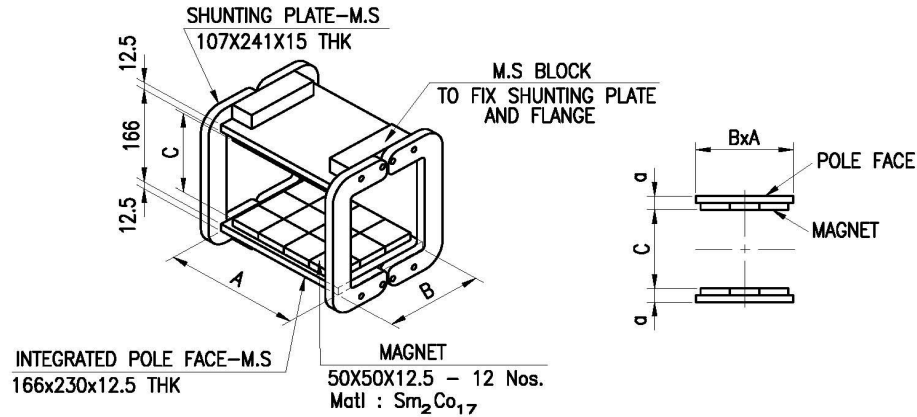
**Table 4.2: Comparison of magnetic properties**

Material	Alnico-V	Alnico-VIII	Sm-Co <sub>5</sub>	Sm <sub>2</sub> Co <sub>17</sub>	Nd-Fe-B
$(BH)_{max}$ , MGOe	6.5	5.3	16-22	24-30	25-50
$B_r$ , Gauss	13300	8200	8300-9500	10000-11600	10000-14000
$H_c$ , Oersted	670	1650	7500-9000	6000-10600	9600-12700
$H_{ci}$ , Oersted	670	1850	16000-30000	7000-26000	1100-41000
Density, g/cc	7.3	7.3	8.4	8.4	7.4
Reversible temperature coefficient, °C	-0.02	-0.025	-0.040	-0.035	-0.090
Curie temperature, °C	860	860	750	825	310
Maximum operating temperature, °C	525	550	300	350	150

The alloy Sm<sub>2</sub>Co<sub>17</sub> is with a chemical composition ratio of 2 rare earth atoms to 17 atoms of transition metals. Transition metal (TM) content is a cobalt rich combination of cobalt, iron and copper. Small amounts of zirconium, hafnium or other elements are also added to enhance the heat treatment response. The rare-earth content of Sm<sub>2</sub>Co<sub>17</sub> materials is typically 23 to 28 weight percent of the alloy.

When the flow meter is operating at a sodium temperature of 550 °C, magnet temperature will be around 100 °C. Maximum operating temperature of  $\text{Sm}_2\text{Co}_{17}$  is 350 °C, which gives a good margin. Rectangular blocks of 50× 50 × 12.5 mm size, magnetically oriented along 12.5 mm, were selected for the flow meter magnet assembly. 24 blocks have been used for making the assembly. This magnet size was based on the design calculations made and the availability of standard size of  $\text{Sm}_2\text{Co}_{17}$  blocks in open market.

To minimize the end effects due to the finite length of the magnetic field in the flow meter, pole face length of the magnet assembly in the direction of flow is about 2.25 times the pipe ID. To minimize the non-uniformity of the magnetic field along the electrode axis, pole face width is taken more than the pipe diameter. It is also preferable that the magnets operate at a relatively lower temperature and this has been achieved by covering the sodium pipe with thermal insulation. For 100 NB pipe flow meter which operates at 550°C, an insulation thickness of 10 mm was considered adequate. Based on the above considerations, the dimensions selected for the magnet assembly are of pole face length - 225 mm, pole face width -166 mm and air gap length -141 mm. These dimensions are very close to the Alnico-V based 100 NB pipe PMFM manufactured earlier as part of the present research work (refer chapter 2). In order to make magnet assembly compact, integrated pole face concept was considered. In this arrangement, magnet blocks are spread over the pole face surface and suitably clamped using magnet holder cover plate. Entire surface area of both the poles are covered with magnet blocks, as shown in Fig. 4.1. Four MS blocks are welded on the outer surface of pole face for fixing the shunting plate and the pipe fixing flange. The cover of the flow meter and the eye bolt of the flow meter are also fixed to these MS blocks.



A : POLE FACE LENGTH-230mm; B : POLE FACE WIDTH-166mm; C : AIR GAP-141mm, a : 25mm

**Fig. 4.1: Dimensions of Sm-Co magnet assembly for 100 NB pipe PMFM**

Dimensions have been selected for the magnet assembly as shown in Fig. 4.1. A reference point is provided to measure the flux density of the assembly during service of the flow meter. Integrated pole face, with magnet blocks linked by shunting plates at both end of the pole face and on both sides makes it a parallel magnetic circuit. This arrangement allows the completion of magnetic circuit through four paths, which helps in achieving uniform flux density in the air gap. SS 316 LN pipe as per ASTM standard is used as the pipe material. SS sheathed MgO insulated cable, with SS316 LN conductor is used as electrode and three pairs of electrodes are provided. The electrode conductor is of the same material as that of the pipe to minimize thermal EMF. All the welds on pipe are carried out by qualified welder and examined by liquid penetrant test. The flow meters are finally qualified by a pneumatic and helium leak tests. The flow meters were covered with nonmagnetic perforated SS sheets for ventilation and cooling the magnet assembly. Thermal insulation is provided on the pipe, between the pipe support flange and the magnet assembly, to limit the temperature of the magnet during operation. A three dimensional view of the Sm-Co PMFM is shown in Fig. 4.2. The pipe and electrode axes are made perpendicular to each other. The electrode axis is made close to the centre line of pole face with a 10 mm shift towards downstream. This is achieved by a stud and slot arrangement in pipe and pipe fixing flange, which also prevents rotation and axial movement of the pipe with respect to the magnet assembly (Refer Fig. 2.4).

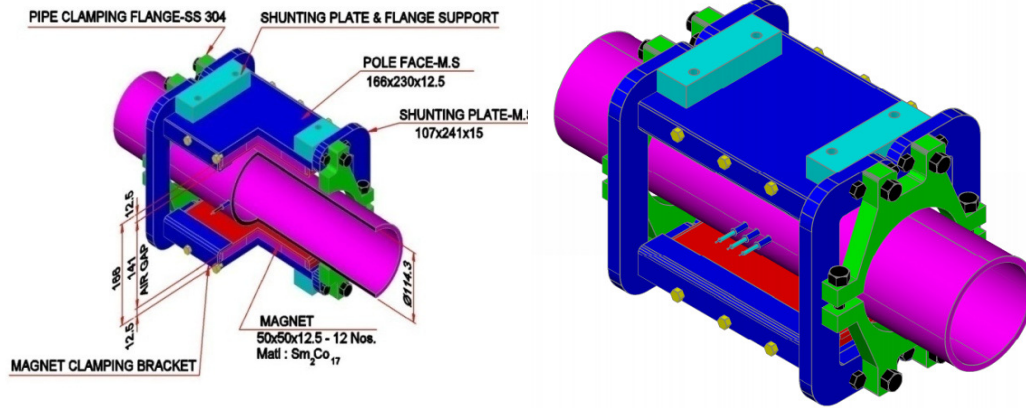


**Fig. 4.2: Three dimensional view of 100 NB pipe Sm-Co PMFM**

Two equations (3.1) and (3.2). control the various parameters involved in the calculation of magnetic circuits with air gap. As per equation (3.4)

$$\frac{B_m}{H_m} = \frac{L.F \times B_g \times A_g \times L_m}{R.F \times H_g \times L_g \times A_m}$$

The assembly under consideration is unique in nature, and no standard formula is available for leakage factor calculation. However, leakage factor was calculated using the following equation which is an approximation [45].

$$L.F = 1 + \left( L_g / A_g \right) \left[ 0.67 U_a \left\{ 1.7 \times 0.67 a / (0.67 a + L_g) + L_g / 2a \right\} \right] \quad (4.1)$$

$A_g, L_g$  : Area and total length of air gap in the magnetic circuit, respectively

$L_g$  : 0.141 m

$A_g$  : 0.03818 m<sup>2</sup>

$a$  : 0.025 m ; Dimension of part,  $a$  in the assembly

$U_a$  : 0.700 m ; Perimeter of cross section of part a, in the assembly

The value of  $LF$  is calculated as 6.2. For this type of assembly,  $RF$  varies from 1.1 to 1.5. An average value of 1.35 is assumed as  $RF$ .

$A_m$ :  $0.03 \text{ m}^2$  ; Area of permanent magnet blocks

$L_m$  :  $0.025 \text{ m}$  ; Total length of permanent magnet blocks

The value of  $B_m/H_m$  as per equation (3.4) is calculated as 1.07. From the demagnetisation curve of  $\text{Sm}_2\text{Co}_{17}$  (Fig 4.3),  $B_m$  corresponding to  $B_m/H_m$  equal to 1.07 is found to be 0.23 Tesla.  $B_g$  is then calculated as 0.7 Tesla using equation (3.1).

$$B_g = \frac{B_m \times A_m}{L.F \times A_g}$$

Various parameters of the magnetic circuit are varied and flux density value in the air gap was determined using a computer code in FORTRAN, developed in house. The design of the magnetic circuit has been carried out using the above procedure and the size and number of magnet blocks required to achieve the required air gap flux density were arrived at. Magnet assembly as per the design has been fabricated and was then magnetized as a whole to saturation with a mild steel keeper block in the air gap. The magnet assembly was magnetically stabilized by AC knockdown process and thermally stabilized at  $150^\circ\text{C}$  by heating and cooling cycles. Flux density at the air gap centre, reference point and various locations in the sodium flow region was measured. The average flux density obtained was 0.1005 Tesla. Procedure as per section 3.10 and 3.13 was followed for magnetization and stabilization respectively. The actual value of flux density obtained was 30% higher than the design value of flux density. This is mainly because of the large value of leakage factor calculated by the equation (4.1) which is not directly applicable for this type of magnet assembly.

#### **4.4 Sensitivity of Sm-Co Flow meter**

Sensitivity of Sm-Co has been estimated in the same way as described in section 2.4. Analytically, the potential difference developed across electrodes

was calculated by dimensional measurements, average flux density measurement in the air gap of the flow meter assembly and by estimating the flow velocity at unit flow rate. Hall probe type gauss meter with an accuracy of  $\pm 1\%$  was used for magnetic flux density measurements. Flux density at various points across the cross section of pipe and at different planes adjacent to electrodes have been measured and averaged. Amplitude of voltage signal developed in a PMFM across a pair of electrodes at unit flow rate was calculated using equation (2.1). Pipe wall correction factor ( $K_1$ ) at  $350^\circ\text{C}$  was calculated as 0.972. End effect correction factor ( $K_2$ ) is a function of pole face length to pipe ID ratio [7]. For a pole face length of 0.225 m and pipe ID 0.1023 m, the above ratio is 2.2 and the correction factor ( $K_2$ ) is 0.975. Temperature correction factor ( $K_3$ ) which takes into account flux change due to temperature is  $1 - (T_m - 30) \times 0.00035$ , where  $T_m$  is the operating temperature of the magnet during operation, and is taken as  $100^\circ\text{C}$ . The temperature coefficient value of 0.00035 is taken for Sm-Co materials and is based on the data available in MMPA standard [31]. So,  $K_3$  was calculated as 0.9755. Analytically, the sensitivity of the flow meter at  $350^\circ\text{C}$  has been calculated as  $0.32 \text{ mV/m}^3/\text{h}$  using equation (2.1).

#### **4.5 Numerical Simulation of Flow Meter**

In PMFM the average sodium flow rate in SS pipe is measured by the voltage generated in liquid sodium due to its motion in the steady magnetic field. To obtain maximum motional voltage for a particular flow rate, magnetic field, sodium velocity and electrode plane are kept mutually perpendicular to each other. Due to PMFM's geometry and working principle, a three dimensional model has to be used to simulate it for its true representation [52, 53, 54, 55]. Multiphysics modelling of PMFM is done in the FEM code COMSOL 3.5a [56]. Modelling involves magnetostatics, incompressible Navier Stokes and DC conduction application modules of the software. Tetrahedral mesh elements were used in simulation. Model becomes highly non linear due to incorporation of BH curves and flow simulation. Hence, the problem was divided into, magnetic circuit simulation, sodium flow velocity simulation and flow meter voltage signal simulation. A sequential approach has been adopted for the solution.

#### 4.5.1 Magnetic circuit simulation

In the first step, liquid sodium was kept stationary and magnetic field generated by magnetic circuit is simulated using demagnetising curves of Sm-Co magnet and mild steel blocks shown in Figs. 4.3 and 4.4 respectively. Three dimensional model of flow meter with dimensions in Fig. 4.2 was used to simulate the magnetic field with magnetostatics application module in FEM code (COMSOL 3.5a). Three dimensional model of the 100 NB pipe Sm-Co flow meter simulated in COMSOL is shown in Fig. 4.5. Magnetostatics problem has been solved with FMGRES iterative solver along with geometric multi grid pre-conditioner. Total number of mesh points which is same as number of nodes taken in simulation are 28291 with 165273 tetrahedral mesh elements. Since many nodes are internal ratio is not matching.

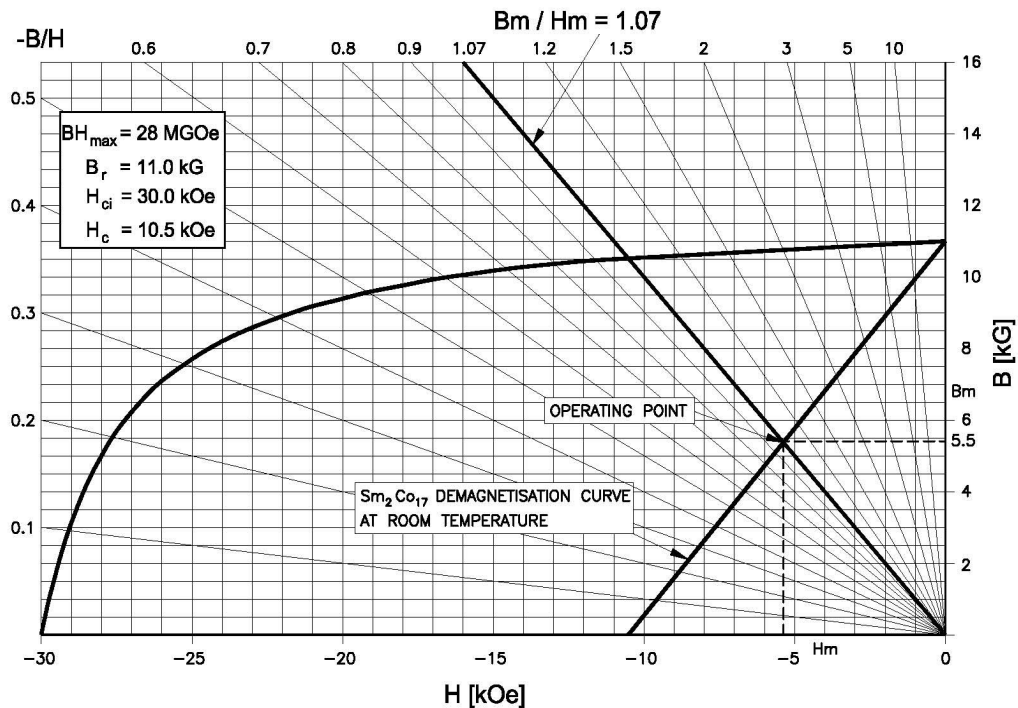
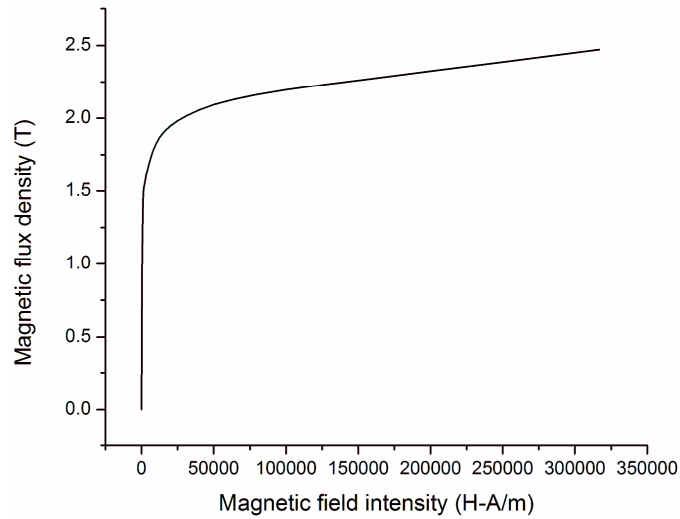
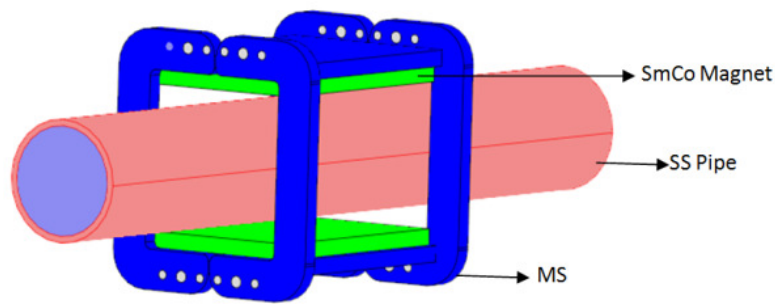


Fig. 4.3: Operating point of PMFM on the demagnetization curve of  $\text{Sm}_2\text{Co}_{17}$



**Fig. 4.4: BH curve for soft iron parts of the Sm-Co magnet assembly**



**Fig. 4.5: 3D model for 100 NB flow meter**

#### 4.5.2 Sodium flow simulation

The pipe through which the liquid sodium flows offers frictional resistance to the flow and this leads to development of a non uniform velocity profile across the flow area of the pipe. This velocity profile attains a fully developed condition and remains invariant after a certain flow length. The steady state profile of the sodium flow velocity across the flow area is predicted by solving three dimensional Navier-Stokes equation with proper boundary conditions. Physical properties like density and dynamic viscosity of sodium corresponding to the sodium temperature has been used for the calculation. No slip boundary condition is chosen at boundary along with SS pipe and inlet boundary condition is

taken as fixed velocity corresponding to sodium flow rate. The position of the electrodes in the model of the flow meter has been kept sufficiently away from the inlet such a way that a fully developed sodium flow profile will form at the electrode location. In testing and calibration of 100 NB Sm-Co flow meter, sodium flowrates were varied from 14 m<sup>3</sup>/h to 146 m<sup>3</sup>/h. Sample velocity profile plots in pipe cross section for flow rates of 14 m<sup>3</sup>/h to 146 m<sup>3</sup>/h are shown in Fig. 4.6 and Fig. 4.7 respectively.

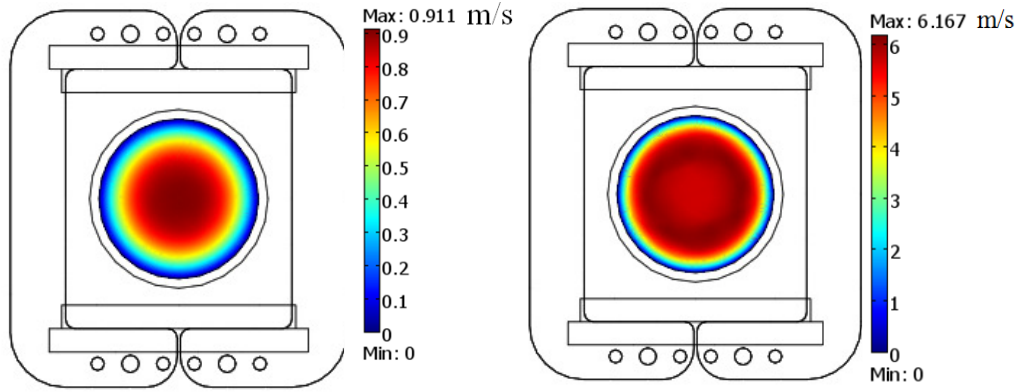


**Fig. 4.6 :** Velocity profile for flow rate of 14 m<sup>3</sup>/h **Fig. 4.7:** Velocity profile for flow rate of 146 m<sup>3</sup>/h

#### 4.5.3 Simulation for flow meter voltage signal

Sm-Co flow meter voltage signal developed for a particular sodium flow is calculated using conductive media DC application module in COMSOL. Loss of voltage signal generated in liquid sodium depends on electrical conductivity values of sodium and SS pipe at the operating temperature. To account for the loss of voltage signal in modelling, electrical conductivities of SS pipe and liquid sodium at different temperatures were calculated using the following equations and used in modelling.

$$\rho(SS) = 6.96 \times 10^{-7} + 8.78 \times 10^{-10} T + 3.01 \times 10^{-13} T^2 \quad (\Omega \cdot m) \quad (4.2)$$

$$\rho(Na) = 8.14 \times 10^{-8} + 2.27 \times 10^{-10} T - 2.98 \times 10^{-13} T^2 \quad (\Omega \cdot m) \quad (4.3)$$

Magnetic flux density distribution in Tesla in the magnetic circuit of the flow meter is shown in Fig. 4.6. From the figure it can be seen that the flux density in all four shunting plates is high but below the saturation value. The relative permeability in different parts of the magnetic circuit is shown in Fig. 4.8. Relative permeability is low at points wherever flux density is high.

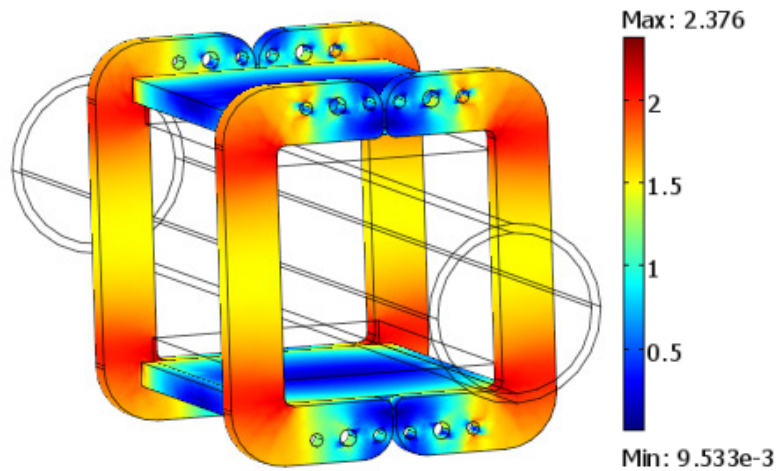


**Fig. 4.8:** Magnetic flux density (T) distribution in the magnetic circuit of the flow meter

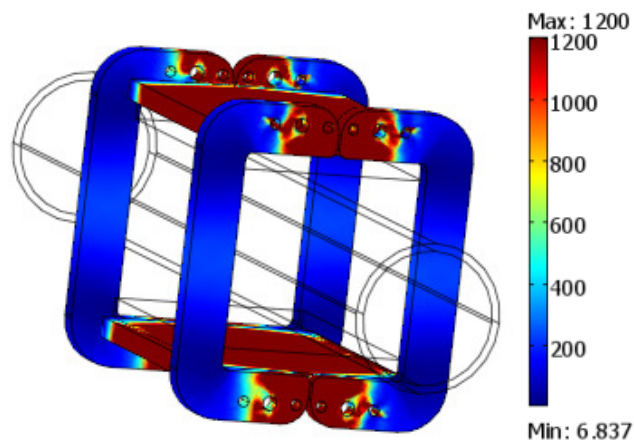


**Fig. 4.9:** Relative permeability in the magnetic circuit of Sm-Co flow meter

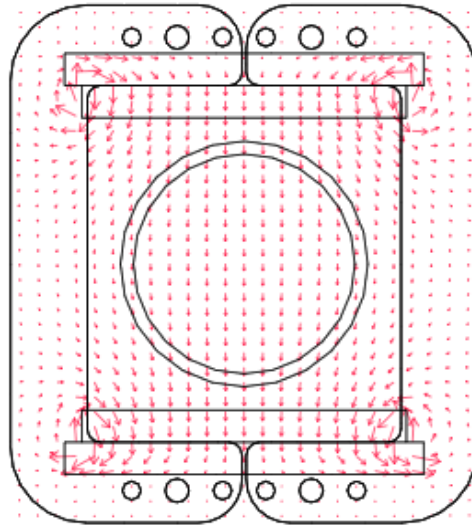


**Fig. 4. 10: Vector plot of magnetic field in the PMFM assembly**

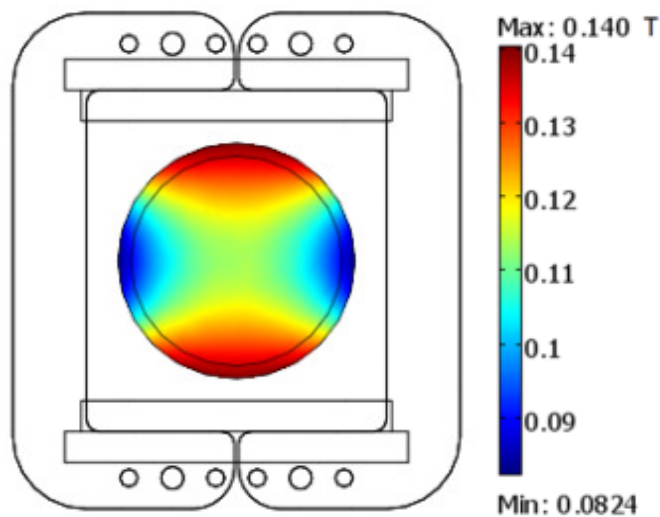


**Fig. 4.11 : Magnetic flux density (T) distribution in pipe**

Vector plot of magnetic flux density on the plane at the centre of pole face and perpendicular to sodium flow is shown in Fig.4.10. Arrows represent the direction of magnetic field. . Amplitude of magnetic flux density distribution at the cross-section of SS pipe at the centre of pole face is shown in Fig. 4.11 The direction of magnetic field is perpendicular to the flow direction and electrode axis in the inner region of the pipe.. Flux density is high near to the pole faces as expected.

The voltage signal generated due to motion of sodium at 17 m<sup>3</sup>/h, in steady magnetic field, across SS electrodes placed at the centerline of the pole face of the magnet assembly is shown in Fig. 4.12. The voltage gradient is uniform across the pipe. The voltage output of the Sm-Co based PMFM at different flow rates for three different sodium temperatures of 250 °C, 350 °C and 450 °C based on analysis is shown in Fig. 4.13. Output of flow meter is linear for flowrates ranging from 14 m<sup>3</sup>/h to 140 m<sup>3</sup>/h..

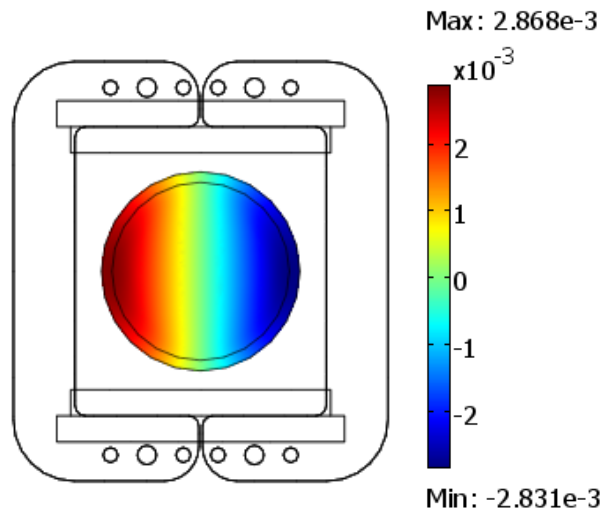


**Fig. 4.12: Voltage across the electrodes at the center line of pole**

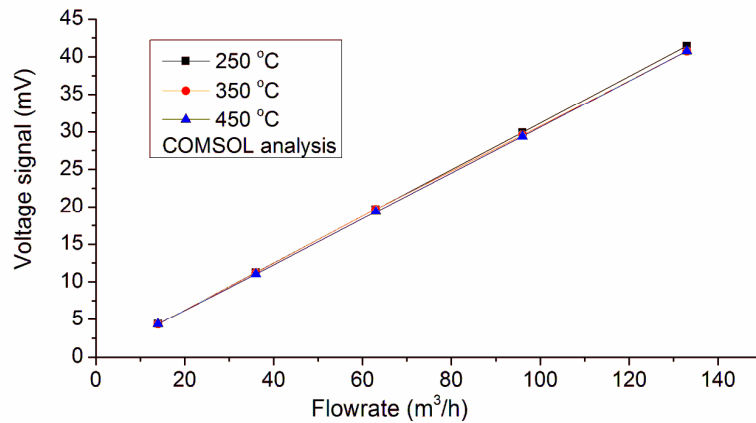


**Fig. 4.13: Output voltage verses flow based on COMSOL analysis**

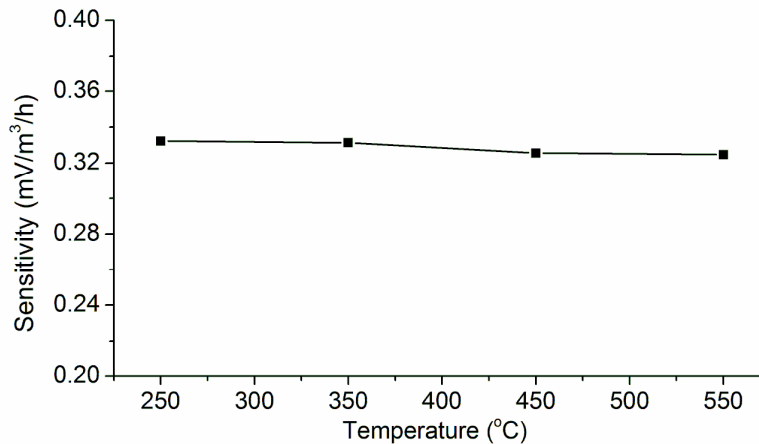


**Fig. 4.14: Predicted sensitivity variation with temperature from COMSOL analysis**

From Fig. 4.13, it is clear that the voltage output is fairly linear with respect to flow. The magnitude of the voltage is good enough for the measurement. The change in the voltage output with respect to temperature is as expected and found to be minimum. The sensitivity of the Sm-Co PMFM for different sodium temperatures is shown in Fig. 4.14. The sensitivity value is almost double that of Alnico-V flow meter of the same size. The sensitivity reduces as temperature increases but very marginally.

#### **4.6 Testing and Calibration of Sm-Co PMFM for Sodium Flow**

The testing and calibration of Sm-Co PMFM with sodium is carried out in the existing calibration setup. The details of the setup are available in section 2.7.1. All the three pairs of signal electrodes were connected to the multichannel data acquisition system. Calibration of the flow meter has been carried out by constant volume method (absolute method) in the sodium system. The procedure followed for calibration was same as the one discussed in section 2.7.3.

The calibration of flow meter has been done at various flow rates and at various sodium temperatures. The trace of the output voltage with respect to time at the sodium flow rate of 133 m<sup>3</sup>/h is shown in Fig. 4.15. The complete area under the flow trace curve corresponds to the total sodium drained. The reduction in flow

with respect to time is due to reduction in head during draining.. The milli volt seconds obtained is equated to the volume of sodium drained and sensitivity of the flow meter is determined. The calibration runs were repeated at 350 °C and 450 °C and at different flow rates for assessing the variation in sensitivity with temperature and flow. The sensitivity of the Sm-Co PMFM at each calibration point is calculated using the equation (2.4), i.e.,

$$\begin{aligned} \text{Sensitivity } S &= (v \times t) / (Q_{SV}) \text{ mVs/m}^3 \\ &= (v \times t) / (Q_{SV} \times 3600) \text{ mV/m}^3/\text{h} \end{aligned}$$

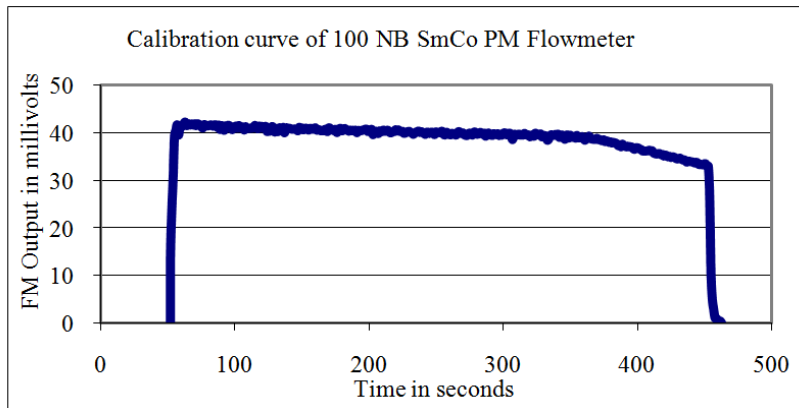


**Fig. 4.15: Output voltage trace during calibration at a sodium flow rate of 133 m<sup>3</sup>/h**

Sm-Co PMFM have three pairs of electrodes to record the voltage signal generated for a particular flow. The upstream pair (UE) was placed 5 mm upstream side of the pole face central line. The central electrode pair (CE) and downstream electrode pair (DE) were positioned 10 mm and 25 mm downstream side of the pole face central line respectively. Plots of Sm-Co PMFM sensitivity, determined by in-sodium calibration of the three pairs of the electrodes at different temperatures (250 °C, 350 °C, 450 °C and at various flow rates are shown in Figs. 4.16-4.18, respectively. The sensitivity marginally reduces (less than 5 %) in the full flow range of testing, at all the temperatures tested. It can be seen from the plots that the downstream electrodes have relatively lower sensitivity at lower flow rates and relatively higher sensitivities at higher flow rates compared to central

electrodes at all the three temperatures. This increase in sensitivity of downstream electrodes at higher flow rates is due to magnetic field sweeping in downstream direction for higher magnetic Reynolds number [14]. Figure 4.19 shows the percentage variation in sensitivity in the three pairs of electrodes at the full flow range of calibration. Variation in the sensitivity of the Sm-Co PMFM and Alnico -V PMFM with sodium temperature is shown in Fig. 4.20. PMFM sensitivity reduces by around 2 %, when the sodium temperature is increased from 250 °C to 450 °C. Sm-Co PMFM voltage acquired across downstream, upstream and central electrode pairs for various sodium flow rates at 350 °C are shown in Fig. 4.21. Sm-Co PMFM voltage varies from 4.74 mV to 39.5 mV in the full flow range.

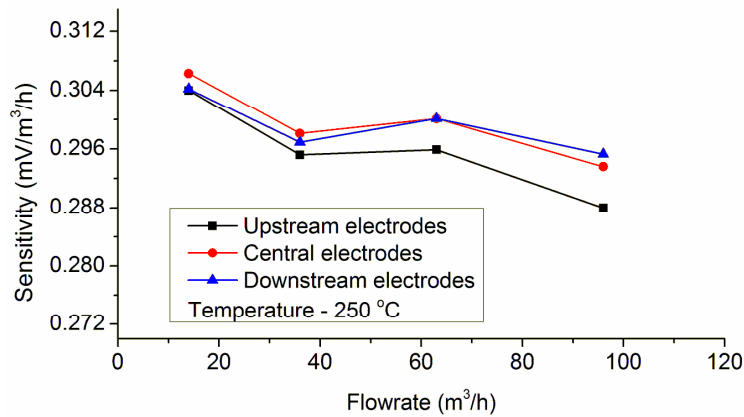


**Fig. 4.16: Sm-Co PMFM sensitivity verses flow rate at 250 °C**

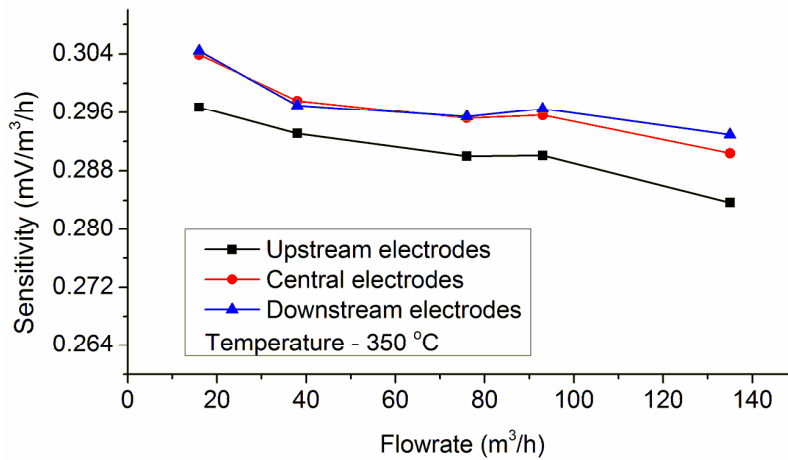


**Fig. 4.17: Sm-Co PMFM sensitivity verses flow rate at 350 °C**

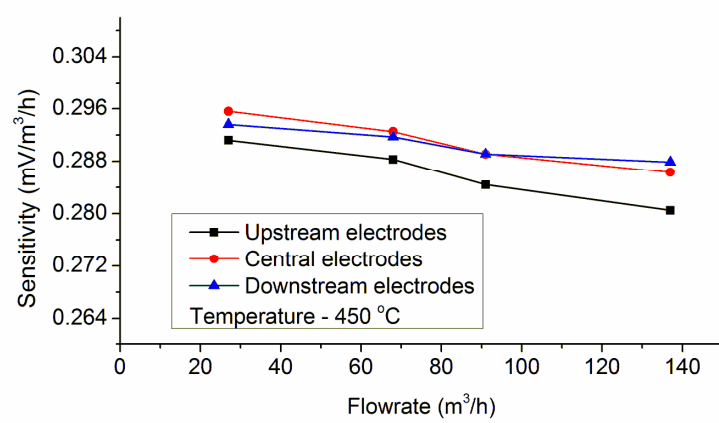


**Fig. 4.18: Sm-Co PMFM sensitivity verses flow rate at 450 °C**

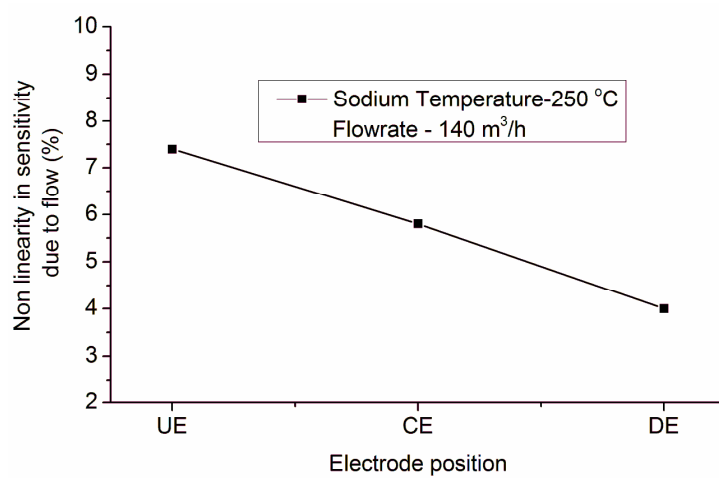


**Fig. 4.19: Non linearity in sensitivity due to flow at 140 m³/h**

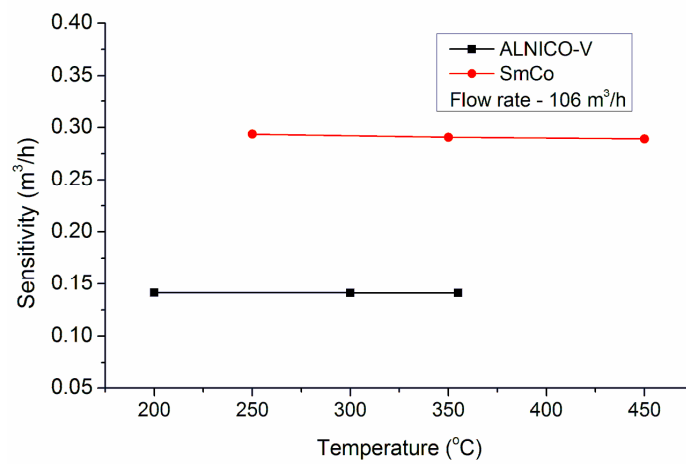


**Fig. 4.20: Sensitivity variation with temperature**

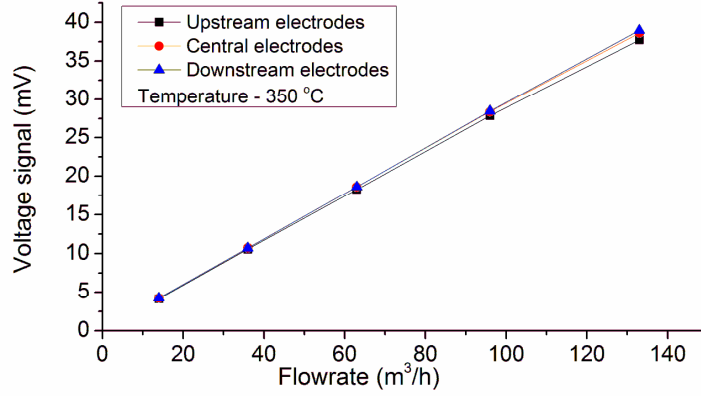


**Fig. 4.21: Experimental voltage of Sm-Co at 350 °C**

#### 4.7 Error Analysis of Sm-Co Flow Meter Sensitivity

The accuracy of calibration or error involved in the calibration is estimated, as in the section 2.8.

$$\Delta S = \left| \frac{\partial(S)}{\partial v} \times \Delta v \right| + \left| \frac{\partial(S)}{\partial t} \times \Delta t \right| + \left| \frac{\partial(S)}{\partial Q_{SV}} \times \Delta Q_{SV} \right|$$

$\Delta v$ ,  $\Delta t$ ,  $\Delta Q_{SV}$  are to be estimated to estimate the error in sensitivity  $\Delta S$ .

Total error in milli volt measurement  $\Delta v$  is estimated as 34.43 micro volts as in section 2.8.1.

$$\left| \frac{\partial(S)}{\partial v} \times \Delta v \right| = 0.00025$$

Total error in time measurement  $\Delta t$  is assumed as one second.

$$\left| \frac{\partial(S)}{\partial t} \times \Delta t \right| = 0.00069$$

Error in SV volume estimation, for an assumed error of 5 mm in the dimensional measurement is calculated in section 2.8.3 as  $0.1158 \text{ m}^3$

$$\left| \frac{\partial(S)}{\partial Q_{SV}} \cdot \Delta Q_{SV} \right| = 0.00209$$

Total error in sensitivity of Sm-Co flow meter calibration is

$$\Delta S = 0.00025 + 0.00069 + 0.00209 = 0.00303$$

$$\% \text{ Error} = (\Delta S/S)100 = (0.00303/ 0.28381)\times 100 = 1.1\%$$

From the error analysis it is clear that the calibration accuracy is 1.1%.

#### 4.8 Comparison Between Analysis and Experimental Results

Experimental and computational results of the flow meter output voltage and the sensitivity are compared in Figs. 4.22 and 4.23 respectively. At a low flow rate of 14 m<sup>3</sup>/h, the variation between the experimental and the computational results is only 1.91 %. This increases with increase in the flow rate and reaches its maximum value of 7.38 % at the maximum flow rate of 133 m<sup>3</sup>/h. In the computations, effects of motional currents and end currents on resultant magnetic flux density have not been considered, which lead to increase in error between simulation and experimental results at higher sodium flows. The difference between simulation and experimental results at higher sodium flows. The difference between experimental and computational voltage is shown in Fig. 4.24. Experimentally observed value of flow meter sensitivity is 0.2837 mV/m<sup>3</sup>/h, while analytically estimated value of flow meter sensitivity as per section 2.4 is 0.32 mV/m<sup>3</sup>/h. The difference between the experimental and analytically estimated values of flow meter sensitivity is around 12%.

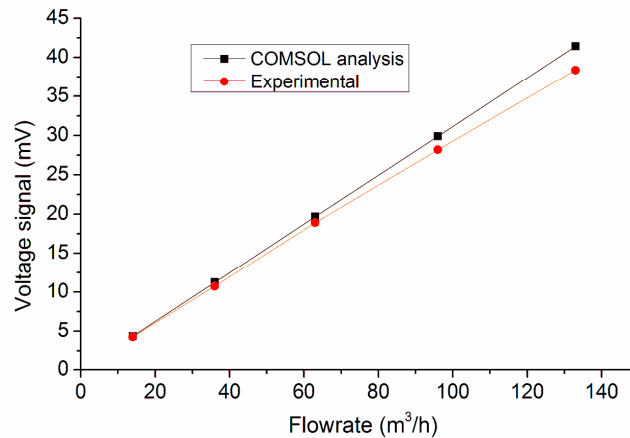


**Fig. 4.22: Comparison between experimental and computational output voltage**

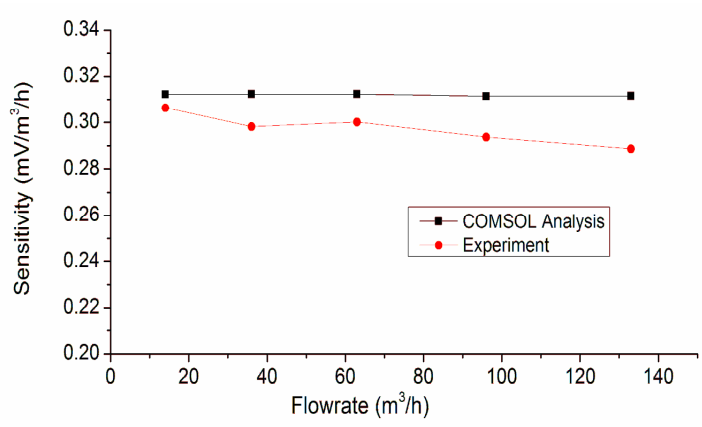


**Fig. 4.23: Comparison between experimental and computed sensitivity for different flow rates**

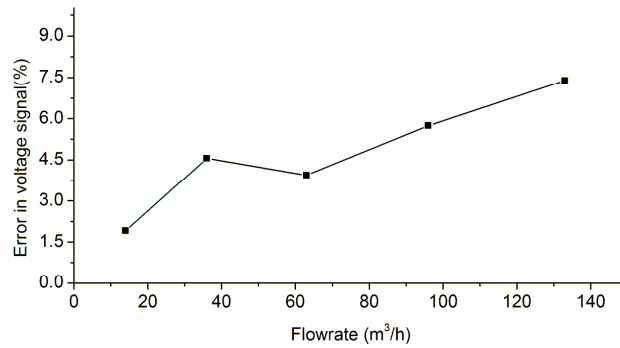


**Fig. 4.24: Error between the experimental and predicted voltage with flow rate**

#### 4.9 Comparison of Sm-Co PMFM with Alnico-V PMFM

The main performance parameters of Alnico-V based permanent magnet flow meter are compared with the Sm-Co flow meter and are tabulated in Table 4.3.

**Table 4.3: Comparison Sm-Co and Alnico-V PMFM**

Property	Alnico-V PMFM	Sm <sub>2</sub> Co <sub>17</sub> PMFM
B <sub>avg</sub> at center of SS pipe	0.0495 T	0.1005 T
Magnet Temperature	<100 °C	<100 °C
Weight	110 kg	49.5 kg
Sensitivity	0.141 mV/m <sup>3</sup> /h	0.285 mV/m <sup>3</sup> /h
Volume of magnet	1512 cm <sup>3</sup>	750 cm <sup>3</sup>

It can be seen from Table 4.3 that Sm-Co flow meter sensitivity increased by 102 % with a net weight reduction of 55%.

#### **4.10 Stability Test on Sm-Co Magnet Assembly**

Stability of the magnetic field with respect to time is the most important requirement of Sm-Co PMFM. Electrical and thermal stabilization procedures of Sm-Co magnet assembly was same as that of Alnico-V assembly, described in Section 3.13.

For conducting long term stability test, two magnet assemblies shown in Fig 4.25 were selected. These magnet assemblies are suitable for 20 NB pipe size flow meter. The magnet blocks used were  $\text{Sm}_2\text{Co}_{17}$ . The operating point of the assembly in the demagnetization curve are in the same region as that of the 100 NB pipe PMFM magnet assembly. Initially, one assembly was stabilized at 150 °C and the stability test was carried out at the normal operating temperature of 100 °C for 5000 hours. Flux density measurement were made after every 1000 hours of ageing. No reduction in the flux density was observed after 5000 hours of ageing.



**Fig. 4.25: Magnet assemblies selected for stability test**

Another assembly was stabilized at 250 °C and the stability testing was carried out at 200 °C. This testing was carried out for 10000 hours and no significant

reduction in the flux density was noticed. The flux density was measured at every 1000 hours at the reference point and at the air gap centre and the results are shown in Fig. 4.26. These test results confirm the satisfactory long term stability of  $\text{Sm}_2\text{Co}_{17}$  magnet assembly.

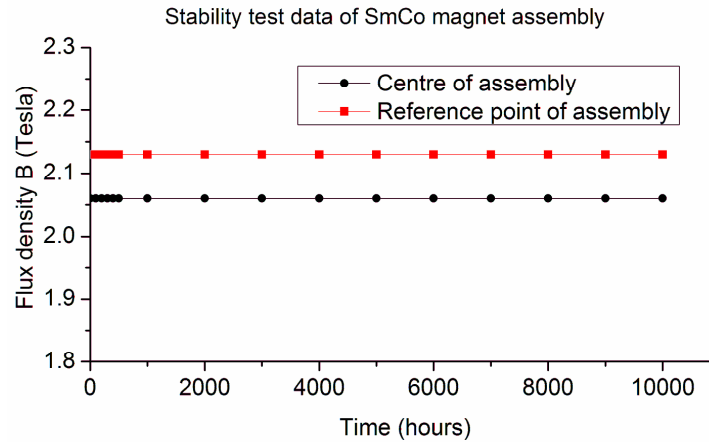


**Fig. 4.26: Stability test data for Sm-Co magnet assembly at 200°C**

#### 4.11 Estimation of Temperature Coefficient of Reversible Losses

The assembly stabilized at 250 °C and aged at 200 °C was used for finding the temperature coefficient of reversible losses of  $\text{Sm}_2\text{Co}_{17}$  magnet assembly. The magnet assembly has been provided with electrical heater for heating, thermocouple to monitor temperature and thermal insulation to prevent heat loss. The hall probe of the gauss meter was positioned at the air gap centre with air cooling arrangement. The probe was maintained at around 40 °C with forced air cooling. The magnet was gradually heated and from 28 °C to 250 °C in steps of 25 °C. At each temperature, the magnet assembly was maintained for 30 minutes. The flux density value at the air the gap centre was measured, while magnet was maintained at a particular temperature. The heating process was continued upto 250 °C and then the magnet was cooled to room temperature gradually. While cooling also, the flux density was measured and recorded. Figure 4.27 shows the flux density versus temperature curve during heating and cooling cycles. The flux density after heating and cooling cycle was found to be exactly the same as the original value of 0.2066 Tesla. This shows the excellent stability of

the magnet assembly with respect to demagnetizing forces and the complete regaining of the reversible losses. The temperature coefficient of reversible losses is calculated for the range of temperatures from 28 °C to 100 °C, which is the expected range of temperatures of the magnet during application. It was found to be 0.0312%/°C which matches with the value reported in MMPA standard [31]. However, for the temperature range of 28-150 °C the average value of reversible loss coefficients works out to be around 0.0505 %/ °C and is acceptable

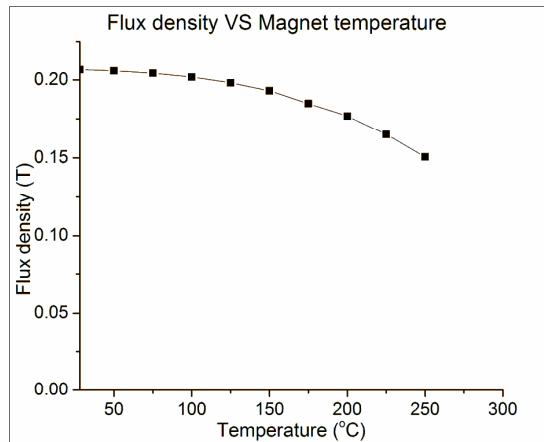


**Fig. 4.27: Magnetic flux density variation with temperature**

#### 4.12 Closure

PMFM for 100 NB pipe with Sm-Co magnet was designed, fabricated and tested in sodium system and the feasibility of its use in SFR circuits has been demonstrated. Proposed design targets were satisfactorily achieved and the weight of the Sm-Co based PMFM is 55 % lower and the sensitivity is improved by 102% as compared to Alnico-V based PMFM. The variation in sensitivity with flow and temperature is minimum and is comparable with Alnico-V PMFM. Three dimensional finite element modeling of the Sm-Co PMFM has been performed for its voltage output signal prediction. In simulation, magnetic field distribution across the flow meter pipe and the flow meter output voltage signal for different flow rates with sodium temperature varying from 250 °C to 450 °C were predicted. It is observed that the variation between the experimental and computational results

of the output voltage at low sodium flow rates is 1.9 %, and at maximum flow rate, it is 7.3%. It is established that FEM analysis can be used for design optimization and sensitivity prediction of PMFM in future. The design and development of 200 NB Sm-Co flow meter is taken up based on this experience. Findings of this research will be very useful for fast reactor instrumentation community in selecting flow measurement methods for future SFRs. However, beyond the size of 200 NB, Sm-Co based flow meter will also be bulky and heavy. This emphasizes the need for developing a still compact flow sensors for large pipes at penalty of reduction in sensitivity. To address this issue, the development of side wall type flow meter was taken up as part of the research and the details are covered in the next chapter.

## CHAPTER 5

### SIDE WALL TYPE PERMANENT MAGNET FLOW METER FOR SODIUM FLOW MEASUREMENT IN LARGE PIPELINES OF SFR's

#### 5.1 Introduction

The secondary sodium heat transport circuit of a typical 500 MWe capacity SFR is of pipe size 800 mm. For the commercial 1000 MWe capacity SFR, the pipe size of the secondary sodium heat transport system will be of the order of 1000 mm. For the auxiliary circuits SFRs, where the pipe is less than 100 NB size, conventional PMFM with Alnico-V magnet assembly is the optimum choice. Internationally, during initial period of SFR development, conventional permanent magnet flow meters and saddle coil type electromagnet flow meters are considered for flow measurement even for the large pipes [7,57]. In large diameter high temperature service pipes, it is difficult to provide the large upstream and downstream straight lengths required for these flow meters, from space constraint and flexibility considerations. For large pipelines conventional Alnico-V based PMFMs become bulky, heavy and have installation difficulties. Alternate methods are to be developed for the flow measurement in large pipelines for the new reactors under design. For sodium flow measurement in the large pipelines, PMFMs with high energy magnetic material Sm-Co, Alnico-V permanent magnet based side wall flow meters (SWFMs), bypass type flow meters, ECFMs [23, 24] and ultrasonic flow meters are the sensors considered. Beyond the size of 200 NB, Sm-Co based PMFM would also become heavy. In permanent magnet based SWFM, an Alnico-V based permanent magnet block is mounted on one side of the large pipe. The magnetic field penetrates through the pipe and interacts with the flowing sodium inducing a motional voltage proportional to the velocity [12]. Permanent magnet based side wall flow meter is passive, non invasive and does

not require any special welding or penetration in the pipe [58, 59]. This is a compact, cost effective, reliable and accurate method for flow measurement in large pipelines. It is suitable for pipelines of size 100 NB and above. An inherent advantage of SWFM is that, it does not need power supply. However, its sensitivity is very low and sensitivity estimation is difficult due to non uniform magnetic field. As part of this research one SWFM, in which an Alnico-V permanent magnet block mounted on one side of a SS pipe of 100 NB size has been analyzed, designed, fabricated and tested. The size selected for design and development is adaptable for calibration and testing at reactor operating conditions using a sodium loop. The relationship between its voltage signal and sodium flow rate has been established. Further three dimensional FEM modeling of SWFM is done using COMSOL 3.5a software and results of modeling are validated with experimental results [56]. FEM model is then used to analyze the effect of electrode position and sodium flow rates on SWFM sensitivity. The feasibility for the use of this type of flow meter for large pipelines of SFRs is demonstrated. The effect of asymmetric magnetic field on flow meter voltage signal and dependence of flow meter voltage signal on position of electrodes are also analyzed. This chapter of the thesis covers the theoretical/numerical and experimental investigation carried out on SWFM.

## **5.2 Flow Measurement Methods in Large Pipes**

A PMFM with Alnico-V magnet considered for 900 mm pipe by INTERATOM weighs 2000 kg and is able to produce 10 mV for 1 m/s of sodium velocity [7]. For Fast Flux Test Facility (FFTF) reactor in US, a 400 mm pipe size flow meter with Alnico-V magnet was developed and tested [57]. In secondary main pipeline of Prototype Fast Reactor in UK, saddle coil flow meter was used for pipe of 355 mm diameter [16]. A saddle coil flow meter was designed by UK for a pipe of 900 mm, and its weight is 1000 kg [16]. Because of the larger number of components required to operate the flow meter system, reliability of the saddle-coil flow meter is less than that of the permanent-magnet flow meter. The

difficulties of the saddle-coil flow meter are also due to its large dimensions and weight.

Bypass type flow meter is used in PFBR and a few other reactors. In the bypass type flow meter, flow in the main line is measured by measuring the flow in a small bypass line using conventional permanent magnet flow meter. Considering the merits, bypass type flow meter is selected for flow measurement in the 800 NB main secondary pipeline of PFBR [4]. Numerical and experimental studies carried out on bypass type of flow meter is also covered in chapter 6. Sm-Co based PMFM developed for large pipes are appropriate for pipe sizes ranging from 100 NB-200 NB. Above 200 NB pipe size, the overall size of the Sm-Co based PMFM could also be large.

SWFM can be electromagnetic or permanent magnet type. The stability of Alnico-V permanent magnet with respect to time and temperature is studied in detail as a part of Alnico-V PMFM development programme and covered in chapter 3. SWFM is compact and it does not need any change in pipe configuration. Maintenance and replacement of magnet block are easy. Like PMFM, multiple output signals are possible from one SWFM assembly.

### **5.3 Description of Side Wall Flow Meter**

The SWFM designed and fabricated consists of a single Alnico-V magnet block of size 200×140×35 mm. One side of the magnet block (200×35 side) is cast to have a curved surface matching to the pipe outer diameter profile and mounted on a 100 NB schedule 40, SS 316LN pipe with thermal insulation of 5 mm thickness between the magnet and the pipe. The magnet is clamped on the pipeline with SS bolts and nuts. Mineral insulated SS sheathed SS conductor of size 4 mm is used as electrode. The SS core conductor of size 1.5 mm diameter is welded outside the SS pipe on either side of the magnet block at angles of 60 and 120 degrees, in line with the centre of the magnet block. The welding of the electrode is carried as per standards. Electrodes are earmarked, routed and

terminated at the terminal box. A perforated stainless steel cover is provided on all sides of the flow meter for natural cooling of the magnet. Entire assembly is supported on a base plate and is also provided with an eye bolt. The cross sectional and the side views of the SWFM are shown in Fig. 5.1. Three dimensional view is shown in Fig. 5.2. Photograph of the SWFM is shown in Fig. 5.3. The flow meter duct assembly is qualified for sodium system application by pneumatic testing and helium testing as per relevant standards.

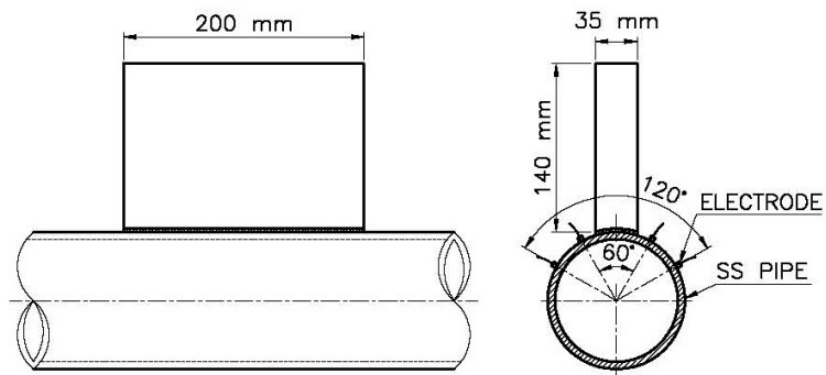


**Fig. 5.1: Cross sectional and side view of SWFM**

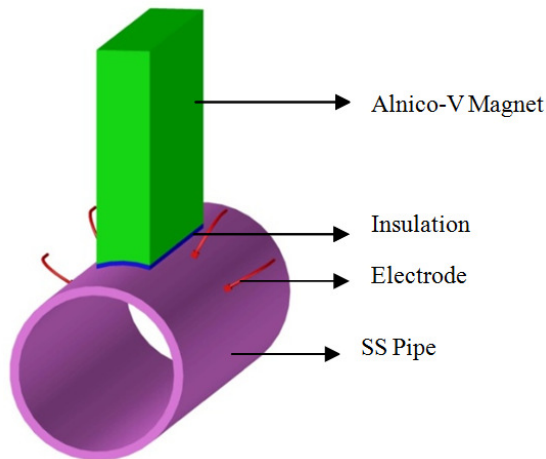


**Fig. 5.2: Three dimensional view of SWFM**



**Fig. 5.3: 100 NB SWFM assembly**

During normal operating conditions, sodium flows in the SS pipe 550 °C. The temperature of magnet during normal operation will be much less than 550 °C as the magnet is thermally insulated from the pipeline. Alnico-V magnet block used in SWFM is electrically stabilized by AC knockdown and thermally stabilized at 550 °C by rapid heating and cooling cycles (RHC) and gradual heating and cooling cycles (GHC), as per the procedure established in chapter 3. Magnetic properties of Alnico-V block [31] used for generating magnetic field are given below.

<b>Magnetic Property</b>	<b>Value</b>
Residual induction (Br)	1.25 T
Coercive force (Hc)	51700 A/m
Max Energy product (BH) <sub>max</sub>	43.8 kJ /m <sup>3</sup>
Curie Temperature	870 °C

#### **5.4 Sensitivity of SWFM**

Sensitivity of a SWFM is defined as the ratio of flow meter voltage output in mV across flow meter electrodes for a unit flow rate. The unit of sensitivity is mV/m<sup>3</sup>/h. The sensitivity of SWFM depends on electrical conductivity

of fluid flowing through the pipe, size of pipe, wall thickness, electrical conductivity, magnetic flux density value across the pipe, velocity profile of sodium in the pipe and electrode position.

Potential difference developed across electrodes is analytically calculated by dimensional measurements, average flux density measurement in the air gap of flow meter assembly and by estimating the flow velocity at unit flow rate. Amplitude  $E_v$  of voltage signal developed in SWFM across a pair of electrodes has been calculated using equation (5.1)

$$E_v = K \cdot d_e \cdot (v_u \times B_g) \times K \times 10^3 \text{ mV} \quad (5.1)$$

where,  $B_g$  :Magnetic flux density (Tesla).

$v_u$  : Velocity of sodium at unit flow rate (m/s).

$d_e$  : Electrodes gap (m).

$K$  is a correction factor, which depends on the variation in magnet temperature, finite length of magnetic circuit and ratio of electrical conductivities of SS and sodium. Thus,  $K$  is a combination of three factors. Correction factors for conventional PMFM can be calculated based on properties of sodium and pipeline material and dimensions of the PMFM. For a side wall configuration, these relations cannot be readily used. The values of  $K$  varies with temperature and is always less than 1. So, the maximum value of sensitivity for both the pairs of electrodes can be approximately calculated assuming  $K$  as 1.

Measured average value of flux density in the zone of interaction of magnetic field is 0.0524 Tesla for 60° angle electrodes. For unit flow rate, the velocity is 0.0340 m/s. The straight distance between the electrodes is 0.0511 m. Hence the voltage signal across the electrodes at 60° is

$$E_{v_{60}} = (0.0511 \times (0.0340 \times 0.0524) \times 1 \times 10^3) = 0.091 \text{ mV/m}^3/\text{h}$$

Measured average value of flux density in the zone of interaction of magnetic field is 0.0287 Tesla for 120° angle electrodes. The straight distance between electrodes is 0.0885 m. The voltage signal across the electrodes at 120° is

$$\begin{aligned} E_{V_{120}} &= 0.0885 \times (0.0340 \times 0.0287) \times 1 \times 10^3 \\ &= 0.0863 \text{ mV/m}^3/\text{h} \end{aligned}$$

This indicates that theoretically the sensitivity of both the electrode pairs is approximately equal.

## **5.5 FEM Analysis of Side Wall Flow Meter**

Side wall flow meter magnetic structure is not symmetric, and hence sensitivity of the flow meter depends on position of electrodes. Three dimensional finite element modeling of SWFM has been carried out to determine the potential difference across the pipe cross section, which helps in deciding electrode position to obtain maximum sensitivity. In the simulation studies, magnetic field distribution across the flow meter pipe and effect of sodium flow on flow meter sensitivity are analyzed. Flow meter sensitivity for different positions of electrodes has been predicted with modeling and compared with experimental results. In modeling, the effect of magnetic field generated by motional currents and end currents in sodium are neglected.

### **5.5.1 Magnetic circuit simulation of SWFM**

Magnetic circuit of side wall flow meter (Fig. 5.1) is made up of a rectangular Alnico-V block. Magnetic field of the Alnico-V block magnet is simulated using magnetostatics application module in the FEM code COMSOL 3.5a. Three dimensional model of the PMFM simulated in COMSOL is shown in Fig. 5.4.

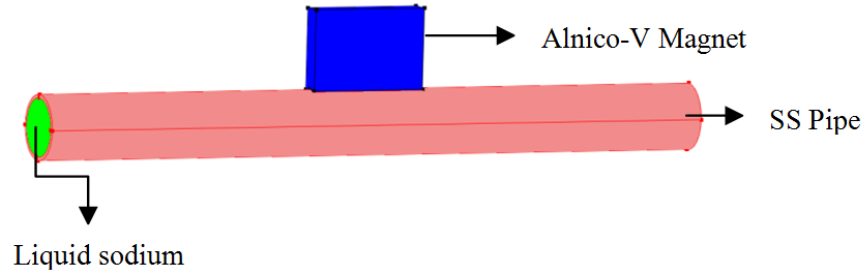


**Fig. 5.4: Three dimensional model of side wall flow meter**

Figure 5.5 shows the distribution of magnetic flux density (T) in the cross section of the SS pipe. It can be seen that the magnetic flux density is non uniform in the pipe cross section and is confined to the region under the pole face of the magnet block. Mathematically,  $J$  is the resulting current density,  $E$  is the electric field and  $u$  is the fluid velocity. The relation between current density and magnetic flux density becomes [56]

$$J = \sigma(E + u \times B) \quad (5.2)$$

Since quasi-steady conditions prevail, continuity equation can be written as

$$\nabla \cdot J = 0 \quad (5.3)$$

Combining the above two equations with  $E = -\nabla E_v$ ,

we get

$$\nabla^2 E_v = \nabla \cdot (u \times B) \quad (5.4)$$

where  $E_v$  is the electrical potential developed by the flow field of the induced motional current.

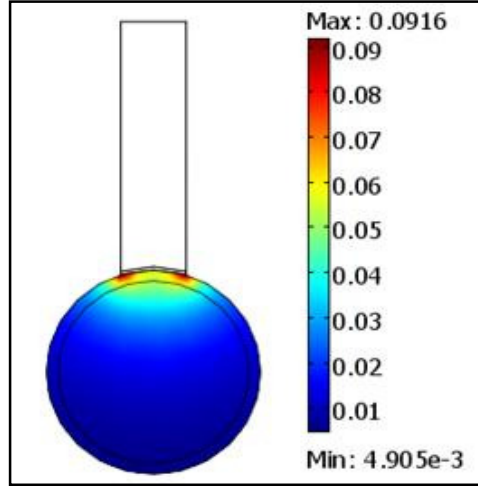


**Fig. 5.5: Magnetic flux density (T) in SWFM pipe cross section**

### 5.5.2 Sodium Flow Simulation

Sodium flow in SS pipe is stimulated in Navier-Stokes application mode in steady state. Sodium velocity is taken as constant and Lorentz forces acting on sodium are neglected, so generalized momentum balance equation in terms of transport properties and velocity gradients can be written as [60]

$$\rho \left( \frac{\partial u}{\partial t} + u \cdot \nabla u \right) = -\nabla p + \mu \nabla^2 u + f \quad (5.5)$$

where  $\rho$  is the density of sodium,  $p$  is the fluid pressure,  $f$  is body forces (per unit volume) and  $\mu$  is dynamic viscosity. For incompressible flow

$$\nabla \cdot u = 0 \quad \text{and} \quad (5.6)$$

$$\rho \frac{\partial u}{\partial t} = 0 \quad (5.7)$$

Sodium velocity profile across the pipe cross section is shown in Fig. 5.6. It can be seen that the velocity profile is axis-symmetric and minimum at the pipe inner surface.

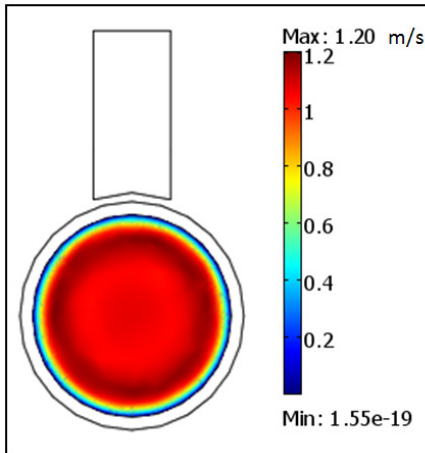


**Fig. 5.6: Sodium flow profile across the pipe cross section.**

### 5.5.3 Flow meter signal estimation

PMFM signal is calculated using 'Conductive media DC' application mode in COMSOL. Due to motional currents in the sodium, electrical potential is developed in the sodium. Direction of current flow is perpendicular to both magnetic field and sodium flow. Magnetic flux density is not uniform across pipe cross section in side wall flow meter, which leads to development of maximum value of potential difference near Alnico-V permanent magnet. In Fig. 5.7, direction of current is represented by vector plot and electrostatic potential developed in the pipe at a flow rate of  $36 \text{ m}^3/\text{h}$  is represented by the raster plot.

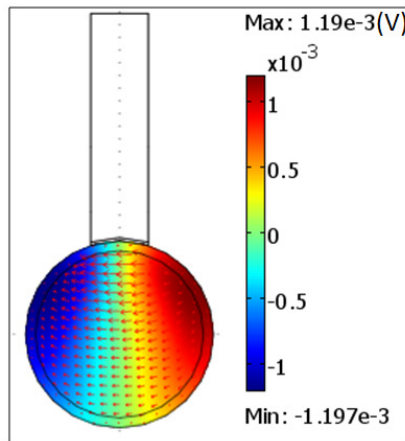


**Fig. 5.7: Electric field distribution within the pipe of SWFM**

## 5.6 Testing and Calibration of PM Based SWFM for Sodium Flow Measurement

Testing and calibration of SWFM is carried out in an existing facility. Section 2.7.1 gives the details of the facility. Both the pairs of signal electrodes are wired and connected to the multi channel HP data logger based data acquisition system. The procedure followed for calibration is same as the one followed in section 2.7.3. The trace of output voltage of SWFM with respect to time at sodium flow rate of  $133 \text{ m}^3/\text{h}$  is shown in Fig. 5.8. The milli volt seconds obtained is equated to the volume of sodium drained and sensitivity of flow meter is determined. The calibration runs are repeated at  $250 \text{ }^\circ\text{C}$ ,  $350 \text{ }^\circ\text{C}$  and  $450 \text{ }^\circ\text{C}$  and at different flow rates for assessing the variation in sensitivity with temperature.

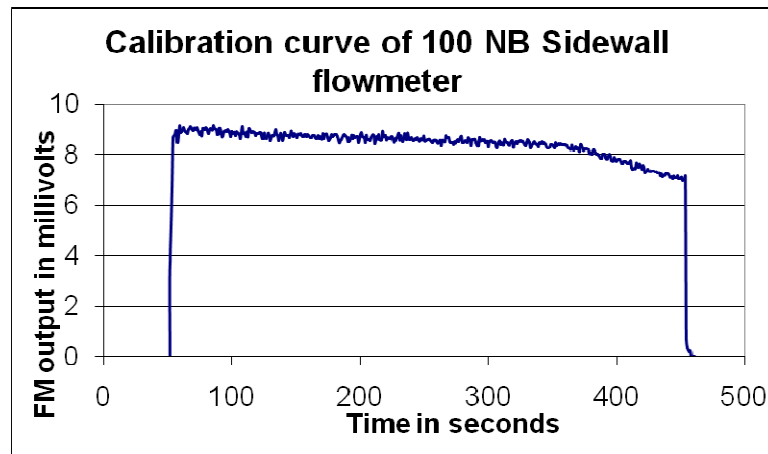
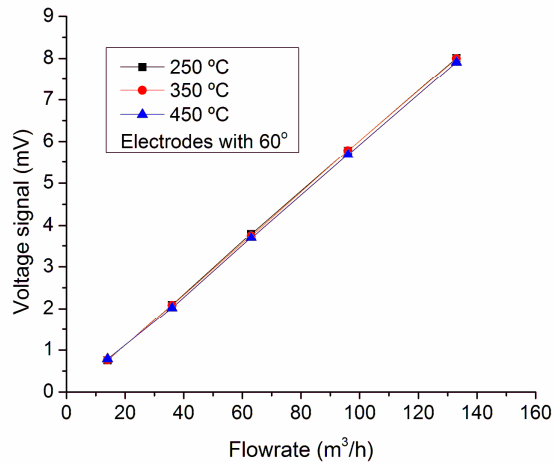


**Fig. 5.8: Output voltage trace during calibration of SWFM**

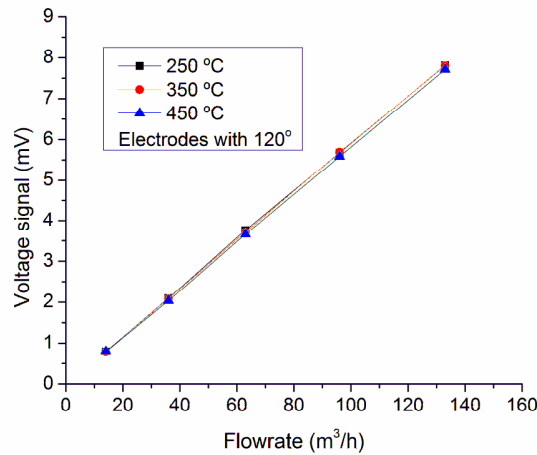
Plots of SWFM voltage measured across SS electrodes welded at  $60^\circ$  angle and  $120^\circ$  angle verses flow rates at different temperatures are shown in Figs. 5.9 and - 5.10 respectively. Both the pairs give measurable output voltage which confirm the functionality of this type of flow meter. The output is found fairly linear over the range of flow upto  $140 \text{ m}^3/\text{h}$ .

Figure 5.11 shows the variation of SWFM sensitivity with respect to the temperature at a flow rate of  $135 \text{ m}^3/\text{h}$  for both the pairs of electrodes. Sensitivity of  $60^\circ$  angle electrode pair is 2.5 % more than  $120^\circ$  electrode pair. The voltage

decreases by 2.5% across electrodes at 60° apart, while it decreases by 2.6 % across electrodes at 120° apart, when temperature of sodium increases from 250 °C to 450 °C. The output and hence the sensitivity of the flow meter decrease with respect to temperature marginally. The above mentioned reduction in sensitivity is due to increase in the ratio of sodium resistivity to SS resistivity with temperature and negative temperature coefficient of the magnetic flux density. Increase in the ratio of resistivity with temperature leads to increase in the loss of voltage signal by short circuiting in the pipe wall and negative temperature coefficient of magnet leads to reduction in the magnetic flux density in the pipe cross section.



**Fig. 5.9: SWFM voltage verses flow for electrodes 60° apart**



**Fig. 5.10: SWFM voltage verses flow for electrodes 120° angle apart**

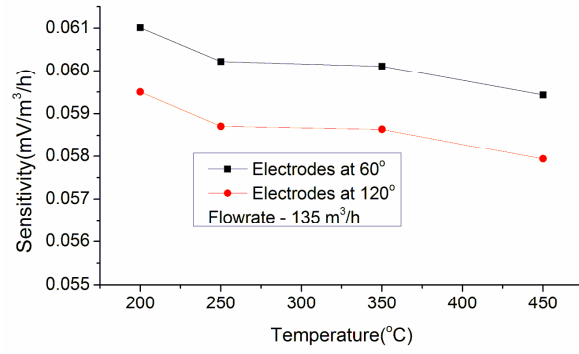


**Fig. 5.11: SWFM voltage versus sodium temperature**

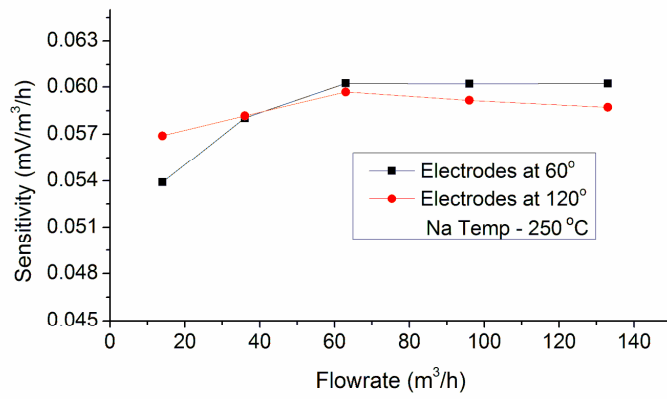


**Fig. 5.12: SWFM sensitivity versus sodium flow rate at 250 °C**

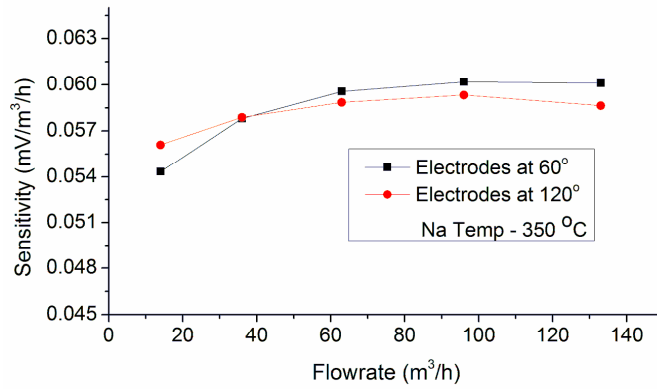


**Fig. 5.13: SWFM sensitivity versus sodium flow rate at 350 °C**

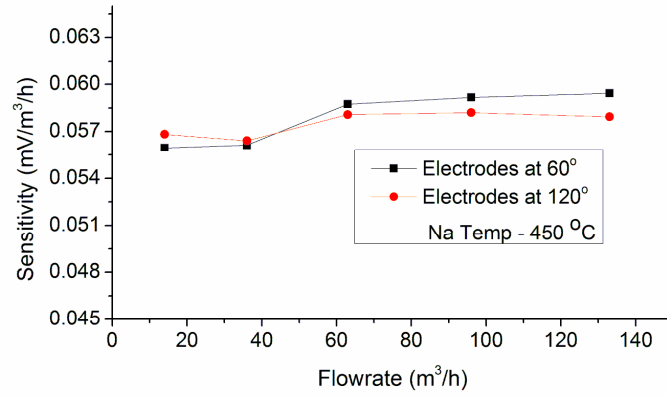


**Fig. 5.14: SWFM sensitivity verses sodium flow rate at 450 °C**

Figures 5.12 to 5.14 show flow versus sensitivity plot of both pairs of electrodes at 250 °C, 350 °C and 450 °C respectively. It can be seen that the electrode pair at 120° angle is more sensitive than the electrodes pair at 60° angle at low sodium flows while the trend reverses at higher flows above 40 m<sup>3</sup>/h irrespective of temperature. The maximum value of the variation in sensitivity in the full flow range is around 9% for 60° angle electrodes pair and 4 % for 120° angle electrodes pair. This implies that the electrodes pair at 120° angle is more linear than the electrodes pair at 60° angle. In SWFM magnetic flux density is not uniform across pipe cross section. Magnetic flux density values are more near the permanent magnet block and reduce gradually with distance from the permanent magnet block. With increase in the sodium flow, flow profile across pipe cross section changes from parabolic to flat profile [60]. The larger weight functions [12] of flow velocity at points near the permanent magnet combined with higher magnetic flux density values lead to marginally higher sensitivities for 60° angle electrode pair than 120° angle electrode pair at high flow rates

### 5.7 Error in Estimated Sensitivity of SWFM

$$\text{Sensitivity } S = (v \times t) / (Q_{SV} \times 3600)$$

$$\Delta S = \left| \frac{\partial(S)}{\partial v} \times \Delta v \right| + \left| \frac{\partial(S)}{\partial t} \times \Delta t \right| + \left| \frac{\partial(S)}{\partial Q_{SV}} \times \Delta Q_{SV} \right|$$

For the flow rate considered,  $v = 8.06 \text{ mV}$

Drain time,  $t = 411 \text{ s}$

The sodium drained  $Q_{SV}$  (refer section 2.7.3) =  $15.632 \text{ m}^3$

$$S = 0.05887 \text{ mV m}^3/\text{h}$$

$\Delta v$ ,  $\Delta t$ ,  $\Delta Q_{SV}$  are to be estimated to determine the error in sensitivity  $\Delta S$ . Total error in milli volt measurement,  $\Delta v$  is estimated as 33.83 micro volts as in section 2.8.1.

$$\left| \frac{\partial(S)}{\partial v} \times \Delta v \right| = 0.00025$$

Total error in time measurement,  $\Delta t$  is assumed as 1 sec.

$$\left| \frac{\partial(S)}{\partial t} \times \Delta t \right| = 0.00014$$

Error in sodium volume estimation, for an assumed error of 5 mm in the dimensional measurement is calculated in section 2.8.3 as  $0.1158 \text{ m}^3$ .

$$\left| \frac{\partial(S)}{\partial Q_{SV}} \cdot \Delta Q_{SV} \right| = 0.00044$$

Total error in sensitivity of SWFM is

$$\Delta S = 0.00025 + 0.00014 + 0.00044$$

$$= 0.00083$$

$$\% \text{ Error} = (\Delta S/S) \times 100 = (0.00083/0.05887) \times 100$$

$$= 1.4 \%$$

From the error analysis, calibration accuracy is determined as 1.4 %.

## 5.8 Comparison of Experimental and FEM Results

Experimental and simulation results of potential difference developed across the electrodes welded at  $60^\circ$  angle and  $120^\circ$  angle at the centre of the magnet have been compared and are shown in Fig. 5.15. At the maximum flow rate of  $140 \text{ m}^3/\text{h}$ , the deviation between experimental and computational results for the potential difference developed across electrodes at  $60^\circ$  and  $120^\circ$  angles is  $-11.6 \%$  and  $+13.2 \%$  respectively. At a flow rate of  $14 \text{ m}^3/\text{h}$ , the variation in the experimental and computational results is only  $\pm 1.66 \%$ . In numerical simulation, the effects of motional currents and end currents on resultant magnetic flux density were neglected, which leads to increase in error between the two results at higher sodium flows. Effect of electrode position on flow meter output voltage is analysed at a flow rate of  $14 \text{ m}^3/\text{h}$ , as at this flow rate both the results are closely matching.

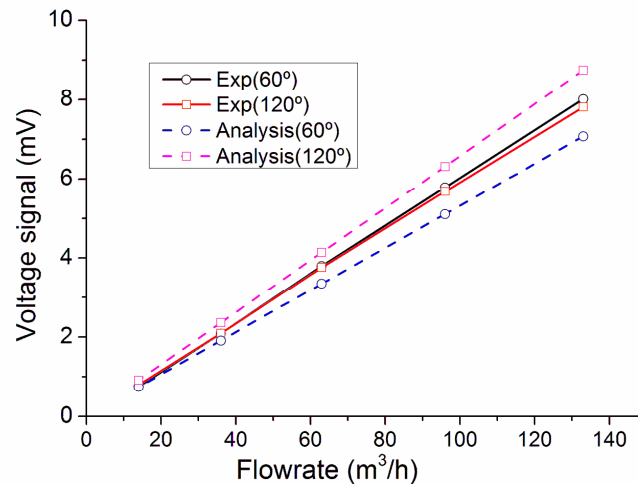


**Fig. 5.15: SWFM flow meter output Vs flow rate**

Potential difference developed across electrodes placed at different angles is simulated using FEM analysis. The voltage developed at a sodium flow rate of  $14 \text{ m}^3/\text{h}$  for electrodes placed at different angles is shown in Fig. 5.16. Voltage signal developed in SWFM for a particular flow depends on magnetic flux density values and distance between the electrodes. As one moves away from the magnet, magnetic flux density values reduce and distance between the electrodes

increases. The voltage signal first increases due to increase in distance between the electrodes, attains a maximum value and then starts decreasing as the reduction in magnetic flux density plays a dominant role. It can be seen that the maximum potential difference for the rated sodium flow is developed across electrodes welded at 120° angle apart. Position of electrodes at 120° angle is optimal and the same is confirmed with analysis as well as experiment results.

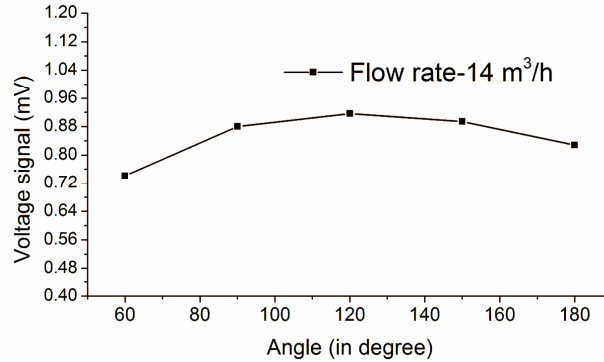


**Fig. 5.16: Variation of SWFM voltage with electrode position**

## 5.9 Closure

Options available for sodium flow measurement in large pipelines are briefly discussed. Difficulties associated with large EM flow meters are highlighted. A SWFM of 100 mm pipe with Alnico-V permanent magnet has been , analysed, designed, fabricated and tested for sodium flow measurements. The flow meter was able to produce measurable output at minimum flow and was found to be fairly linear with flow. Experimental results show that sensitivity of SWFM increases with increase in sodium flow rate and decreases with increase in sodium temperature marginally. A three dimensional Finite Element Model (FEM) was also made for sensitivity estimation of the flow meter in COMSOL 3.5a and results of simulation were validated with experimental results. FEM simulation shows that sensitivity of SWFM is maximum with electrodes positioned at 120° angle. The feasibility of using this type of flow meter, for sodium flow measurements in large pipelines of SFRs is demonstrated by modelling and experiments. The roadmap for development and testing of SWFM for 200 and 800 mm pipe is brought out. However, the

sensitivity of the flow meter is low and hence the resolution in flow measurement. Moreover, different flow measurement methods are to be developed and final choice can be based on techno-economic considerations. Ultrasonic flow meters are also considered for sodium flow measurement in large pipes. Bypass type of flow meters are used in large pipelines of a few reactors elsewhere and in PFBR. Experimental and theoretical investigations carried on bypass type flow meter is described in the next chapter.

## CHAPTER 6

### BYPASS TYPE FLOW METERS FOR FLOW MEASUREMENT IN LARGE SFR PIPELINES

#### 6.1 Introduction

Alternative methods are developed for flow measurement in the large pipelines of new SFRs under design. Considering the merits, bypass type flow meter is selected for flow measurement in the 800 NB main secondary sodium pipeline of PFBR [2] and a few other SFRs [20]. The schematic of PFBR heat transport system indicating the location of the secondary flow measurement is shown in Fig. 1.10. As part of this research, the bypass flow measurement configuration selected for PFBR is numerically modelled and flow ratio is predicted. A scaled-down model of the system is tested in water and the model is validated. To address the need of future SFRs, an optimisation study is conducted to increase the sensitivity of the bypass flow meter by changing the bypass circuit geometry, which increased the flow through the bypass line. A combined numerical and experimental approach is adopted for design and validation of the optimised bypass flow meter configuration. The optimised configuration increases the bypass flow by 71% of the original value. Numerical results of the optimised bypass circuit are again validated by experiments in water with the scaled-down models. With the validated numerical procedure, the flow multiplication factor at different flow rates, for the optimised bypass circuit of future SFRs is established. This chapter contains the details of studies, experiments, modelling and analysis carried out on bypass type flow meter for measuring sodium flow in large pipelines.

#### 6.2 Bypass Type Flow Meter

In the bypass type flow meter, flow in the main line is inferred by measuring the flow in a small bypass line using conventional permanent magnet flow meter [19]. The main flow in the large pipeline can be estimated from the

previously determined ratio of main flow to bypass flow [60,61]. Bypass flow meters give fairly good accuracy and sensitivity for liquid sodium flow measurements in large pipes. The hydraulic characteristics of the bypass flow system that can be analysed using hydraulic models and the PMFM, which is the sensor of the bypass flow meter system, can be conveniently calibrated in sodium. Alnico-V based flow meters are used in the bypass line [47]. This is an invasive method of sodium flow measurement with variable volumetric flow ratio with respect to the volumetric flow in the main line. The accuracy of the flow readings, experience in other SFRs and flexibility makes bypass flow meter system suitable for liquid sodium flow measurement in large size secondary main pipes of SFRs.

### 6.2.1 Description of bypass flow meter

In bypass flow meters, when sodium flows through the large diameter main line, a definite portion of the flowing sodium will pass through the small diameter bypass line where the PMFM is installed. The volumetric flow ratio,  $F_m$  is defined as the ratio between volumetric fluid flow through the main line to the volumetric fluid flow through the bypass line. The flow measurement in the small bypass line with a PMFM, and computing the main flow from the previously determined flow ratio is a convenient and compact arrangement, compared to the direct flow measurement system in large size pipes. Figure 6.1 shows the schematic of a bypass type flow meter.

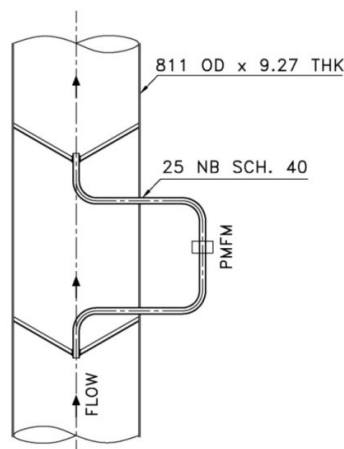


**Fig. 6.1: Bypass flow meter geometry for PFBR secondary sodium flow measurement**

The ratio of the volumetric sodium flow through main line to the bypass line is decided by the flow resistances of the flow paths which are purely decided by hydraulic characteristics of the flow path. Hence the volumetric sodium flow rate in the main line can be determined from the bypass flow meter reading by multiplying it with  $F_m$ .

The bypass flow path of flow measurement system should cause minimum disturbance in the main circuit and the pressure drop in the main pipeline due to introduction of bypass tapping should also be as low as possible. To make the total system compact, the bypass line should be of optimum size. The upstream and downstream tapplings are taken from the centre line of the pipe where maximum velocity occurs at all flow conditions. In order to avoid flow induced vibration, the bypass tapplings are rigidly supported within the main pipe. The shape, orientation and spacing of the supports are selected, to ensure minimum pressure drop and flow induced vibration. The upstream tapping faces flow direction and the downstream tapping leaves the pipe opposite to the flow direction. This arrangement enhances the velocity in the bypass line and is finalised after preliminary studies as well as experiments in water using scale down models. The radius of bend in the bypass circuit would be five times the pipe diameter to minimise the pressure drop. The edges of the tapplings should be tapered suitably for smooth flow transition. The penetrations should be suitably designed as per structural design codes and the joints are to be inspected and qualified by ultrasonic methods.

### **6.2.2 Bypass flow meter for secondary main line flow measurement in PFBR**

The bypass circuit geometry for the measurement of main secondary sodium flow in PFBR is shown in Fig. 6.1. The bypass flow upstream tapping is taken with a 25 NB scheduled 40 pipe of inner diameter 26.6 mm, from the centre of main pipeline with 792.6 mm inside diameter. The downstream sodium flowing through the bypass line leaves at the centre portion of the main line. This geometry imparts negligible additional resistance to the sodium flowing through the main line. Bypass circuit design ensures minimum pressure drop in the bypass line. This was confirmed by pressure drop calculations using conventional methods as well as CFD tools.

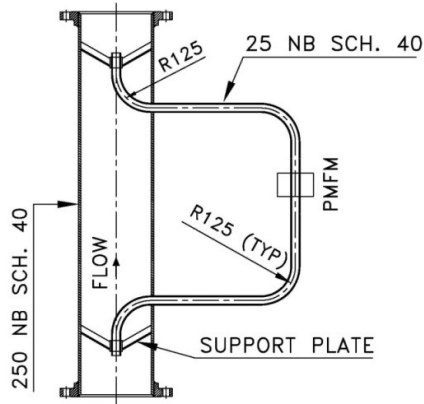


**Fig. 6.2: Scale down model of PFBR bypass circuit**

The hydraulic characteristics of the bypass flow meter system have been evaluated numerically and experimentally using water as simulant for a scaled-down model of the PFBR secondary bypass flow meter. To reduce the cost and complexity of the experimental validation the model for the studies is scaled down. The scaling down is done only for the main line from 792.6 to 254.5 mm diameter by keeping the bypass line geometry same (Fig. 6.2). This is performed by keeping the velocity of the fluid flowing through the main line of the model equal to the actual system. However, the pressure drop in the main line of the prototype and the model will be different but the velocity and head will be same which is the major driving force for the bypass flow. The scaled-down geometry has been modelled and analyzed with three dimensional 180° symmetric model using CFD. The pressure and velocity profiles in the system have been obtained by analysis. The bypass flow covering the full range of main flow velocity is evaluated by numerical calculations.

Then experiments have been carried out in water for validating the numerical results with the same scaled down model, that was used for numerical study. During experiments, volumetric flow rate of water through main line is measured by an EM flow meter suitable for water flow measurement with a calibration uncertainty of  $\pm 0.15\%$  of the reading. The volumetric flow rate of water through bypass line is measured with ultrasonic flow meter which is calibrated in-situ by absolute weight collection method with an uncertainty of  $\pm 0.75\%$ . The uncertainty in the estimation of  $F_m$  is about  $\pm 1.5\%$  of the reading. The comparison

of the volumetric water flow rate through the bypass line obtained from numerical calculations and experimental evaluation is shown in Fig. 6.3. The result obtained by the experiments was used to validate the numerical procedure and this validated numerical tools are used to evaluate the volumetric flow ratio,  $F_m$  of the actual system in sodium. The experimentally obtained points and numerically derived trend are in good agreement with an average deviation of +3.48% and a maximum deviation of +3.85%. This close agreement validated the numerical method adopted for predicting the flow through the bypass line. Using the same validated numerical tool with suitable correction factor, flow ratio for full scale PFBR circuit is computed. Figure. 6.4 shows the established relation between the computed sodium flow through the bypass line and the total sodium flow through the main line at two different sodium temperatures.

The PMFM sensor used in the bypass line is calibrated with an accuracy of  $\pm 2\%$  of the measured value. The uncertainty in the flow ratio derived by numerical methods which is validated and corrected by experiments is estimated as  $\pm 1.5\%$  of the reading based on statistical methods with 99.7% confidence level. The overall accuracy achieved in PFBR secondary flow measurement is  $\pm 2.5\%$  which is adequate from the process and safety considerations.

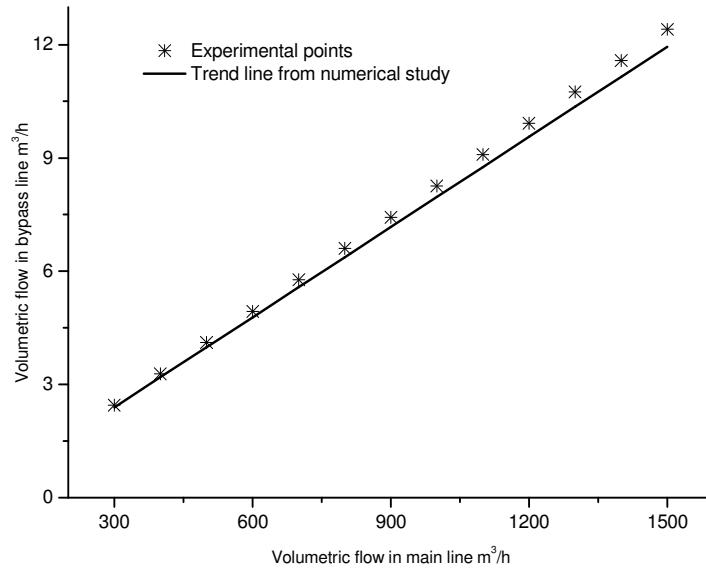


**Fig. 6.3: Main flow versus bypass flow for the scale down model of PFBR bypass configuration**

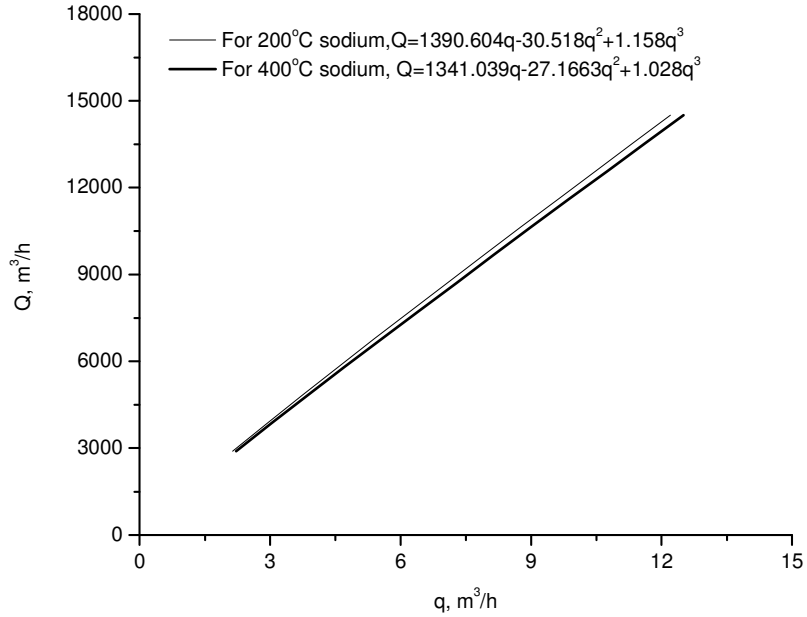


**Fig. 6.4: Relation between the measured sodium flow through bypass line and total sodium flow through the main line for PFBR geometry**

### 6.2.3 Optimisation of bypass circuit geometry

The induced voltage is directly proportional to the velocity of sodium flowing through the bypass line which is proportional to the velocity of sodium flow through the main line. In PMFM

$$Ev = C_1 B d_b v_b \quad (6.1)$$

where

$Ev$ : Induced voltage

$B$  : Flux density in the flow meter

$d_b$  : diameter of bypass pipeline

$v_b$  : velocity in bypass pipeline

$C_1$  : constant

In the bypass flow meter system, velocity of the fluid in the main line ( $V_m$ ) is proportional to the velocity of the fluid in the bypass line ( $v_b$ ).

$$v_b \propto V_m$$

or

$$v_b = C_2 V_m \quad \text{or} \quad V_m = v_b/C_2 \quad (6.2)$$

where  $C_2$  is a constant

$$V_m = \frac{1}{C_1 C_2} \frac{Ev}{B d_b}$$

$$Q_m = \frac{1}{C_1 C_2} \frac{\pi D_m^2}{4} \frac{Ev}{d_b B}$$

$$= \frac{1}{C} \frac{D_m^2}{d_b} \frac{Ev}{B} ; \text{ Where } C = \frac{4C_1 C_2}{\pi}$$

$D_m$  : Diameter of main line

$Q_m$  : flow rate in main line

And sensitivity,

$$\frac{Ev}{Q_m} = C \frac{d_b B}{D_m^2} \quad (6.3)$$

For a given value of  $d_b$  and  $D_m$ , the sensitivity of the bypass flow meter can be increased by high value of  $C$  or  $B$ . With the given geometry of magnet assembly,  $B$  is constant and  $C$  can be increased by an increase in the sodium velocity through the PMFM. The sensitivity and resolution of the bypass flow meter system will increase with increase in the fluid velocity in bypass line for the same main flow conditions. The magnitude of the induced voltage signal ( $Ev$ ) is directly proportional to the velocity of the sodium in bypass line. With constant sodium velocity in the main line ( $V_m$ ), an increase in the sodium velocity in the bypass line ( $v_b$ ) will increase the induced voltage across the electrodes of PMFM. This will increase the sensitivity of bypass flow meter system and reduce the measurement error of EMF.

The static pressure difference responsible for sodium flow in the bypass line  $\Delta P_m$  is given by the following relation [60, 62].

$$\Delta p_m = k_m \frac{\rho V_m^2}{2} \quad (6.4)$$

where  $k_m$ : Resistance L coefficient for friction in main line

$\rho$  : density of sodium

Pressure drop in bypass line:

$$\Delta p_{by} = k_{by} \frac{\rho v_b^2}{2} \quad (6.5)$$

where

$k_{by}$  : Resistance coefficient for bypass line

$v_b$ : velocity in bypass line

$$k_{by} = k_{fr} + k_e + k_{be} + k_{red}$$

$k_{fr}$  : Resistance coefficient of friction bypass line

$k_e$  : Resistance coefficient at entry and exit of bypass line

$k_{be}$  : Resistance coefficient due to bends in bypass line

$k_{red}$  : Resistance coefficient reducers in bypass line

As static pressure difference responsible for sodium flow in the bypass line is equal to pressure drop in the bypass line.  $\Delta p_m = \Delta p_{by}$  and from equations (6.4) and (6.5)

$$k_m \frac{\rho V_m^2}{2} = k_{by} \frac{\rho v_b^2}{2}$$

$$V_m = v_b \sqrt{\frac{k_{by}}{k_m}} \quad (6.6)$$

For a given velocity,  $V_m$ , in the main line, the fluid velocity in the bypass line depends on the numerical value of  $\sqrt{\frac{k_{by}}{k_m}}$ . To get a higher  $v_b$ , the resistance  $k_m$  should be increased and/or resistance  $k_{by}$  should be decreased. The value of  $k_m$  is not recommended to be increased because, it will increase the pressure drop in the main line. Hence, the value of  $k_{by}$  is required to be reduced to get higher sodium velocity in the bypass line. An optimisation study is carried out to reduce the pressure drop in the bypass line without increasing the pressure drop in the main line to get a higher sodium velocity and volumetric flow rate through the bypass line. The liquid sodium velocity in the bypass line at normal operating condition is limited to around 10 to 12 m/s due to erosion and flow induced vibration considerations. In order to respect the flow velocity restriction in the bypass line, the size of the bypass line is increased by keeping the inside diameter of the PMFM section same. Only standard pipe sizes were considered for the optimisation study for the convenience of manufacturing. From the numerical study conducted with various pipe sizes possible and within the feasible velocity range, it is found that, with 35.1 mm inside radius for the bypass line with 26.6 mm inside diameter PMFM section is the optimum geometry.

Numerical and experimental studies for the search of optimum bypass geometry have been done with a main line size of 254.5 mm and water as flowing fluid. The schematic of the modified bypass geometry used for numerical analysis is shown in Fig. 6.5. By increasing the bypass pipe diameter, the component of flow resistance  $k_{by}$  reduces significantly. From the numerical analysis, it has been observed that the sodium velocity at PMFM section in the scaled down model of modified geometry is 71% more than that with the scaled down PFBR geometry. Thus,  $F_m$  is lower than that for the present PFBR bypass configuration. The velocity vectors and pressure profile for the model obtained from numerical studies of the optimised geometry are shown in Fig. 6.6 and Fig. 6.7. To validate the numerical results, and reconfirm the methodology, experiments have been conducted with the model of the optimized geometry. Figure 6.8 shows the comparison between the numerical and experimental results for the optimized geometry along with the experimental results of the present geometry. The mean deviation between experimentally obtained volumetric flow rate in bypass line with numerically

evaluated trend line is +2.15% with maximum deviation as +2.3%. The bypass flow estimation with numerical analysis fairly matched with the experimental value. Thus, this validated CFD model can be used for numerical prediction of bypass flow rate for optimized configuration of bypass geometry in future SFRs.

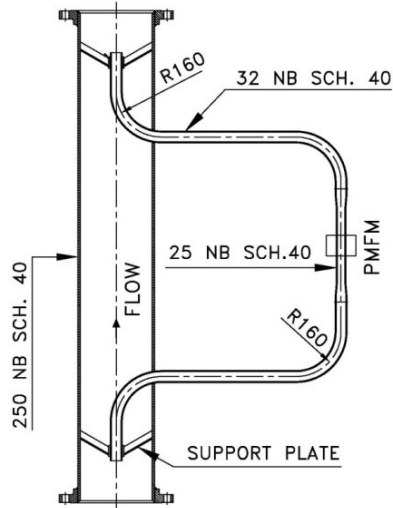


**Fig. 6.5: Model for optimized bypass loop for experimental and numerical studies**

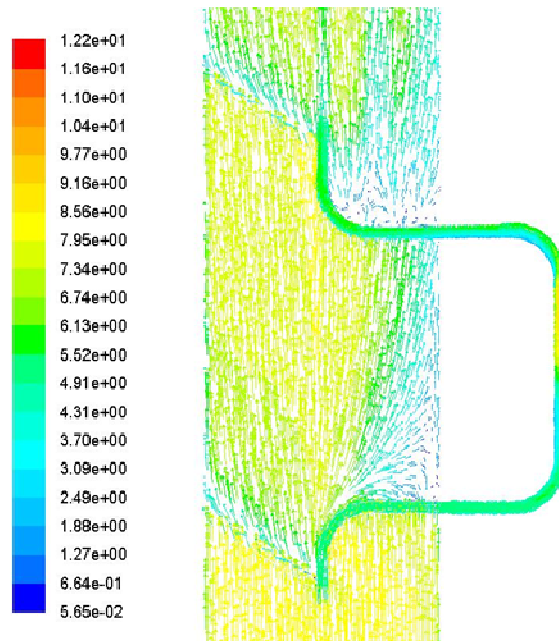


**Fig. 6.6: Schematic of velocity vector profile in optimized bypass geometry (m/s)**

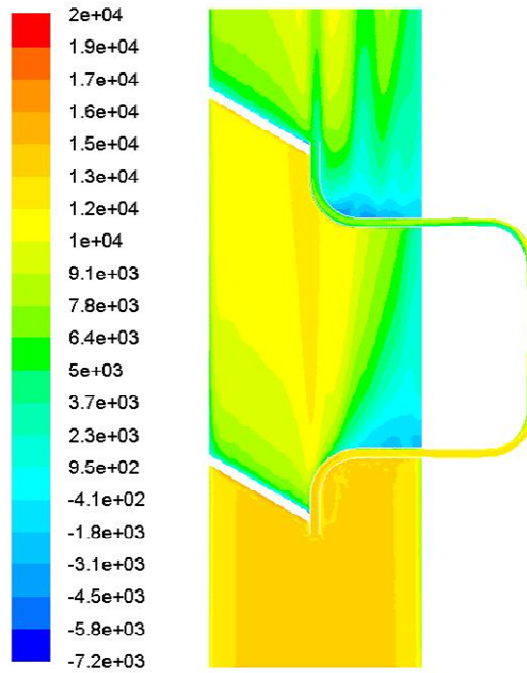


**Fig. 6.7: Schematic of pressure contour profile in optimized bypass geometry (Pa)**

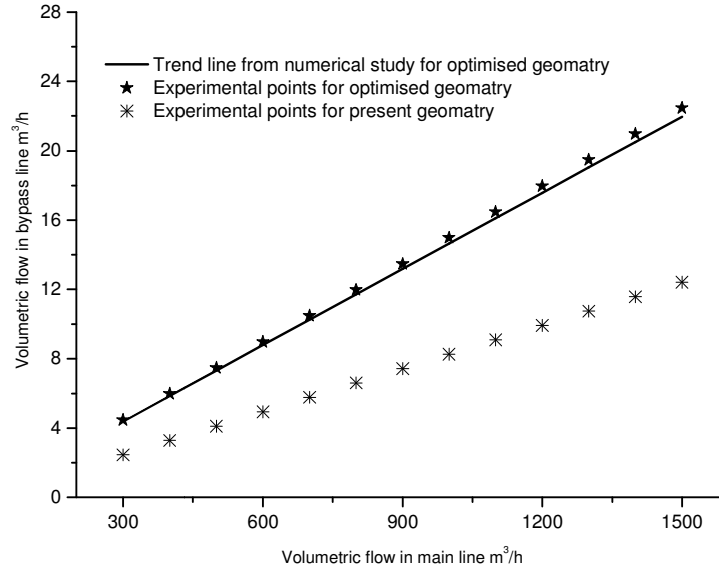


**Fig. 6.8: Comparison of volumetric flow rate through bypass line and main line between PFBR and optimised configuration**

#### 6.2.4 Numerical estimation of flow multiplication factor

The schematic of the optimized bypass flow meter geometry for the usage in future SFRs is arrived at based on the optimisation study shown in Fig. 6.9. A numerical study has been conducted using the validated procedure to predict the characteristics of optimized bypass flow meter geometry. The variation of flow ratio for the optimized configuration is given in Fig. 6.10. The characteristic equation obtained from this study for  $F_m$  is given below.

$$F_m = 709.58 + 141.63e^{-Re/5.76E6}$$

where  $Re$  is the Reynolds number. The volumetric flow rate obtained through the bypass line of optimized geometry is 71% higher than that existing in PFBR bypass geometry. This increased volumetric flow rate gives an increased velocity of sodium at the PMFM section and an increase in the sensitivity of the bypass flow measurement system by the same percentage. As explained earlier, the uncertainty of the estimated sodium flow through main line using the PMFM sensor installed in the bypass line is estimated as 2.3% which is better than that of PFBR configuration. Figure 6.11 shows the relation between sodium flow through the bypass line and the total sodium flow through the main line for optimized bypass flow meter geometry.

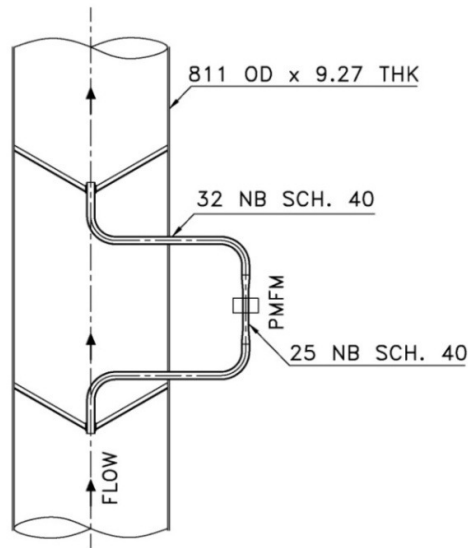


**Fig. 6.9: Optimized bypass configuration for new reactor designs**

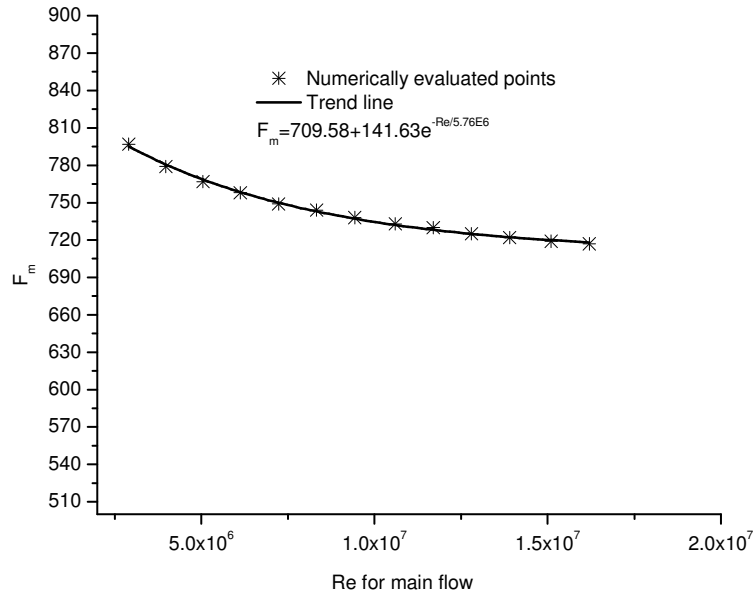


**Fig. 6.10: Variation of  $F_m$  with respect to  $Re$  for optimized bypass configuration**

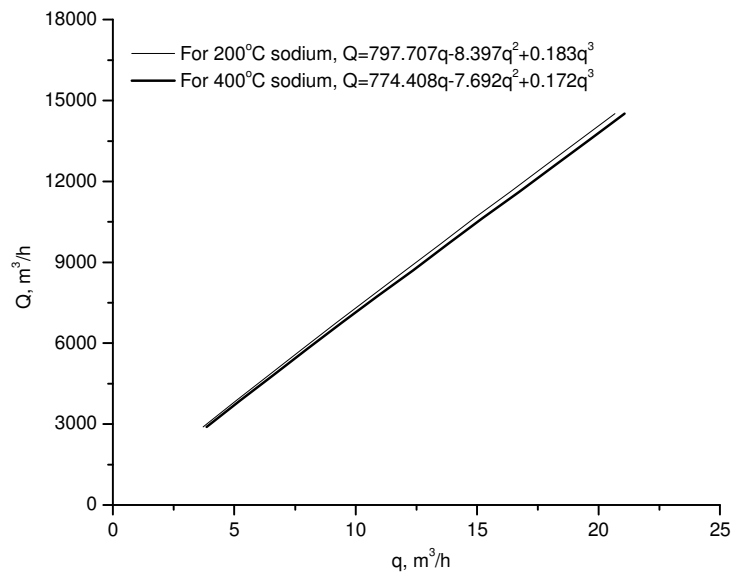


**Fig. 6.11: Relation between sodium flow through bypass line and main line for optimized geometry**

### 6.3 Closure

Bypass type permanent magnet flow meter has been used for sodium flow measurements in secondary loop of PFBR. Estimation of flow multiplication factor,  $F_m$  is performed with a numerical model which has been validated by experiments with scaled down models in water. Further, an optimization study has been conducted to increase the sensitivity and resolution of the bypass flow meter by changing the bypass configuration. From the study, it is observed that, the increase of inside diameter of bypass line from 26.6 mm to 35.1 mm by keeping the PMFM section size same, will increase the sensitivity of the flow meter system by 71%. With the increase in the inside diameter of bypass line, the flow resistance of the bypass line, reduces allowing enhanced flow to pass through it. This reduces the value of  $F_m$  and consequently the influence of geometrical tolerances on the level of uncertainty for bypass flow meter system decreases. The numerical procedure to arrive at the relation between the sodium flow in the main line and the bypass line is established. This leads to a compact, accurate, sensitive and reliable flow measurement method for large pipelines of SFR circuits.

## CHAPTER 7

### CONCLUSION AND SCOPE FOR FUTURE WORKS

#### 7.1 Conclusions

The focus of the research of this thesis is in the analysis, design, modeling, testing and calibration of different types of pipeline flow meters used in various sodium circuits of SFRs. Detailed literature survey was carried out on sodium flow measurement methods in SFR circuits and challenges faced as on today have been identified. Flow measurement methods followed in SFRs all over the world was summarized and methods followed in Indian SFRs viz. FBTR and PFBR have been detailed in the first chapter.

The second chapter described the research activities carried out on Alnico-V based permanent magnet sodium flow meters. The analytical procedure followed for estimating the sensitivity has been described and various factors affecting the sensitivity have been indicated and explained. The facility established for sodium calibration and the procedure followed for calibration have been explained with a typical example of 100 NB Alnico-V based PMFM. The methodology followed for error analysis of sensitivity has been explained and the error in the sensitivity estimated by sodium calibration has been derived. To ensure and confirm the stability of the sensitivity during the life of reactor, in-situ calibration of the flow meter is desirable. In-situ calibration of a 100 NB flow meter used in an experimental facility was carried out using cross correlation of noise signals from different pairs of electrodes of the PMFM. This would be a very useful tool for in-situ performance evaluation of reactor flow meters.

Permanent magnet assembly is the most critical part of the flow meter. The long term performance of the flow meter mainly depends on the ability of the magnet assembly to provide constant magnetic field with respect to time. Detailed studies on losses in permanent magnets have been carried out and the procedure

for magnetization, electrical stabilization and thermal stabilization have been established. Accelerated stability test was carried out on a typical Alnico-V based flow meter magnet assembly and experimentally demonstrated that the magnetic flux density remains stable for an assembly which was treated as per established procedure. Chapter-3 of the thesis covered the results of these studies in detail.

For pipelines of size below 100 NB, the choice of Alnico-V based flow meter appears appropriate. But for larger pipes above 100 NB size, these flow meters become bulky and heavy. To address this issue various options were studied in detail and PMFM based on high energy rare earth magnets is found as an option. A flow meter suitable for 100 NB pipe size was designed and manufactured with Sm-Co magnet assembly. This flow meter was modeled using COMSOL software and flow meter sensitivity has been predicted at different temperatures and flow rates. The stability of the magnetic field was experimentally studied by conducting accelerated stability test at 200°C for 10000 hours and found stable. This flow meter is able to provide double the sensitivity, with weight reduced to 55% as compared to Alnico-V based PMFM. Sm-Co based PMFM found to be suitable for 100 to 200 NB pipe sizes. The analysis, design and studies on this design are significant contribution to the fast reactor programme. Details of this study was covered in Chapter 4 of this thesis.

Redundant flow measuring methods are desirable in SFR circuits. The alternative method developed for large pipes is side wall type of flow meter. A side wall flow meter of 100 NB size, with Alnico-V magnet block and two pairs of electrodes has been analysed, designed, and manufactured. This flow meter has been modeled using COMSOL software and sensitivity is predicted at different flow rates and temperatures. The sensitivity though low, is adequate for flow measurement. SWFM has been calibrated in sodium and the numerical model is validated. This design emerges as a viable alternative for flow measurement in all pipe sizes above 100 NB. Chapter 5 of the thesis gave the full details of this work.

The main secondary circuit SFR pipeline will be of the size 800 NB or above. Different flow measurement methods are considered for research and development. An attractive method is bypass type flow meter. Detailed

investigations have been carried out on bypass type flow meter. Flow and pressure drop characteristics of the bypass circuit have been analyzed using a commercial CFD software and the flow ratio has been predicted. The model has been experimentally validated by conducting water testing in a scaled down model. Further analysis and studies have been carried to optimize the design of bypass circuit to improve the sensitivity. A bypass circuit configuration was arrived at for future reactors which is more sensitive than the existing arrangement. Chapter 6 of the thesis gave details of the work carried out.

The research work of this thesis has been focused on the issues presently facing in pipeline sodium flow measurement in SFRs. These issues have been addressed satisfactorily and redundant, alternative, cost effective, sensitive and accurate flow measurement techniques have been developed. All the research works carried out as part of this thesis was with the direct involvement of the author with significant contributions. However for fabrication of the magnet assembly and flow meter support of industry was utilized. Various experimental and practical works including data acquisition was carried out as a team work with the guidance of the author. Expertise available in different areas in the authors lab was utilized during the course of work by useful discussions and is acknowledged. Based on the findings of the research work redundant methods have been proposed for flow measurement in the sodium circuits of future SFRs. Table 7.1 gives the details of the pipeline flow measurement followed in existing Indian SFRs and the proposed methods in future SFRs.

**Table 7.1 : Sodium flow measurement in Indian SFRs**

<b>Reactor</b>	<b>15-100 NB</b>	<b>100-200 NB</b>	<b>200-800 NB</b>
<b>FBTR</b>	Alnico-V based PMFM	Alnico-V based PMFM	No pipe above 200
<b>PFBR</b>	Alnico-V based PMFM	Alnico-V based PMFM	Alnico-V based PMFM in bypass line of 25 NB
<b>Future SFRs</b>	Alnico-V based PMFM	Sm-Co based PMFM Side wall flow meter	Alnico-V based PMFM in bypass line of 32/25 NB Side wall flow meter

## **7.2 Scope for Future Research**

### **7.2.1 Alnico-V based PMFM**

Alnico-V based PMFM will continue to be the option for flow measurement in small pipes upto 100 NB size in SFRs. These small flow meters will form large percentage of the total number of flow meters required in the reactor. Research and development to improve the performance of these flow meters will continue in the following lines.

- a) Optimization of the magnetic assembly design to minimize the size, weight and cost.
- b) Numerical finite element modeling considering reaction field and its validation to achieve an accuracy of around 2%, so that calibration with sodium can be avoided.

### **7.2.2 Sm-Co flow meter for large 200 NB pipe**

Design analysis of Sm-Co flow meter for single wall pipelines and double wall pipelines upto 200 NB pipe size can be taken up by numerical modeling and validation by calibration with sodium. Further long term stability test on Sm-Co magnet assembly under accelerated conditions needs be carried out to evaluate the stability of magnetic flux density.

### **7.2.3 SWFM for large pipes**

Low sensitivity is one of the disadvantages of SWFM. Analysis, design and modeling of side wall flow meter with Sm-Co magnet appears essential for pipe sizes ranging from 100 NB to 800 NB. These designs and models needs to be validated by testing with sodium in experimental facilities and in reactor circuits.

#### **7.2.4 In-situ calibration methods**

In-situ calibration of sodium flow meters by noise analysis techniques such as cross correlation should be further focused to improve the accuracy and repeatability.

#### **7.2.5 Development of flow straightners**

The large straight length of piping is required to achieve axi-symmetric velocity in the flow meter section in sodium systems. This is difficult to achieve because of the expansion bends provided in piping to accommodate large thermal expansion of stainless steel pipes at high temperature of operation. To achieve axi-symmetric velocity, flow straightners are required to be provided at the upstream side of the flow meter. Design and development of flow straightner and optimizing the design with minimum pressure drop can be the target.

#### **7.2.6 PMFM for heavy liquid metals**

Alternative coolant of FBR is lead or lead-bismuth alloy. Work on application of PMFM for these heavy liquid metals along with numerical modeling and analysis can be taken up as future work [63]

## REFERENCES

- [1] Website, <http://www.world-nuclear.org/info/Current-and-Future-Generation/Nuclear-Power-in-the-World-Today/>, World nuclear association, updated on April, 2014
- [2] Website, [https://www.gen-4.org/gif/jcms/c\\_59461/generation-iv-systems](https://www.gen-4.org/gif/jcms/c_59461/generation-iv-systems).
- [3] G. Srinivasan, K.V. Suresh Kumar, B. Rajendran, P.V. Ramalingam, The Fast Breeder Test Reactor—Design and operating experiences, Nuclear Engineering and Design, Volume 236, Issues 7–8, April 2006, pp, 796–811.
- [4] S.C.Chetal, V.Balasubramaniyan, P.Chellapandi, P.Mohanakrishnan, P.Puthiyavi-nayagam, C.P.Pillai, S.Raghupathy, T.K.Shanmugham, C.S.Pillai, The design of the prototype fast breeder reactor, Nuclear Engineering and Design, 236 (2006), pp, 852–860.
- [5] Prahalad B, Swaminathan K, Kale R D, Determination of response time of core thermocouples of the Fast Breeder Test Reactor, Proceedings of the 6th Heat and Mass Transfer conference, 1985, pp, B 35-39.
- [6] R.G. Affel, G.H. Burger, C.L. Pearce, Calibration and testing of 2 and 3 ½ inch magnetic flow meter for high temperature NAK service, Oak Ridge National laboratory, U S atomic energy commission.(ORNL-2793), March 1960.
- [7] Hans, R., Knaak, J., Weiss, H.J., 1979; Flow measurement in main sodium pipes. Atomic Energy Review 17 (4), 1979.
- [8] Prashant Sharma, S.Suresh Kumar, B.K. Nashine, R.Veerasingam, B.Krishnakumar, P. Kalyanasundaram, G. Vaidyanathan, Development, computer simulation and performance testing in sodium of an eddy current flow meter, Annals of Nuclear Energy, 37 (2010), pp, 332-338.
- [9] S. Suresh Kumar, Mohammad Sabih, S. Narmadha, N. Ravichandran, R. Dhanasekaran, C. Meikandamurthy, G. Padmakumar, R. Vijayashree, V. Prakash, K.K. Rajan; Utilization of eddy current flow meter for sodium flow measurements in FBR's; Nuclear Engineering & Design, 265 (2013), pp, 1223-1231.

- [10] Poornapushpakala S., Gomathy C., Sylvia J.I., Babu B, Design, development and performance testing of fast response electronics for eddy current flow meter in monitoring sodium flow, *Flow Measurement and Instrumentation* 38, (2014), pp,98–107.
- [11] D.W. Clarke, J. Hemp, Eddy-current effects in an electromagnetic flow meter, *Flow Measurement and Instrumentation* 20 (2009),pp, 22-37.
- [12] J.A Shercliff, *The Theory of Electromagnetic Flow-Measurement*, University Press, Cambridge, UK, 1962.
- [13] J Hemp and H K Versteeg, Prediction of electromagnetic flow meter characteristics, *J. Phys. D: Appl. Phys.* 19 (1986),pp, 1459-1476.
- [14] Mahmud Tarabad, Roger C Baker, Integrating electromagnetic flow meter for high Reynolds numbers, *J. Phys. D: Appl. Phys.*, 15 (1982), pp,739-745.
- [15] C. Thatcher, P.G. Bentley, G. Mc Gonigal, Sodium flow measurement in PFR, *Nuclear Engineering International*, 1970, pp, 822-825.
- [16] C. Thatcher, Electromagnetic flow meters for large sodium flows, *Proceedings of IAEA Specialists Meeting on Sodium Flow Measurements in Large LMFBR Pipes*, INTERATOM, Bensberg, W. Germany, 1980, pp,21–33.
- [17] H. Araki, S. Horikoshi, N.Sekiguchi, H. Kitagwa, K.Sano, O.Uno, Design criteria and current status of research and development on LMFBR large pipe sodium flow meter in Japan. *IAEA Specialists Meeting on Sodium Flow Measurements in Large LMFBR Pipes*, INTERATOM, Bensberg, W. Germany, 1980, pp, 161–171.
- [18] Kamanin, Y.L., Kuzavkov, 1989. Measurement of coolant flow rate through the fuel assemblies in BN-350 and BN-600 reactors, *Proceedings of IAEA/IWGFR Specialists' Meeting on Instrumentation for Supervision of Core-Cooling in Fast Breeder Reactors*, Kalpakkam, India, pp, 143–153.
- [19] Fontaine, B., Martin, L., Core flow measurement at Phenix, In: *Proceedings of CEA-IGCAR Technical Seminar on Liquid Metal Fast Reactor, Safety Aspects Related to Severe Accidents*, Kalpakkam, 2007.
- [20] Lions N. Et al., 1976,Utilization and performance of sodium instrumentation during start-up and initial operation of Phenix, *proceedings international conference liquid metal technology in energy production*, Champion, Pennsylvania, United States of America (USA); 3 - 6,May 1976,pp,755-761.

- [21] L.J. Christensen, ANL, Experimental Breeder Reactor II (EBR II), Instrumentation for Core Surveillance, IAEA/IWGFR-Specialists Meeting on Instrumentation for Supervision of Core-Cooling in Fast Breeder Reactors, Kalpakkam, India, 12-15, December, 1989.
- [22] Status on National Programme on Fast Breeder Reactors, 24th Annual meeting, Tsuruga, Japan, April, 1991, A review of the collaboration programme on the European Fast Reactor.
- [23] Engineering aspects of Pool type LMFBR, 1000 MWe, EPRI NP-645 Vol.2 April 1978, prepared by M/s Rockwell International and M/s Bechtel Corporation.
- [24] Pool type LMFBR plant, 1000 MWe Phase A design; prepared by M/s General Electric company EPRI NP 646, Vol.4, April 1978.
- [25] Pool type LMFBR plant, 1000 MWe Phase A – Extension I design prepared by M/s General Electric company EPRI NP 882, Vol.6.
- [26] Joachim Knak, Joachim Barzantny, Ultrasonic and flux distortion flow meter, two likely methods of sodium flow measurement in ducts of large nominal bore, IAEA specialist meeting on sodium flow measurements in large pipes, Interatom, Bensberg, W Germany, February 1980, pp,116-128.
- [27] E. Duncombe, R.D.Watkins, Likely future requirements for main duct sodium flow measurements, IAEA specialists meeting on Sodium Flow Measurements in Large LMFBR Pipes, INTERATOM, Bensberg, W. Germany, February 1980, pp 173-182.
- [28] D. Letainturier et al, Measurement of Core Thermal Hydraulic Characteristics, Nuclear Science and Engineering, Vol 106, September 1990.
- [29] G.E.Turner, Liquid Metal Flow Measurement (Sodium) State-of-the-Art Study LMEC-Memo-68-9, June 28, 1968.
- [30] K.K. Rajan; P.Kalyanasundaram; G.Vaidyanathan, Flow meter for sodium systems, Global conference and exhibition – FLOTEK.G, FCRI, Palghat, 2007.
- [31] Standard specifications for Permanent magnet materials, MMPA Standard No. 0100-00, Magnet materials producers association, December 1998.
- [32] T Miyazawa, et al., Toshiba corporation, Electromagnetic flow meter development for LMFBR; Proceedings of the IAEA Specialists meeting on sodium flow measurements in large LMFBR pipes, Bergisch Gladbach, Germany, 4-6, February, 1980, pp, 46-57.

- [33] G. Vijayakumar., et al., Calibration of permanent magnet flow meters in sodium, Proceedings of National Symposium on Instrumentation-30, Cochin (2005),pp, 337-343.
- [34] Uiju Jeong, Yun Ho Kim, Jong-Man Kim, Tae-Joon Kim, Sung Joong Kim, Experimental evaluation of permanent magnet probe flow meter measuring high temperature liquid sodium flow in the ITSL, Nuclear Engineering and Design 265, (2013), pp,566–575.
- [35] J. Hemp, A technique for low cost calibration of large electromagnetic flow meters, Flow Measurement and Instrumentation, 12 (2001),pp,123–134.
- [36] Vitaly Minchenya, Christian Karcher, Yuri Kolesnikov, André Thess, Calibration of the Lorentz force flow meter, Flow Measurement and Instrumentation 22, (2011), pp,242–247.
- [37] Ernest O. Doebelin, Department of Mechanical Engineering, The Ohio State University; Measurement Systems Application and Design; 5<sup>th</sup> Edition, Mc Graw Hill Higher Education, Page 67-91.
- [38] Akira Endou, In-service calibration method of electromagnetic flow meter for LMFBR utilizing cross correlation of output voltage fluctuation, Journal of nuclear science and technology (1984),pp,501-514.
- [39] W. Reimche., et al., Velocity profile and flow measurement in liquid sodium by signal correlation of fast intrinsic thermocouple and electromagnetic flow meters, Progress in nuclear energy 15 (1985),pp,727-734.
- [40] C. Raptis and G. A. Forster, A signal analysis method using cross-correlation of turbulence flow signals to determine calibration of permanent magnet sodium flow meters, IEEE Transactions on Nuclear science 25(1) (1978),pp,278-281.
- [41] M. Fujino., et al., Development of calibration method of electromagnetic flow meters by average frequency technique, Proceeding of the specialist meeting on sodium flow measurements in large LMFBR pipes (1980), pp, 130-138.
- [42] W.Q.Yang., et al., An intelligent cross correlator for pipeline flow velocity measurement, Flow Measurement and Instrumentation, 8(2) (1997),pp, 77-80.
- [43] R.Prabhakar., et al., Calibration of PM flow meters in sodium by noise cross correlation technique, Liquid metal engineering and technology, 1 (1985),pp, 449-450.
- [44] Permanent magnets and their application, Rollin J. Parker, Robert J. Studders, Wiley, 1962.

- [45] R K Tenser, Design and application of permanent magnets, Indiana general, Magnet products, Valparaiso, Indiana 46383, a division of Electronic memories and magnetics Corporation, 1963, pp, 15-17.
- [46] George A. Forster, Irradiation of Alnico magnets in EBR-II,ANL-ETD-71-03,January 1971.
- [47] G.Vijayakumar, R.Rajendraprasad, S.P.Pathak, K.K.Rajan, P.Kalyanasundaram and G.Vaidyanathan, Manufacturing of Permanent Magnet Flow meters, INSAC-2009, Chennai.
- [48] St.Muller, G.Thun, W. Glauner, Two novel probes for flow measurement in liquid metal pipes of great nominal width, Proceedings of the IAEA Specialists meeting on sodium flow measurements in large LMFBR pipes, Bergisch Gladbach, Germany, 4-6, February, 1980; pp 83-93.
- [49] R. Veerasamy, B. Srinivasa Rao, K.K.Rajan and R. Prabhakar, Development of electromagnetic sodium flow meters for the primary circuit of prototype fast breeder reactor, Fourth international conference on liquid metal engineering and technology, 1988.
- [50] Proceedings of the Specialists meeting on sodium flow measurements in large LMFBR pipes, Bergisch Gladbach, Germany, 4-6, February, 1980, pp, 1-188.
- [51] G Vijayakumar, B.K.Nashine, K. K. Rajan and P.Kalyanasundaram, Development and Testing of PM Flow meter with Samarium Cobalt Magnet Assembly; Asian Nuclear Prospects 2010;Energy Proceedia, Volume 7, 2011, pp, 630–637.
- [52] Vijay Sharma, G. Vijaya Kumar, S.K. Dash, B.K. Nashine and K.K. Rajan; Modelling of permanent magnet flow meter for voltage signal estimation and its experimental verification; Flow measurement and instrumentation, Elsevier, Vol. 28, pp,22–27, December, 2012.
- [53] Bo Lu, Liangwang Xu, Xiaozhang Zhang, Three-dimensional MHD simulations of the electromagnetic flow meter for laminar and turbulent flows, Flow Measurement and Instrumentation 33, (2013),pp,239–243.
- [54] Carmen Stelian, Calibration of a Lorentz force flow meter by using numerical modeling, Flow Measurement and Instrumentation 33, (2013), pp, 36–44.
- [55] Torben Amby Christensen, Morten Willatzen, Investigating the effect of magnetic pipes connected to electromagnetic flow meters using experimentally validated finite element models, Flow Measurement and Instrumentation 21 (2010), pp, 62-69.

- [56] COMSOL 3.5a, Reference Manual, 2009; COMSOL AB, Stockholm, Sweden.,2013
- [57] V. Devita and L. Fletcher, US large pipe sodium flow meter test experience, IAEA specialist meeting on sodium flow measurements in large pipes, Interatom, Bensberg, W Germany, February 1980, pp, 35-34.
- [58] Gautam Pulugundla, Christiane Heinicke, Christian Karcher, André Thess, Lorentz force velocimetry with a small permanent magnet, European Journal of Mechanics B/Fluids 41, (2013),pp,23–28.
- [59] T. Asada, D. Kittaka, M. Komai, M. Enomoto, H. Ota, E. Hoashi, S. Suzuki, H. Horiike, M. Hirabayashi, M. Otaka, K. Ara, Development of a new electromagnetic flow meter for fast reactor, Feasibility of EMF composed of multi-unit, International Conference on Fast Reactor and Related Fuel Cycles: Safe Technologies and Sustainable Scenarios, Conference (FR-13), Paris, France,4-7, March 2013.
- [60] Frank M White, Fluid Mechanics, 6th edition, The McGraw-Hill companies, New Delhi, 2008
- [61] Z. Wang, G.Y. Tian, G.P. Lucas, Relationship between velocity profile and distribution of induced potential for an electromagnetic flow meter, Flow Measurement and Instrumentation 18 (2007),pp,99–105.
- [62] K.K.Rajan, etal, Bypass type flow meter for PFBR primary pump sodium flow measurement, National Symposium on Instrumentation (NSI-22), New Delhi,1997.,
- [63] Thomas Schulenberg, Robert Stieglitz, Flow measurement techniques in heavy liquid metals, Nuclear Engineering and Design, 240, (2010), pp,2077–2087.